Ocean-glacier interaction on the large regional scale

Dissertation

A dissertation submitted to
Fachbereich 8
University of Bremen

for the degree
Doktor der Naturwissenschaften

submitted by
Beatriz Margarita Recinos Rivas

supervised by
Prof. Ben Marzeion and Asst. Prof. Fabien Maussion

reviewed by
Prof. Ben Marzeion and Dr. Robert McNabb

Bremen, December 2020.

Date of doctoral colloquium: Monday 21st of December 2020.

This work was typeset using LaTeX
Produced by Joel Goop.

Dedication

This work is dedicated to my dad Rene Recinos.

Abstract

Glaciers are important regulators of water availability in many regions of the world and their retreat can lead to increased geohazards. Glacier melt has contributed significantly to sea-level rise in the past and has become the biggest single source of observed sea-level rise since 1900, even if the ice mass stored in glaciers is small compared to the Greenland and Antarctic ice sheets ($< 1\%$). Glacier melt has and will continue to be a major source of sea-level rise in the 21st century. Therefore, it is a pressing task to improve the knowledge of how glaciers change when subjected to climate change, both natural and anthropogenic. About 30% of the glaciers on earth terminate in the ocean and frontal ablation (mass loss by calving and frontal melting) is a major component of the mass budget of tidewater glaciers, strongly affecting their dynamics.

Most global scale ice volume estimates to date still suffer from considerable uncertainties related to i) the implemented frontal ablation parameterization or ii) not accounting for frontal ablation at all in the glacier model. To improve estimates of the ice thickness distribution of tidewater glaciers, it is thus important to identify and test low-cost and robust parameterizations of this process. By implementing such parameterization into the ice-thickness estimation module of the Open Global Glacier Model (OGGM v1.1.2), this thesis conducts a first assessment of the impact of accounting for frontal ablation on the estimate of ice stored in glaciers located in Alaska and Greenland.

OGGM is the first globally applicable, open source, community-driven model for consistently simulating past and future global scale glacier change. It's ice thickness inversion scheme relies on a mass-conservation approach, this thesis found that if frontal ablation is neglected from the mass balance budget, the

model systematically underestimated the mass turnover, and therefore the thickness and volume of tidewater glaciers. This underestimation can amount to up to 19% on a regional scale in Alaska, and up to 14% in Greenland's Peripheral glaciers (PG's). For individual glaciers volume underestimation can be up to 30% (e.g Columbia Glacier in Alaska). The effect is independent of the size of the glacier.

Additionally, this study performs different sensitivity experiments to study the influence of i) a constant of proportionality (k) used in the frontal ablation parameterization, ii) Glen's temperature-dependent creep parameter (A) and iii) a sliding velocity parameter (f_s) on the regional dynamics of Alaska tidewater glaciers. OGGM is able to reproduce previous regional frontal ablation estimates by applying a number of combinations of values for k, Glen's A and f_s. The sensitivity studies also show that differences in thickness between accounting for and not accounting for frontal ablation occur mainly at the lower parts of the glacier, both above and below sea level. This indicates that not accounting for frontal ablation will have an impact on the estimate of the glaciers' potential contribution to sea-level rise.

In Greenland, there are no regional observations or estimates of frontal ablation to constrain model parameters. Forcing the study to develop two independent methods to calibrate the calving parameterization implemented in OGGM. The first method constrains the calving constant of proportionality k, with surface velocity fields derived from the MEaSUREs Multi-year Greenland Ice Sheet Velocity Mosaic. Whereas the second method constrains the k parameter using frontal ablation fluxes, derived from Surface Mass Balance (SMB) means over an equilibrium reference period (1961-1990), obtained from the monthly output of the Polar Regional Climate Model RACMO, statistically downscaled to 1 km resolution. The second calibration method is based on the strong assumption that most PG's during that time have a balanced budget (i.e. did not experience any mass loss or gain). Considering an equilibrium between what the glacier gained and calved might not reflect real frontal ablation fluxes, but such estimates, serve as a base to asses the dynamic mass loss of glaciers when combined with frontal ablation estimates constrained from velocity observations. By comparing the model output after applying both calibration methods, this thesis finds that the model is not able to predict individual tidewater glacier dynamics, if it relies only on SMB estimates and the assumption of a closed budget to constrain k values. Velocity observations are essential to constrain model parameters and estimate the dynamic mass loss of PG's.

Zusammenfassung

Gletscher sind wichtige Regulatoren der Wasserverfügbarkeit in vielen Regionen der Erde und der Rückzug der Gletscher kann zu vermehrten Georisiken führen. Die Gletscherschmelze hat in der Vergangenheit signifikant zum Meeresspiegelanstieg beigetragen und ist die größte Einzelquelle des beobachteten Meeresspiegelanstiegs seit 1900, obwohl die gespeicherte Eismasse in Gletschern klein ist im Vergleich zu den Eisschilden Grönlands und der Antarktis ($\leq 1\%$). Die Gletscherschmelze war und wird auch weiterhin ein bedeutender Grund des Meeresspiegelanstiegs im 21. Jahrhundert sein. Daher ist es eine dringende Aufgabe unser Wissen darüber zu verbessern, wie sich Gletscher aufgrund des Klimawandels verändern, sowohl dem natürlichen als auch dem anthropogenen. Etwa 30 % der Gletscher der Erde enden im Ozean und frontale Ablation (Masseverlust durch Kalbung und frontales Schmelzen) ist eine bedeutende Komponente des Massebudgets von Gezeitengletschern, weil sie starke Auswirkungen auf deren Dynamik hat.

Die meisten heutigen weltweiten Schätzungen des Eisvolumens leiden immer noch unter erheblichen Unsicherheiten im Zusammenhang mit i) der implementierten Parametrisierung der frontalen Ablation oder ii) der fehlenden Berücksichtigung der frontalen Ablation im Gletschermodell. Um die Schätzungen der Eisdickenverteilung von Gezeitengletschern zu verbessern, ist es daher wichtig kostensparende robuste Parametrisierungen dieses Prozesses zu identifizieren und zu testen. Durch die Implementierung einer solchen Parametrisierung in das Eisdickenschätzungsmodul des Open Global Glacier Model (OGGM v1.1.2), führt diese Arbeit eine erste Beurteilung des Einflusses durch, die eine Berücksichtigung der frontalen Ablation auf die Schätzung der in den Gletschern Alaskas und Grönlands gespeicherten Eismasse hat.

OGGM ist das erste global anwendbare, Open Source, von der Gemeinschaft geleitete Modell, um konsistent vergangene und zukünftige globale Gletscheränderungen zu simulieren. Sein Inversionsschema der Eisdicke beruht auf einem Massenerhaltungsansatz. Diese Arbeit kommt zu dem Ergebnis, dass wenn die frontale Ablation in der Massebilanz vernachlässigt wird, das Modell systematisch den Masseumsatz unterschätzt und damit auch die Dicke und das Volumen von Gezeitengletschern. Diese Unterschätzung kann sich auf bis zu 19% auf einer regionalen Skala in Alaska summieren und bis zu 14% bei den Gletschern der Grönländischen Peripherie (PG's). Die Unterschätzung für einzelne Gletschervolumen kann bis zu 30% betragen (z.B. Columbia Gletscher in Alaska). Der Effekt ist unabhängig von der Größe des Gletschers.

Außerdem führt diese Arbeit verschiedene Sensitivitätsexperimente durch, um den Einfluss i) der Proportionalitätskonstanten (k) in der Parametrisierung der frontalen Ablation, ii) Glen's temperaturabhängigem Kriechparameter (A) und iii) einem Gleitgeschwindigkeitsparameter (f_s) auf Grundlage der regionalen Dynamik von Alaskas Gezeitengletschern zu bestimmen. OGGM ist in der Lage frühere regionale Schätzungen der frontalen Ablation zu reproduzieren, indem verschiedene Kombinationen für Werte von k, Glen's A und f_s angewandt werden. Die Sensitivitätsstudien zeigen auch, dass Unterschiede in der Dicke unter Berücksichtigung oder Nicht-Berücksichtigung der frontalen Ablation einen Einfluss auf die Schätzung des potenziellen Beitrags eines Gletsches zum Meeresspiegelanstieg haben.

In Grönland gibt es keine regionalen Beobachtungen oder Schätzungen der frontalen Ablation um Modellparameter zu beschränken. Dies führte dazu, dass in dieser Arbeit zwei unabhängige Methoden entwickelt wurden, um die Kalbungsparametrisierung in OGGM zu kalibrieren. Die erste Methode beschränkt die Proportionalitätskonstante der Kalbung k mit Oberflächengeschwindigkeitsfeldern, welche aus dem MEaSUREs Multi-year Greenland Ice Sheet Velocity Mosaic stammen. Während die zweite Methode den Parameter k beschränkt indem der Fluss der frontalen Ablation genutzt wird, der aus Mittelwerten der Oberflächenmassebilanzen (SMB) über eine Equilibriumsreferenzperiode (1961-1990) stammen. Diese Daten werden aus dem monatlichen Ergebnis des Polar Regional Climate Model RACMO gewonnen, welches auf eine Auslösung von 1 km reduziert wurde. Die zweite Kalibrierungsmethode basiert auf der starken Annahme, dass die meisten PG's während dieser Zeit ein ausgeglichenes Budget hatten (d.h. sie haben weder Masse gewonnen noch verloren). Betrachtet man ein Gleichgewicht zwischen der Masse die gewonnen wird und der

Masse die durch das Kalben verloren geht, so spiegelt dies nicht unbedingt den realen Fluss der frontalen Ablation wieder. Allerdings dienen solche Schätzungen als Basis um den dynamischen Masseverlust von Gletschern zu bestimmen, wenn man diese mit Schätzungen der frontalen Ablation kombiniert, welche durch Geschwindigkeitsbeobachtungen beschränkt sind. Durch den Vergleich der Modellergebnisse nach der Anwendung beider Kalibrierungsmethoden findet diese Arbeit heraus, dass das Modell nicht in der Lage ist einzelne Dynamiken von Gezeitengletschern vorherzusagen, wenn es nur auf SMB-Schätzungen und der Annahme eines geschlossenen Budgets für die Beschränkung des k-Wertes beruht. Geschwindigkeitsbeobachtungen sind essentiel, um die Modellparameter zu beschränken und den dynamischen Massenverlust der PG's abzuschätzen.

Preface

The work presented in this thesis constitutes of an overview part and a collection of papers that partially fulfil the requirements for the degree of Doctor of Natural Science (*Dr.rer.nat.*) at the Institute of Geography, University of Bremen, Germany.

The first chapter of the thesis is an overview of the study. It comprises of an introduction, where the main research questions and the motivation of the thesis are addressed. Then each following chapter corresponds to three papers submitted to, or publish by, international peer reviewed journals. These papers are:

- **Paper I:**
  Maussion, F., Butenko, A., Champollion, N., Dusch, M., Eis, J., Fourteau, K., Gregor, P., Jarosch, A. H., Landmann, J., Oesterle, F., **Recinos, B.**, Rothenpieler, T., Vlug, A., Wild, C. T., and Marzeion, B.: The Open Global Glacier Model (OGGM) v1.1, Geosci. Model Dev., 12, 909-931, `https://doi.org/10.5194/gmd-12-909-2019`, **2019**.

- **Paper II:**
  Recinos, B., Maussion, F., Rothenpieler, T., and Marzeion, B.: Impact of frontal ablation on the ice thickness estimation of marine-terminating glaciers in Alaska, The Cryosphere, 13, 2657–2672, `https://doi.org/10.5194/tc-13-2657-2019`, **2019**.

- **Paper III:**
  Recinos, B., Maussion, F., B. Noël, Möller, M., and Marzeion, B.: Cali-

bration of a frontal ablation parameterization applied to Greenland's peripheral calving glaciers. Journal of Glaciology, **submitted.**.

In the last chapter, these three papers are summarised and a synthesis of the conclusion for each paper is presented. This chapter ends with a discussion and outlook on future work.

Acknowledgements

I would like to express my sincere gratitude to my supervisors Ben Marzeion and Fabien Maussion for first giving me the opportunity to pursue a post graduate education within their research group and for their constant support and guidance during the past five years. Without their patience and innovated thinking this work would not have been possible. I am especially thank full for their encouragement to push beyond my limits and for all their investment on my professional development. A huge thanks to all members of the OGGM team specially Fabien Maussion, Timo Rothenpieler and Julia Eis for their technical help with running the model and for innumerable discussions about OGGM and science in general. I would like to also acknowledge all my colleagues at the University of Bremen, specially those in the Climate Lab and within ArcTrain for their support and advice during my PhD. A major fraction of this PhD thesis is a result to several research stays done at the University of Innsbruck and this wouldn't have been possible without the financial support of ArcTrain and the willing of Fabien Maussion to host me. Thanks for helping complete the job!

And in a more personal level I would like to thank my family and friends especially my mom, dad (even if you are no longer here to witness this), sisters and my husband since they are the people that had led me to complete my degree successfully by not letting me give up despite the hard times. Special thanks to my husband Ben Jones for his patience in proof-reading all my manuscripts and thesis.

Contents

List of Figures

List of Tables

1

Overview

1.1 Introduction

Glaciers are formed where climate conditions and topographic characteristics allow snow to accumulate over several years. The snow is gradually transformed into glacier ice, in a process highly dependent on temperature and that is often long and complex (Cuffey and Paterson, 2010). Just like any other object on earth, glaciers experience the force of gravity and flow loss to elevations with higher temperatures, where various processes of ablation (lost of snow and ice) dominate over accumulation (gain of snow and ice). The sum of all accumulation and ablation processes determines the mass balance of a glacier. Glaciers are important indicators of changes in climate, because they adjust their geometry in response of changes in temperature and precipitation (Vaughan et al., 2013). During the past century, glaciers have lost a substantial fraction of their mass, with several studies suggesting that this would almost certainly not have happened, if the Earth was not experiencing a rapid warming increase caused by anthropogenic sources (Marzeion et al., 2014a). But the impacts of glacier changes - whether they grow or shirk - go beyond this sentimental aspect: by changing the seasonality of runoff, glaciers are also important regulators of water availability in many regions of the world (Marzeion et al., 2012b). Glacier retreat often leads to the destabilization of mountain slopes and formation of unstably dammed melt water lakes, increasing geohazards (e.g. landslides, floods. Richardson and Reynolds, 2000). Finally, glaciers have added more mass to the

ocean than the Greenland and Antarctic ice sheets during the past century, despite storing a smaller volume of ice. This section gives a brief overview of the contribution of glaciers to sea-level rise, the methods developed to measure this contribution at a global scale and the interaction between glaciers and the ocean, thought to be a crucial link between climate, ice mass loss and sea-level change.

1.1.1 Glaciers and sea-level rise

In the Fifth Assessment Report of the Intergovernmental Panel on Climate Change (AR5 IPCC, Church et al., 2013b) glaciers are defined as all land-ice masses, including those peripheral to (but not including) the Greenland and Antarctic ice sheets. In the report, glacier mass budgets for the 2003 - 2009 period were reconciled in order to obtain an estimate of the glacier contribution to sea-level. This was achieved by combining traditional observations with satellite altimetry and gravimetry as a way of filling regional gaps and obtaining global coverage (Zemp et al., 2015). Additionally, glacier models were used that when combined with the observations, indicated that a net decline of global glacier volume began in the 19th century, before significant anthropogenic climate forcing had started and was probably the result of warming associated with the termination of the Little Ice Age (Church et al., 2013b). At the beginning of the 20th century, Fig. 1.1b shows a slight increase in the glaciers' contribution to sea-level but it is not until the period between 1993-2015, that glacier mass loss accounts for a 22% of the observed sea-level. Together with the thermal expansion of the oceans (42% of the observed Global Mean Sea-Level rise) account for more than half of the observed GMSL rise.

Observational and model based studies (e.g. Leclercq et al., 2014; Marzeion et al., 2015) estimate the glaciers contribution during the period of 1902 - 2005 to be between 68.2 $\pm$ 6.9 and 80.4 $\pm$ 21.1 mm SLE, becoming the biggest single source of observed sea-level rise since 1900 (Gregory et al., 2013a).

A more recent study by Zemp et al. (2019) estimates that glaciers contributed 27 $\pm$ 22 mm SLE to global mean sea-level rise from 1961 to 2016 (or a contribution of 0.5 $\pm$ 0.4 mmyr^{-1}). Regional specific-mass-change rates for 2006-2016 range from -0.1 to -1.2 m.w.e yr^{-1}, resulting in a global sea-level contribution of 335 $\pm$ 144 Gt, or 0.92 $\pm$ 0.39 mm yr^{-1} (see Fig. 1.2). This suggest that glacier mass loss may be larger than previously reported and that glaciers were playing

and will continue to play an important part of the sea-level budget in the near future. Zemp et al. (2019) state that the present glacier mass loss is equivalent to the sea-level contribution of the Greenland Ice Sheet, and accounts for 25 to 30% of the total observed sea-level rise.

Understanding the causes, mechanisms and time scales of glacier change, when subjected to climate change, both natural and anthropogenic, is thus paramount to identify successful strategies for mitigation and adaptation to rising sea levels (Marzeion et al., 2018). The main challenge to achieve progress in this task is a severe undersampling problem: direct glaciological measurements of mass balance have been performed on ∼300 glaciers world wide (≈ 0.1% of all glaciers on Earth, see Fig. 1.2). The number of glaciers on which these types of measurements have been carried out for time periods longer than 30 years, i.e. over periods that potentially allow for the detection of a climate change signal, is one order of magnitude smaller (Maussion et al., 2019; Zemp et al., 2009).

The number of glaciers with ice thickness observations is equally limited. The Glacier Thickness Database (GlaThiDa), which centralizes ice thickness measurements outside the two ice sheets, presently contains information for only about 1,000 out of the 250,000 glaciers worldwide (Farinotti et al., 2019). From these 1,000 glaciers, only ∼ 800 have measurements that fall inside a glacier outline defined in the latest Randolph Glacier Inventory (RGI) (Castellani, 2019).

Length variations of glaciers have been observed for substantially longer periods of time (Oerlemans, 1994, 2005). These variations are, however, much more difficult to understand, as large glacier length fluctuations may arise from intrinsic climate variability (Roe, 2011; Roe and O'Neal, 2009). Data obtained by remote sensing allow for gravimetric assessments of ice mass change or volume change estimates, by differencing digital elevation models. Unfortunately, they are only available for the past decade (e.g. Gardner et al., 2013) on longer time scales. Therefore, to assess the evolution of glaciers when subjected to climate change it is necessary to rely on glaciodynamical models. Most models require the glacier ice-thickness distribution as an initial condition. Measuring glacier thickness and deriving an estimate of its total volume is not, however, an easy task (Farinotti et al., 2009) and as mentioned before very few measurements exist. To overcome this undersampling problem, a number of numerical methods have been developed to infer the total volume and/or the ice thickness distribution of glaciers from characteristics of the glacier surface properties (Farinotti et al., 2017).

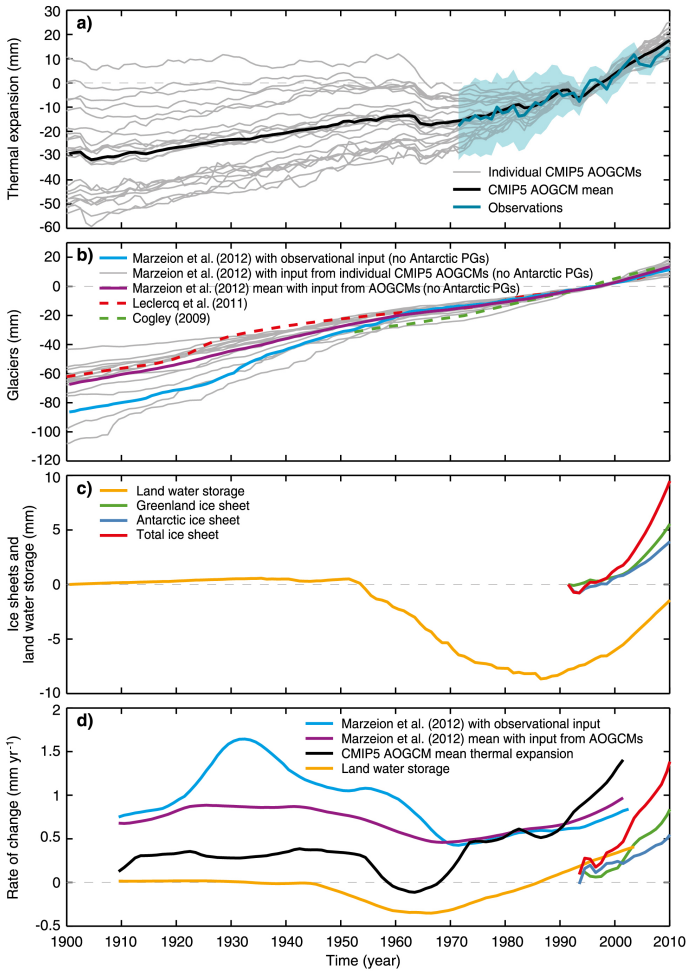

Figure 1.1: Changes in glaciers, ice sheets and land water storage are shown as positive sea-level rise when mass is added to the ocean. (a) Ocean thermal expansion. (b) Glaciers (excluding Antarctic peripheral glaciers). Model simulations by Marzeion et al. (2012b). The observational estimates by Cogley (2009b) are shown in green (dashed) and by Leclercq et al. (2011) in red (dashed). (c) Changes in land water storage (yellow/orange, the sum of groundwater depletion and reservoir storage) start at zero in 1900. The Greenland ice sheet (green), the Antarctic ice sheet (blue) and the sum of the ice sheets (red), start at zero at the start of the record in 1991. (d) The rate of change (19-year centred trends) for the terms in (a)–(c), and for the ice sheets (5-year centred trends). All curves in (a) and (b) are shown with zero time-mean over the period 1986-2005 and the colours in (d) are matched to earlier panels. (Taken from Church et al., 2013b)

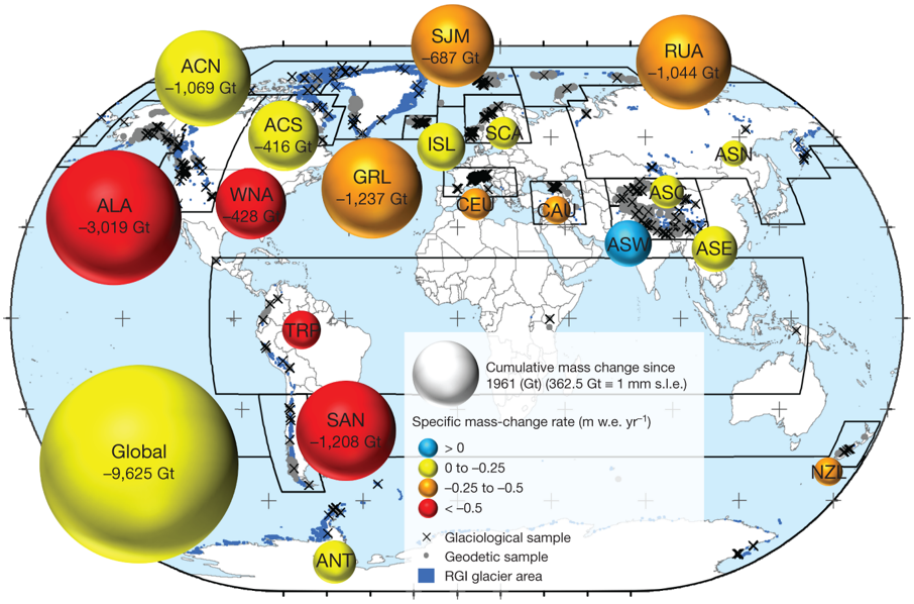

Figure 1.2: Regional glacier contributions to sea-level rise from 1961 to 2016. The cumulative regional and global mass changes (in Gt, represented by the volume of the bubbles) are shown for the 19 first-order regions (outlined with bold black lines). Specific mass-change rates (m.w.e. yr^{-1}) are indicated by the colours of the bubbles. In the background, the locations of glaciological and geodetic data samples are plotted over the glacier polygons from RGI 6.0. The grey plus signs mark latitudes and longitudes. (Taken from Zemp et al., 2019)

1.1.2 Ice thickness estimation methods

Simulations and projections of global mass changes of glaciers and ice caps have relied on low-complexity models of surface mass balance and glacier dynamics. These modeling studies have commonly assumed that the main drivers of glacier mass balance are air temperature and precipitation (Radić et al., 2014), while glacier dynamics, involved in changes of glacier area and thickness, are assumed to be successfully simulated by using a variety of methods (see Farinotti et al. (2017), for a review of all methods).

Scaling approaches are among the simplest methods and more popular, relating the length, slope and area of the glacier to its total volume (e.g. Bahr et al., 1997; Grinsted, 2013; Lüthi, 2009; Radić and Hock, 2011). However, they yield only to a mean ice thickness estimate and total glacier volume, without

providing any information on the ice thickness distribution. Methods that seek to obtain a distribution, must rely on certain ice dynamics theoretical considerations (Farinotti et al., 2017).

Nye (1952), for example, noted that for the case of an idealized glacier of infinite width, ice thickness can be calculated from the surface slope using estimates of basal shear stress and assuming that the glacier ice moves with a perfect plastic behaviour, an approach that was later extended and applied to valley glaciers of idealized shapes (Nye, 1965). Li et al. (2012) extended Nye's approach, accounting not only for the basal shear stress effect on the ice velocity but also for the effect caused by the lateral drag at the glacier margins. All these three approaches, assumed a constant and known basal shear stress (Farinotti et al., 2017) thus limiting the method to regions where ice thickness observations are available. Observations of ice thickness are necessary to calibrate basal shear stress parameterisations. Haeberli and Hoelzle (1995) additionally showed that it was possible to estimate the basal shear stress from the glacier elevation range, this approach and the corresponding parameterisation has been used in a series of studies covering entire glaciated regions (e.g. Frey et al., 2014; Gantayat et al., 2014; Linsbauer et al., 2012; Paul and Linsbauer, 2012). Gantayat et al. (2014) for example used surface velocities and mass balance observations to estimate mean ice flux. However there are many regions of the world where these observations are not available, making the method highly dependent on data availability.

There is another collection of methods, that rely on mass conservation and combine different aspects of ice flow dynamics, such as applying the shallow-ice approximation (SIA e.g. Cuffey and Paterson, 2010; Oerlemans, 1997) and/or an integrated form of Glen's flow law (Glen, 1995). The SIA neglects longitudinal (along flow stretching and compression) and transverse stresses (lateral drag against slower ice for an ice stream or valley walls for a valley glacier), and vertical stress gradients (Adhikari and Marshall, 2012b). Despite these neglections, the SIA is computationally efficient and works reasonably for valley glaciers when a set of correction factors (shape factors) are imposed upon SIA flowline models (e.g. Anderson et al., 2008; De Smedt and Pattyn, 2003; Nye, 1965). Glen's flow law on the other hand, describes how individual ice crystals deform in response to stress, it considers ice as a non-linear viscoelastic fluid (exhibits both viscous and elastic characteristics when undergoing deformation), and relates strain rates to stresses mostly to the third power (Glen, 1995). The rate of deformation for a given stress depends on the temperature and fabric of the ice; warmer ice deforms

more easily (Davies and Lea, 2015). Both approximations when combined to form a flowline model will simulate ice-flow along a single, one-cell wide centreline. The idea of combining these methods goes back to Budd and Allison (1975) and Rasmussen (1988), whose ideas were further developed by Fastook et al. (1995) and Farinotti et al. (2009) the later approach being successfully applied several times since (e.g. Clarke et al., 2013; Huss and Farinotti, 2012; Maussion et al., 2019; Morlighem et al., 2011).

Farinotti et al. (2009) estimate ice-thickness distribution from a given glacier surface topography, by inferring the ice thickness from estimates of ice fluxes, derived from the assumption that ice fluxes balance the surface mass budget. The results are thus sensitive to the spatial distribution of the mass flux and the mass balance. The method was originally applied to valley glaciers (land-terminating glaciers), which mass balance components comprise of accumulation (via the precipitation of snow) and ablation (via ice melting due to energy balance changes). But for calving glaciers (marine- and lake-terminating glaciers), the surface mass budget cannot be considered closed, even assuming equilibrium between glacier and climate. The derived ice thickness estimate for these glaciers hence depends on estimates of frontal ablation (mass loss by calving, subaerial frontal melting and sublimation and subaqueous frontal melting).

1.1.3 Ocean-glacier interactions

There are 3,222 glaciers classified as calving (marine- and lake- terminating) glaciers in the latest Randolph Glacier Inventory (RGI v6.0, RGI Consortium, 2017), from these glaciers nearly 40% of them drain directly into the ocean (Cuffey and Paterson, 2010). It is in these oceanic margins that we see the most rapid changes: ice stream acceleration, thinning and grounding line migration.

Calving glaciers

Calving, or the mechanical loss of ice from glaciers and ice shelves, is an important component of the mass budget of many glacier systems worldwide (Benn et al., 2007b). Calving is most common when a glacier flows into water (i.e. lakes or the ocean) but can also occur on dry land, where is known as dry calving (Diolaiuti et al., 2004). Iceberg calving is a dominant ablation mechanism, that can allow much larger volumes of ice to be lost than would otherwise be

possible through surface ablation (Van der Veen, 1996). Calving is not a single process, but a family of related processes that can take place in a wide variety of settings (Benn et al., 2007b). There are two main factors that determine the type of calving, whether the glacier is cold or temperate and whether the terminus is grounded or floating. This gives four possible combinations. However, no temperate floating ice tongues are known to exist and many, if not most, polar glaciers entering the sea have floating termini. Thus, most calving glaciers are of just two types, temperate grounded glaciers and polar and subpolar glaciers with floating termini (Nick, 2006).

There are several main calving mechanisms, all of which are related to stress at the glacier terminus. Figure 1.3 summarises the different possible situations, where stresses can be high enough to allow fractures to propagate through glacier ice, and trigger calving events: (i) during the stretching of ice associated with spatial gradients in the velocity of a glacier (Fig. 1.3a); (ii) as the result of force imbalances in the vicinity of ice cliffs (Fig. 1.3b); (iii) where ice cliffs are undercut by preferential melting at or below the waterline (Fig. 1.3c and d); and (iv) where torque is introduced by buoyant forces (Fig. 1.3e Bendle, 2018; Benn et al., 2007b).

In addition to mechanical processes occurring at the glacier front, calving is strongly coupled with dynamical processes upstream of the glacier terminus. An increase in the ice flux can trigger a calving event and in turn this event can accelerate the movement of the ice. External aspects like ocean temperature, fjord bathymetry and, in polar areas, sea-ice concentration along the calving front can also influence the discharge of solid ice to the ocean (Straneo et al., 2013). Figure 1.4, summarises internal and external glacier processes that can influence frontal ablation.

Straneo et al. (2013) suggested that frontal ablation and tidewater glacier retreat are closely interlinked. If ice loss at the terminus is more rapid than the delivery of ice from higher up the glacier, the terminus will retreat. A leading hypothesis attributes the recent rapid retreat of many of Greenland's tidewater glaciers to an increase in submarine melting, and consequently calving, in response to oceanic warming. However, Cowton et al. (2018) found that over a 20-y period much of the observed tidewater glacier retreat can be explained as a predictable response to combined atmospheric and oceanic warming. The study included 10 large tidewater glaciers along the east of the coast of Greenland. Ocean/atmosphere forcing can explain up to 76% of the variability in terminus

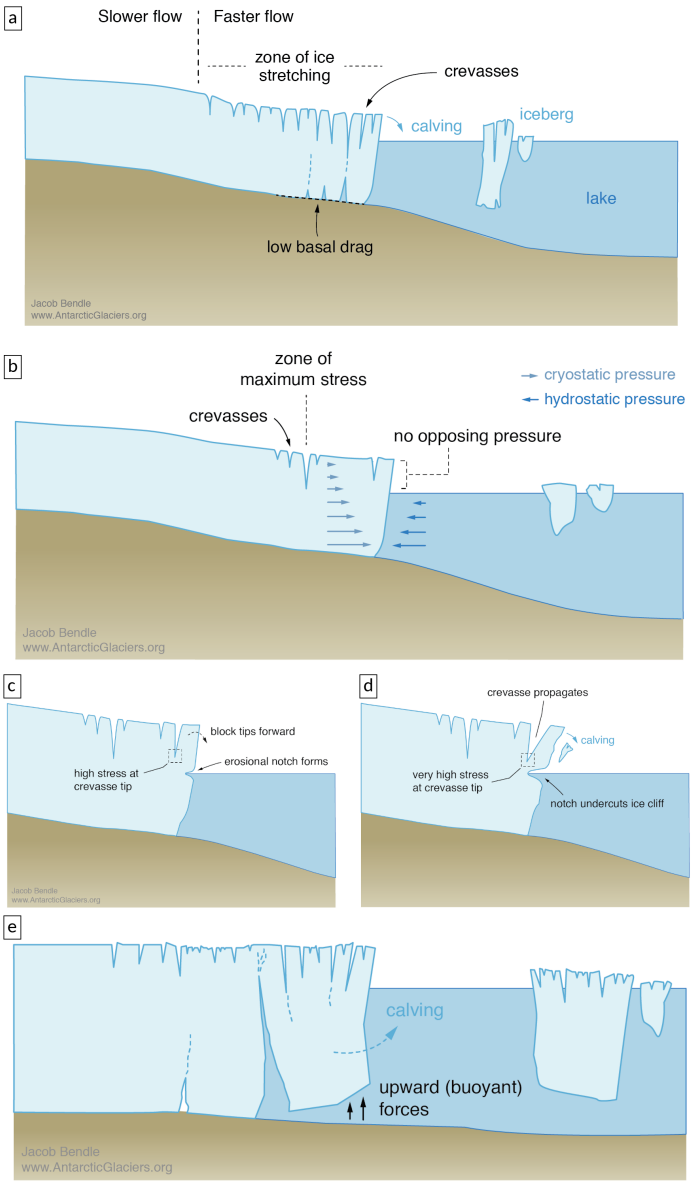

Figure 1.3: Main calving mechanisms at a tidewater glacier caused by: a) stretching of the ice and crevasses formation. b) forces imbalances at the glacier terminus. c and d) melting at or below the waterline, this can erode a notch into a terminal ice cliff (c), then calving occurs when the cliff becomes unstable (d). e) buoyant forces at a glacier terminus. (Taken from Bendle, 2018)

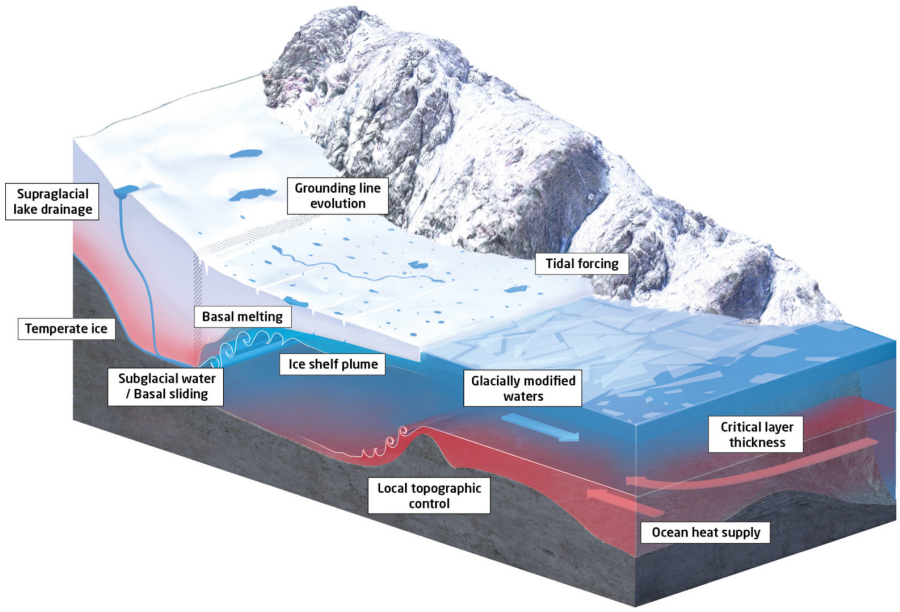

Figure 1.4: Schematic of mechanisms that influence a tidewater glacier retreat and iceberg calving. (Infographic credit: Mario Hoppman and Martin Künsting Turton, 2019)

position at individual glaciers and 54% of variations in terminus position across all 10 glaciers. Cowton et al. (2018) demonstrate that while increased melting and runoff in response to atmospheric warming can explain much of the temporal variability in glacier terminus position, the temperature of the adjacent ocean waters is also a strong determinant of the absolute magnitude of retreat. By including simple parameterizations linking terminus retreat to runoff and ocean temperature, models simulating the response of tidewater glaciers to atmospheric and oceanic warming will improve, and so the accuracy of sea-level rise predictions (Cowton et al., 2018).

1.1.4 Calving models and parameterisations

As a consequence of the diverse nature of the calving process described in sect. 1.1.3, the development of parameterisations of frontal ablation in numerical ice sheet and glacier models, remains an important challenge in glaciology. There is a wide spectrum of approaches that vary in scale and complexity, justified

through the diversity of intended applications of the models (Price et al., 2015).

Early attempts to model calving dynamics began with empirical relationships between frontal ablation and external variables such as water depth (Brown et al., 1982) or terminus height (Pfeffer et al., 1997). Later studies (van der Veen, 2002; Vieli et al., 2001, 2002) included ice properties and dynamics to specify calving front positions. In these studies, the ice front position is based on a height-above-buoyancy criterion (HAB), with which recent numerical models have been able to reproduce more complex observed behaviours of Arctic glaciers (Choi et al., 2018). Benn et al. (2007b) introduced a crevasse-depth criterion (CD), which defines the calving front position as being where the surface crevasses reach the waterline. This criterion was then expanded in Nick et al. (2010), to include basal crevasses and their propagation along the terminus thickness (see Fig. 1.3e), with the objective of determining calving front positions in a flowline model.

Since then, there have been many successful efforts to model calving processes for individual glaciers (e.g. Åström et al., 2014; Nick et al., 2013; Oerlemans et al., 2011; Todd and Christoffersen, 2014; Ultee and Bassis, 2016). Most of these models have been tested on idealised or single, real-world geometries. They have yet to be tested on a wide range of glaciers. However, it is unlikely that they can be implemented in a global glacier model anytime soon, because of the amount and quality of data needed to constrain these types of models.

The crevasse-depth criterion proposed by Nick et al. (2010) for example, requires knowledge of surface melt and refreeze rates at the crevasses of the glacier tongue, and crevasse depth observations to calibrate and validate these rates. These kinds of observations are hard to obtain for entire glaciated regions: e.g., the 3,222 glaciers classified as calving (marine- and lake- terminating) glaciers in the RGI v6.0. Other recent calving models that use discrete particles or a full-Stokes model approach (e.g. Åström et al., 2014; Todd and Christoffersen, 2014; Todd et al., 2018) are too computationally expensive to be included in global glacier models that seek to consistently simulate past and future global scale glacier changes.

1.2 Objectives

At the regional (Blaszczyk et al., 2009; Burgess et al., 2013; McNabb et al., 2015) and global (Huss and Hock, 2015) scale, few estimates of frontal abla-

tion fluxes of glaciers outside the ice sheets exist. From all the global glacier models published in the last decade, only Huss and Hock (2015) account for frontal ablation of marine-terminating glaciers. However, this model, along with the rest of ice thickness inversion methods, still suffers from considerable uncertainty associated with the uncertainty of the frontal ablation parameterisation. For improving ice thickness distribution estimates at the global scale, it is thus important to identify and test low-cost and robust parameterisations of frontal ablation that might not resolve all the dynamical processes at the calving front described in Fig.1.4 (e.g. subaqueous frontal melting, subaerial frontal melting and sublimation), but that can estimate the amount of ice passing through the terminus of the glacier during a mass balance year.

The main objective in this thesis is to conduct a first assessment, of the impact of accounting for frontal ablation on the estimate of ice stored in marine-terminating glaciers (from a regional to a global scale) that will potentially contribute to sea-level rise.

Specifically, the aims of this study are:

- to implement a simple parametrisation of frontal ablation in the Open Global Glacier Model (OGGM v1.1 Maussion et al., 2019), following the approaches proposed by Oerlemans and Nick (2005) and Huss and Hock (2015). In order to improve the first ice thickness estimation of OGGM for marine-terminating glaciers.
- to perform sensitivity studies on the model and investigate the effect of accounting for frontal ablation on the estimated glacier thickness, volume and ice flow velocity for marine-terminating glaciers.
- to develop methods for calibrating the model in areas with non or few frontal ablation observations (e.g. Alaska and Greenland).
- and asses the model performance for Greenland peripheral marine-terminating glaciers by using glacier velocities derived from remote sensing.

2

Paper I: The Open Global Glacier Model (OGGM) v1.0

Maussion, F., Butenko, A., Champollion, N., Dusch, M., Eis, J., Fourteau, K., Gregor, P., Jarosch, A. H., Landmann, J., Oesterle, F., **Recinos, B.**, Rothenpieler, T., Vlug, A., Wild, C. T., and Marzeion, B.

Abstract

Despite their importance for sea-level rise, seasonal water availability, and being a source of geohazards, mountain glaciers are one of the few remaining sub-systems of the global climate system for which no globally applicable, open source, community-driven model exists. Here we present the Open Global Glacier Model (OGGM, `www.oggm.org`), developed to provide a modular and open source numerical model framework for simulating past and future change of any glacier in the world. The modelling chain comprises data downloading tools (glacier outlines, topography, climate, validation data), a preprocessing module, a mass-balance model, a distributed ice thickness estimation model, and an ice flow model. The monthly mass-balance is obtained from gridded climate data and a temperature index melt model. To our knowledge, OGGM is the first global model explicitly simulating glacier dynamics: the model relies on the shallow

ice approximation to compute the depth-integrated flux of ice along multiple connected flowlines. In this paper, we describe and illustrate each processing step by applying the model to a selection of glaciers before running global simulations under idealized climate forcings. Even without an in-depth calibration, the model shows very realistic behaviour. We are able to reproduce earlier estimates of global glacier volume by varying the ice dynamical parameters within a range of plausible values. At the same time, the increased complexity of OGGM compared to other prevalent global glacier models comes at a reasonable computational cost: several dozen glaciers can be simulated on a personal computer, while global simulations realized in a supercomputing environment take up to a few hours per century. Thanks to the modular framework, modules of various complexity can be added to the codebase, which allows new kinds of model intercomparisons studies in a controlled environment. Future developments will add new physical processes to the model as well as automated calibration tools. Extensions or alternative parameterizations can be easily added by the community thanks to a comprehensive documentation. OGGM spans a wide range of applications, from ice-climate interaction studies at millenial time scales to estimates of the contribution of glaciers to past and future sea-level change. It has the potential to become a self-sustained community-driven model for global and regional glacier evolution.

2.1 Introduction

Glaciers constitute natural low-pass filters of atmospheric variability. They allow people to directly perceive slow changes of the climate system, that would otherwise be masked by short-term noise in human perception. Since glaciers form prominent features of many landscapes, shrinking glaciers have become an icon of climate change.

However, impacts of glacier change – whether growth or shrinkage – go far beyond this sentimental aspect: glaciers are important regulators of water availability in many regions of the world (Huss, 2011; Immerzeel et al., 2012; Kaser et al., 2010), and retreating glaciers can lead to increased geohazards (see Richardson and Reynolds, 2000, for an overview). Even though the ice mass stored in glaciers is small compared to the Greenland and Antarctic ice sheets ($< 1\%$),

glacier melt has contributed significantly to past sea-level rise (SLR; e.g. Cogley, 2009a; Gardner et al., 2013; Leclercq et al., 2011; Marzeion et al., 2012b). They probably have been the biggest single source of observed SLR since 1900 and they will continue to be a major source of SLR in the 21st century (e.g. Church et al., 2013a; Gregory et al., 2013b).

It is therefore a pressing task to improve the knowledge of how glaciers change when subjected to climate change, both natural and anthropogenic (Marzeion et al., 2014a). The main obstacle to achieve progress is a severe undersampling problem: direct glaciological measurements of mass balances have been performed on ∼300 glaciers world wide (≈ 0.1% of all glaciers on Earth). The number of glaciers on which these types of measurements have been carried out for time periods longer than 30 years, i.e. over periods that potentially allow for the detection of a climate change signal, is one order of magnitude smaller (Zemp et al., 2009). Length variations of glaciers have been observed for substantially longer periods of time (Oerlemans, 1994, 2005). These variations are, however, much more difficult to understand, as large glacier length fluctuations may arise from intrinsic climate variability (Roe, 2011; Roe and O'Neal, 2009). Data obtained by remote sensing allow for gravimetric assessments of ice mass change or volume change estimates obtained by differencing digital elevation models. Unfortunately, they are only available for the past decade (e.g. Gardner et al., 2013).

During the past few years, great progress has been made in methods to model glaciers globally (Giesen and Oerlemans, 2012, 2013; Huss and Hock, 2015; Marzeion et al., 2012a,b, 2014a,b; Radić and Hock, 2011, 2014). While these approaches yield consistent results at the global scale, all of them suffer from greater uncertainties at the regional and local scales. These stem from the great level of abstraction of the key processes (Marzeion et al., 2012b, 2014b), from the need to spatially interpolate model parameters (Giesen and Oerlemans, 2012, 2013; Radić and Hock, 2011, 2014), and from uncertainties of the boundary and initial conditions. All models lack ice dynamics, most lack frontal ablation (with the exception of Huss and Hock, 2015), and all lack modulation of the surface mass balance by debris cover and snow redistribution (wind and avalanches). Only one model (Marzeion et al., 2012b) was able to provide estimates of past glacier volume changes for the 20th century. None of these models is open-source.

Mountain glaciers are one of the few remaining subsystems of the global climate system for which no globally applicable, open source, community-driven

model exists. The ice sheet modelling community shows a better example, with models such as the *Parallel Ice Sheet Model* (Winkelmann et al., 2011), *Elmer/Ice* (`http://elmerice.elmerfem.org/`), Glimmer-CISM (`https://csdms.colorado.edu/wiki/Model:Glimmer-CISM`), or ISSM (`https://issm.jpl.nasa.gov/`). These models have been applied to mountain glaciers as well, but cannot be applied globally out-of-the-box. While the atmospheric modelling community has a long tradition of sharing models (e.g. the *Weather Research and Forecasting model*, or WRF) or comparing them (e.g. the *Coupled Model Intercomparison Project* or CMIP), recent initiatives originating from the glaciological community show a new willingness to better coordinate global research efforts following the CMIP example (e.g. the *Glacier Model Intercomparison Project*[1] or the *Glacier Ice Thickness Estimation Working Group*[2]).

In the recent past, great advances have been made in the global availability of data and methods relevant for glacier modelling, spanning glacier outlines (RGI Consortium, 2017), automatized glacier centerline identification (e.g., Kienholz et al., 2014), bedrock inversion methods (e.g. Huss and Farinotti, 2012), and global topographic data sets (e.g. Farr et al., 2007). Taken together, these advances now allow the ice dynamics of glaciers to be simulated at the global scale, provided that adequate modelling platforms are available. In this paper, we present the **Open Global Glacier Model (OGGM)**, developed to provide a modular and open source numerical model framework for consistently simulating past and future global scale glacier change.

Global not only in the sense of leading to meaningful results for all glaciers combined, but also for any small ensemble of glaciers, e.g. at the headwater catchment scale. *Modular* to allow different approaches to the representation of ice flow and surface mass balance to be combined and compared against each other. *Open source* so that the code can be read and used by anyone and so that new modules can be added and discussed by the community, following the principles of open governance. *Consistent* between past and future in order to provide uncertainty measures at all realisable scales.

This paper describes the basic structure and primordial assumptions of the model (as of version 1.1). We present the results of a series of single glacier and global simulations demonstrating the model's usage and potential. This will be followed by a description of the software requirements and the testing

[1] `http://www.climate-cryosphere.org/activities/targeted/glaciermip`
[2] `http://www.cryosphericsciences.org/wg_glacierIceThickEst.html`

framework. Finally, we will discuss the potential for future developments that could be conducted by any interested research team.

2.2 Fundamental principles

The starting point of OGGM is the Randolph Glacier Inventory (RGI; Pfeffer et al., 2014; RGI Consortium, 2017): our goal is to simulate the past and future evolution of all of the 216,502 inventoried glaciers worldwide (as of RGI V6). This "glacier centric" approach is the one followed by most global and regional models to date; its advantages and disadvantages will be discussed in Sect. 2.3.6. Provided with the glacier outlines, topographical and climate data at reasonable resolution and accuracy, the model should be able to (i) provide a local map of the glacier including topography and hypsometry, (ii) estimate the glacier's total ice volume and compute a map of the bedrock topography, (iii) compute the surface climatic mass balance and (if applicable) at its front via frontal ablation, (iv) simulate the glacier's dynamical evolution under various climate forcings, and (v) provide an estimate of the uncertainties associated with the modelling chain.

For each of these steps, several choices are possible regarding the input data to be used, the numerical solver or the parameterisations to be applied. Any given choice is driven by subjective considerations about data availability, the estimated accuracy of boundary conditions (such as topography), and by technical considerations such as the available computational resources. In this paper we present one way to realize these steps using OGGM, which to date is in our opinion the best compromise between model complexity, data availability and computational effort. The OGGM software, however, is built in such a way that future improvements and new approaches can be implemented, tested, and applied at minimal cost by ourselves or a larger community.

2.2.1 Example workflow

We illustrate with an example how the OGGM workflow is applied to Tasman glacier, New Zealand (Fig. 4.3). Here we describe shortly the purpose of each processing step, and more details will be provided in Sect. 2.3:

Preprocessing The glacier outlines extracted from the RGI are projected onto

a local gridded map of the glacier (Fig. 4.3a). Depending on the glacier's location, a suitable source for the topographical data is downloaded automatically (here SRTM) and interpolated to the local grid. The map's spatial resolution depends on the size of the glacier (here, 150 m).

Flowlines The glacier centerlines are computed using a geometrical routing algorithm (adapted from Kienholz et al., 2014, Fig. 4.3b), filtered and slightly modified to become glacier flowlines with a fixed grid spacing.

Catchment areas and widths The geometrical widths along the flowlines are obtained by intersecting the normals at each grid point with the glacier outlines and the tributaries' catchment areas (Fig. 4.3c). Each tributary and the main flowline has a catchment area, which is then used to correct the geometrical widths so that the flowline representation of the glacier is in close accordance with the actual altitude-area distribution of the glacier (Fig. 4.3d, note that the normals are now corrected and centred).

Climate data and mass balance Gridded climate data (monthly temperature and precipitation) are interpolated to the glacier location and temperature is corrected for altitude using a linear gradient. These climate time series are used to compute the glacier mass balance at each flowline's grid point for any month in the past.

Ice thickness inversion Using the mass balance data computed above and relying on mass-conservation considerations, an estimate of the ice flux along each glacier cross-section can be computed. By making assumptions about the shape of the cross-section (parabolic or rectangular) and using the physics of ice flow, the model computes the thickness of the glacier along the flowlines and the total volume of the glacier (Fig. 4.3e).

Glacier evolution A dynamical flowline model is used to simulate the advance and retreat of the glacier as a response of the surface mass-balance forcing. Here (Fig. 4.3f), a 100-yr long random climate sequence leads to a glacier advance.

2.2.2 Model structure

The OGGM model is built around the notion of tasks, which have to be applied sequentially to single or a set of glaciers. There are two types of tasks:

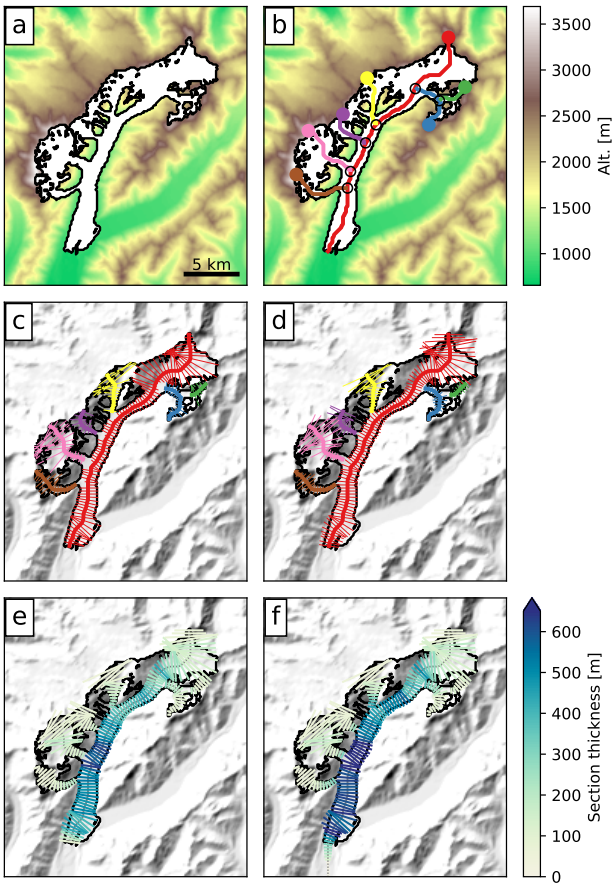

Figure 2.1: Example of the OGGM workflow applied to Tasman glacier, New Zealand; **a**: topographical data preprocessing; **b**: computation of the flowlines; **c**: geometrical glacier widths determination (the colors indicate the different flowlines); **d**: width correction according to catchment areas and altitude-area distribution (see Fig. 2.2 and main text for details); **e**: ice thickness inversion; **f**: random 100-yr long glacier evolution run leading to a glacier advance. See Sect. 2.2.1 for details.

Entity tasks are tasks which are applied on single glaciers individually and do not require information from other glaciers (this encompasses the majority of OGGM's tasks). Most often they need to be applied sequentially (for example, it is not possible to compute the centerlines without having read the topographical data first).

Global tasks are tasks which are run on a set of glaciers. This encompasses the calibration and validation routines, which need to gather data across a number of reference glaciers.

This model structure has several advantages: the same entity task can be run in parallel on several glaciers at the same time, and they allow a modular workflow. Indeed, a task can seamlessly be replaced by another similar one, as long as the required input and output formats are agreed upon beforehand. The output of each task is made persistent by storage on disk, allowing a later use by a subsequent task, even in a separate run or on another machine. For example, the preprocessing tasks store the topography data in a netCDF file, which is then read by the centerlines task, which itself writes it's output in a vector file format.

In this paper we will refrain from naming the tasks by their function name in the code, as these are likely to change in the future and are sometimes organised in a non-trivial way as a result of implementation details. The next section therefore is called "Modules", where each module can be seen as a collection of tasks developed towards a certain goal.

2.3 Modules

The modules are described in the order in which they are applied for a model run. When we provide a specific value for a model parameter in the text, we refer to the model's default parameter value: it can be changed by the user at runtime.

2.3.1 Preprocessing

The objective of the preprocessing module is to set up the geographical input data for each glacier (the glacier outlines and the local topography). First, a Cartesian local map projection is defined: we use a local Transverse Mercator

projection centred on the glacier. Then, a suitable topographical data source is chosen automatically, depending on the glacier's location. Currently we use:

- the Shuttle Radar Topography Mission (SRTM) 90m Digital Elevation Database v4.1 (Jarvis et al., 2008) for all locations in the [60°S; 60°N] range (data acquisition: 2000)
- the Greenland Mapping Project (GIMP) Digital Elevation Model (Howat et al., 2014) for mountain glaciers in Greenland (data acquisition: 2003 to 2009)
- the Radarsat Antarctic Mapping Project (RAMP) Digital Elevation Model, Version 2 (Liu et al., 2015) for mountain glaciers in Antarctica with the exception of some peripheral islands (data acquisition: 1940 to 1999)
- the Viewfinder Panoramas DEM3 product (`http://viewfinderpanoramas.org/dem3.html`) elsewhere (most notably: North America, Russia, Iceland, Svalbard)

All datasets have a comparable spatial resolution (from 30 to 90 m, or 3 arcseconds). Using different data sources is problematic but unavoidable since there is no consistent, gap-free and globally available Digital Elevation Model (DEM) to date. The Advanced Spaceborne Thermal Emission and Reflection Radiometer (ASTER) Global Digital Elevation Model Version 2 (GDEM V2) is available globally but was quickly eliminated because of large data voids and artefacts, in particular in the Arctic. These artefacts are often tagged as valid data and cannot be detected automatically in an easy way. The Viewfinder Panoramas products rely on the same sources but have been corrected manually (mostly with topographic maps; J. de Ferranti, Pers. Comm.) and thus ensure a more realistic void filling. Although having a nearly global coverage, the DEM3 products are not used in place of established and citable digital elevation models such as SRTM, GIMP or RAMP, because it is not easy to retrieve the original data sources used to generate them (the information is scattered around the website, although ASTER and SRTM are the main data sources in most cases). It must be noted that a number of glaciers will still suffer from poor topographic information, and/or a date of data acquisition which doesn't match that of the RGI outlines. Either the errors are large or obvious (in which case the model won't run), or they are left unnoticed. The importance of reliable topographic

data for global glacier modelling will be the topic of a follow-up study[3].

The spatial resolution of the target local grid depends on the size of the glacier: the default is to use a square relation to the glacier size ($dx = aS^{\frac{1}{2}}$ with $a = 14$ and S the area of the glacier in km^2) clipped to a predefined minimum (10 m) and maximum (200 m) value. After the interpolation to the target grid, the topography is smoothed with a Gaussian filter of 250 m radius (this value does not change with the local glacier map resolution because it is meant to be applied to the original DEM, not the interpolated one). This smoothing is driven by practical considerations, since the model becomes unstable if the boundary conditions are too noisy (see also Bahr et al., 2014, for a discussion about the unavoidable trade-off between resolution and accuracy).

2.3.2 Flowlines and catchments

The glacier centerlines are computed following an algorithm developed by Kienholz et al. (2014) and adapted for our purposes. This algorithm was chosen because it allows one to compute multiple centerlines and to define a main branch fed by any number of tributaries. In general we found the method to be very robust, although some glaciers obviously won't have the optimal number of centerlines, with either too many (frequent in the case of large cirque glaciers) or not enough (some tributary branches have no centerlines). These errors however are assumed to play a relatively minor role compared to other uncertainties in the model chain.

In the model semantics, the original "centerlines" are then converted to "flowlines": the points defining the line geometries are interpolated to be equidistant from each other (the default spacing along the line is twice that of the local glacier map, i.e. varying between 20 m and 400 m depending on glacier size), and the tail of the tributaries are cut before reaching their descendant (see the differences between Figs. 4.3b and c, or between Figs. 2.2a and b). Each grid point's elevation is obtained from the underlying topography. By construction, upslope trajectories or sinks along the flowline are rare: this can still occur when the glacier outlines are poorly defined or because of errors in the gridded topography. In these cases, we interpolate the heights (in the case of a deepening) or cut the first grid points of the line (in case of an upslope starting from the

[3] See also `https://rgitools.readthedocs.io/en/latest/dems.html` for an ongoing evaluation of further DEM products.

flowline's head) until only positive slopes larger than 1.5° remain. This is necessary because sinks along a flowline are incompatible with the forward dynamical model, which will fill them with ice and create undesirable spin-up issues.

The flowlines are then sorted according to their Strahler number (a measure of branching complexity defined by Strahler, 1952, and commonly used in hydrological applications), from the lowest (line without tributaries but with possible descendants) to the highest (the main – and longest – centerline). This ordering is important for the mass flow routing: indeed, each flowline contains a reference to its descendant, and this reference is used by the inversion and dynamical models to transfer mass from the tributaries towards the main flowline.

The width of each grid point along the flowline is computed in four steps. First, the catchment area of each flowline is computed using a routing algorithm similar to that used to compute the centerlines (Fig. 2.2a). Then the geometrical widths are computed by intersecting the flowline's normal to the boundaries of either the individual catchments or the glacier itself (Fig. 2.2b). These geometrical widths are then corrected by a factor specific for each altitudinal bin (Fig. 2.2c), so that the true altitude area distribution of the glacier is approximately preserved (Fig. 2.2d). Finally, these widths are multiplied by a single factor ensuring that the total area of the glacier is the exact same as the one provided by the RGI, ensuring consistency with future model intercomparisons.

At this stage, it is important to note that the map representation of the flowline glacier presented in Fig. 2.2c is purely artificial. The fact that the glacier cross-sections are overlapping is irrelevant: the role of the flowlines is to represent the actual flow of ice as accurately as possible while conserving the fundamental aspects of the real glacier: slope, altitude, area, geometry. The flowline approximation is going to work better for valley glaciers (like Tasman glacier shown above) than for cirque glaciers (like the Upper Grindelwald). For ice-caps, the flowline representation is likely to work poorly, as discussed in Sect. 2.3.6. From Fig. 2.2c one can see that future improvements of the mass balance model based on e.g. topographical shading or snow redistribution are made possible by the knowledge about the flowlines' location.

2.3.3 Climate data and mass balance

The mass balance model implemented in OGGM is an extended version of the temperature index melt model presented by Marzeion et al. (2012b). The

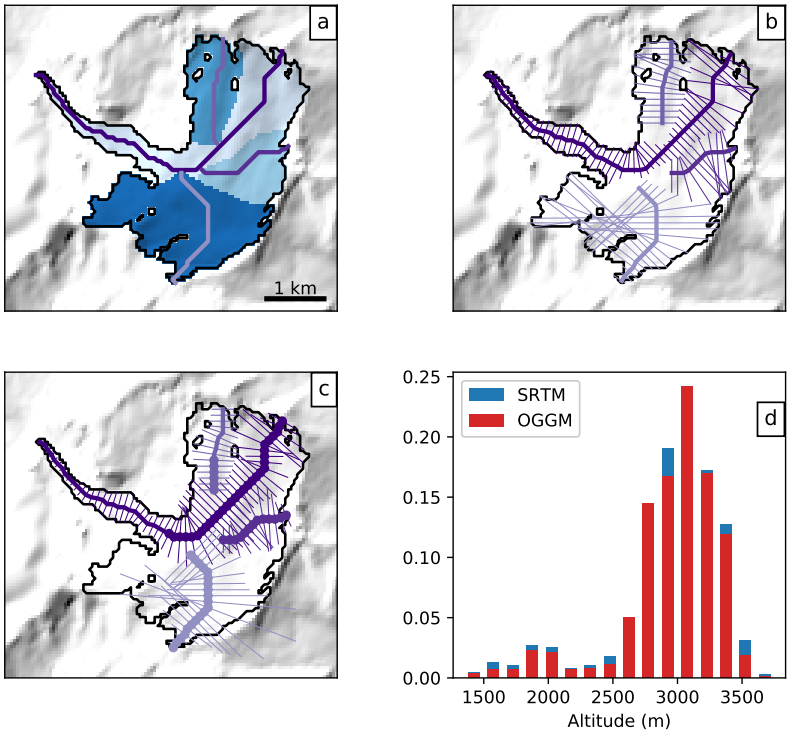

Figure 2.2: Example of the flowlines' width determination algorithm applied to the Upper Grindelwald glacier, Switzerland; **a**: determination of each flowline's catchment area; **b**: geometrical widths; **c**: widths corrected for the altitude-area distribution, the bold lines representing the grid points where the cross-section touches a neighbouring catchment; **d**: frequency distribution of the glacier area per altitude bin, as represented by OGGM and by the SRTM topography.

monthly mass balance m_i at an elevation z is computed as:

$$m_i(z) = p_f \, P_i^{Solid}(z) - \mu^* \; max\left(T_i(z) - T_{Melt}, 0\right) + \varepsilon \tag{2.1}$$

where P_i^{Solid} is the monthly solid precipitation, p_f a global precipitation correction factor (defaults to 2.5, see Appendix A.1), μ^* the glacier's temperature sensitivity, T_i the monthly air temperature, T_{Melt} the monthly air temperature above which ice melt is assumed to occur (default: -1°C, chosen because melting days can occur even if the monthly average temperature is below 0°C), and ε a residual (or bias correction) term. Solid precipitation is computed as a fraction of the total precipitation: 100% solid if $T_i <= T_{Solid}$ (default: 0°C), 0% if $T_i >= T_{Liquid}$ (default: 2°C), and linearly interpolated in between. The parameter μ^* indicates the temperature sensitivity of the glacier and needs to be calibrated. For this paper, the temperature and precipitation time series (1901–2016) are obtained from gridded observations (CRU TS4.01; Harris et al., 2014, see Appendix A.1). The temperature lapse-rate is set to a constant value (default: 6.5 K km^{-1}) or it can be time-dependant and computed from a linear fit of the 9 surrounding grid-points.

For the calibration of the temperature sensitivity parameter μ^* we use the method described by Marzeion et al. (2012b) and successfully applied many times since then (e.g. Marzeion et al., 2014a, 2015, 2018). Although the general procedure didn't change, its peculiarity justifies describing it here. We will start by noting that μ^* depends on many factors, most of them being glacier-specific (e.g. avalanches, topographical shading, cloudiness), and others being related to systematic biases in the input data (e.g. climate, topography). As a result, μ^* can vary greatly between neighbouring glaciers without obvious physical reasons. The calibration procedure implemented in OGGM makes use of these apparent handicaps by turning them into assets.

The procedure begins with glaciers for which we have direct observations of specific mass balance ($N = 254$, see Appendix A.2). For each of these glaciers, annual sensitivities $\mu(t)$ are computed from Eq. 2.1 by requiring that the glacier specific mass balance $\overline{m}(t)$ is equal to zero[4]. $\overline{m}(t)$ is the glacier integrated mass balance computed for a 31-yr period centred around the year t and *for a constant glacier geometry fixed at the RGI outline's date* (e.g. 2003 in the Alps). The

[4] Note that this is not valid for water-terminating glaciers where mass loss happens at the glacier front and the equilibrium surface mass-balance budget doesn't have to be closed. See Sect. 2.3.6 for more details.

process is illustrated in Fig. 2.3c (blue line): around 1920 the climate was cold and wet (Figs. 2.3a and b), and as a consequence the hypothetical temperature sensitivity required to maintain the 2003 glacier geometry needs to be high. Inversely, the more recent climate is warmer and the temperature sensitivity needs to become smaller for the glacier to remain stable.

These hypothetical, time-dependent $\mu(t)$ are called "candidates": it is likely (but not certain) that at least one of them is the correct μ^*. To determine which of the candidates is suitable, we then compute the mass balance time series for each of the $\mu(t)$ and compute their bias ε with respect to observations (red line in Fig. 2.3c). Note that the period over which the observations are taken is not relevant for the bias computation: each μ candidate can produce a mass balance for any year, as per Eq. 2.1. In comparison to observations, $\mu(t = 2000)$ is too low and produces mass balances with a positive bias. Inversely, $\mu(t = 1920)$ is too high and leads to a negative bias. For three years, the bias is close to or crossing the zero line and $\mu(t)$ is therefore very close to the ideal μ^*. These dates represent the center of a 31-yr long climate period where *today's* glacier would be in equilibrium and maintain its *current* geometry. From these three candidates, we pick the date with the smallest bias and call it t^*. This t^* is an actual date but is mostly an abstract concept: we are going to make use of it for the next step.

For the vast majority of the glaciers, μ^* and t^* are unknown. For these we could interpolate the μ^* (probably the most obvious solution), or we could interpolate t^*: indeed, the procedure above can be reversed and t^* can be used to retrieve μ^*, again by requiring that $\overline{m}(t^*)$ is equal to zero (Eq. 2.1). We interpolate t^* to all glaciers without observations using inverse distance interpolation from the 10 closest locations (which can be quite far away, see Appendix A.2 and A.3). The residual bias ε for glaciers with observations can be close to zero (the case for Hintereisferner in Fig. 2.3, where the bias curve crosses the zero line) but can also be higher (indicating that no 31-yr period in the last century would sustain the current glacier geometry). When no perfect t^* is found, the date with the smallest absolute bias is chosen. This residual ε is also interpolated between locations and added to the modelled mass balance. This residual may be significant at certain locations (up to 1.5 m yr^{-1}, median of 6 cm yr^{-1}) and would benefit from further calibration e.g. with regional geodetic mass-balance estimates. The benefit of this approach is best shown by cross-validation (Fig. 2.4), where one can see that the error increases considerably when using μ^* interpolation instead of the proposed method. This is due to several factors:

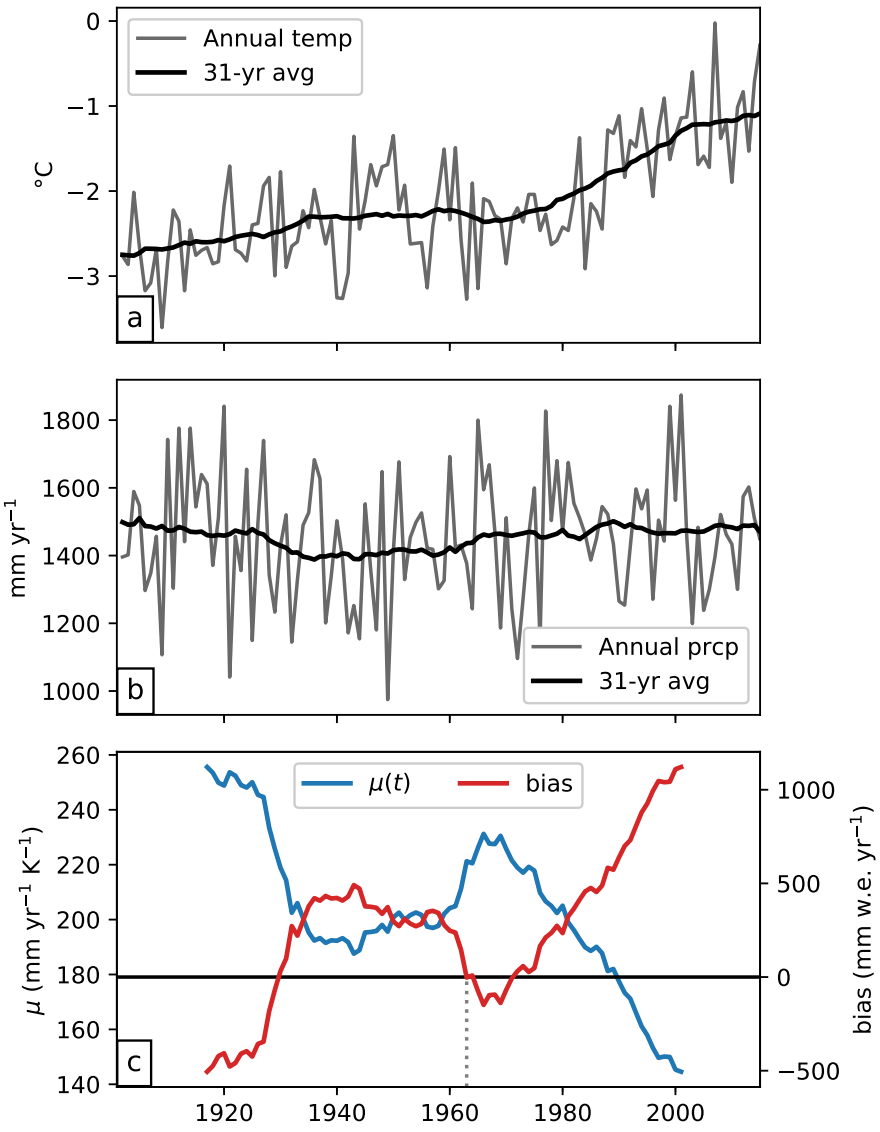

Figure 2.3: Calibration procedure for μ^* applied to the Hintereisferner glacier, Austria. **a** and **b**: annual and 31-yr average of temperature and precipitation obtained from the nearest CRU grid point (altitude 2700 m a.s.l.). **c**: time series of the μ candidates (mm yr^{-1} K^{-1}) and their associated mass balance bias (mm w.e. yr^{-1}, right-axis) in comparison to observations. The vertical dashed line marks the time where the bias is closest to zero (t^*).

- the equilibrium constraint applied on $\mu(t)$ implies that the sensitivity cannot vary much during the last century. In fact, $\mu(t)$ at one glacier often varies less in one century than between neighbouring glaciers, because of the local driving factors mentioned earlier. In particular, it will vary comparatively little around a given year t: errors in t^* (even large) will result in relatively small errors in μ^*.

- the equilibrium constraint will also imply that systematic biases in temperature and precipitation (no matter how large) will automatically be compensated by all $\mu(t)$, and therefore also by μ^*. In that sense, the calibration procedure can be seen as an empirically driven downscaling strategy: if a glacier is located there, then the local climate (or the glacier temperature sensitivity) *must* allow a glacier to be there. For example, the effect of avalanches or a negative bias in precipitation input will have the same impact on calibration: the value of μ^* should be lowered to take these effects into account, even though they are not resolved by the mass balance model.

The most important drawback of this calibration method is that it assumes that two neighbouring glaciers should have a similar t^*. This is not necessarily the case, as other factors than climate (such as the glacier size) will influence t^* too. Our results (and the arguments listed above) show however that this is an approximation we can cope with.

In a final note, it is important to mention that μ^* and t^* should not be over-interpreted in terms of real temperature sensitivity or response time of the glacier. This procedure is primarily a calibration method, and as such it can be statistically scrutinized (for example with cross-validation). It can also be noted that the mass balance observations play a relatively minor role in the calibration: they could be entirely avoided by fixing a t^* for all glaciers in a region (or even worldwide), without much performance loss. The observations, however, play a major role for the assessment of model uncertainty (Fig. 2.4). For more information about the climate data and the calibration procedure, refer to Appendix A.1.

2.3.4 Ice thickness

Measuring ice thickness is a labour-intensive and complex task, therefore only a fraction of the world's glaciers is monitored and direct measurements are

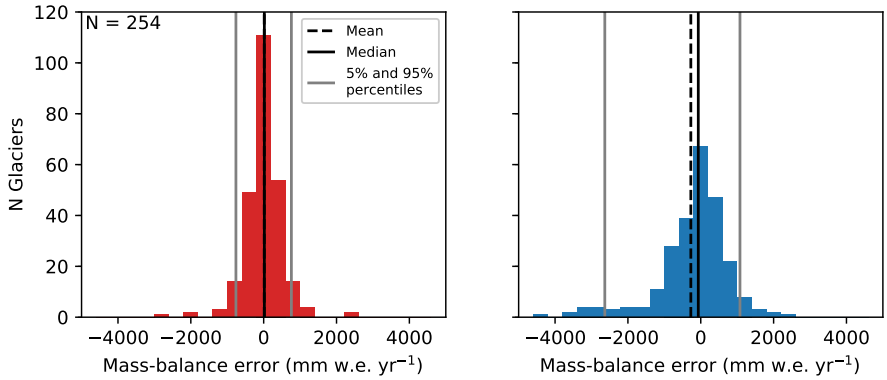

Figure 2.4: Benefit of spatially interpolating t^* instead of μ^* as shown by leave-one-out cross-validation ($N = 254$). **Left**: error distribution of the computed mass balance if determined by the interpolated t^*. **Right**: error distribution of the mass balance if determined by interpolation of μ^*. The vertical lines indicate the mean, median, 5% and 95% percentiles. See `https://cluster.klima.uni-bremen.de/~github/crossval` for an online visualisation of model performance for each glacier.

sparse. A physical or statistical approach is necessary for modelling glacier evolution at the global scale. For a recent review of available techniques for ice thickness modelling, see Farinotti et al. (2017). OGGM implements a new ice thickness inversion procedure, physically consistent with the flowline representation of glaciers and taking advantage of the mass balance calibration procedure presented in the previous section. It is a mass-conservation approach largely inspired by Farinotti et al. (2009), but with distinct characteristics.

The principle is quite simple. The flux of ice q [m^3 s^{-1}] through a glacier flux-gate (cross-section) of area S [m^2] reads:

$$q = uS \tag{2.2}$$

with u the average velocity [m s^{-1}]. Using an estimate for u and q obtained from the physics of ice flow and the mass balance field, S and the local ice thickness h [m] can be computed relying on some assumptions about the bed geometry. We compute the depth-integrated ice velocity using the well known

shallow-ice approximation (Hutter, 1981, 1983):

$$u = \frac{2A}{n+2} h \tau^n \tag{2.3}$$

with A the ice creep parameter [s^{-1} Pa^{-3}], n the exponent of Glen's flow law (n=3), and τ the basal shear stress, computed as:

$$\tau = \rho g h \alpha \tag{2.4}$$

with ρ the ice density (900 kg m^{-3}), g the gravitational acceleration (9.81 m s^{-2}) and α the surface slope computed numerically along the flowline. Optionally, a sliding velocity u_s can be added to the deformation velocity to account for basal sliding. We use the same parameterisation as Oerlemans (1997), who relied on Budd et al. (1979a):

$$u_s = \frac{f_s \tau^n}{h} \tag{2.5}$$

with f_s a sliding parameter (default: 5.7×10^{-20} s^{-1} Pa^{-3}). If we consider a point on the flowline and the catchment area Ω upstream of this point, mass conservation implies:

$$q = \int_\Omega (\dot{m} - \rho \frac{\partial h}{\partial t}) \, dA = \int_\Omega \widetilde{m} \, dA \tag{2.6}$$

with $\dot{m}$ the mass balance [kg m^{-2} s^{-1}], and $\widetilde{m} = \dot{m} - \rho \partial h / \partial t$ the "apparent mass balance" after Farinotti et al. (2009). If the glacier is in steady state, the apparent mass balance is equivalent to the actual (and observable) mass balance. In the non-steady state case, $\partial h / \partial t$ is unknown, and neither is the time integrated (and delayed) mass balance $\int_\Omega \dot{m}$ responsible for the flux of ice through a section of the glacier at a certain time. Farinotti et al. (2009) and Huss and Farinotti (2012) deal with the issue by prescribing an apparent mass balance profile as a parameterized linear gradient which is, arguably, more a semantic than a physical way to deal with the transience of the problem.

Like Huss and Farinotti (2012), OGGM cannot deal with the transient problem yet: we deliberately assume steady state and therefore set $\widetilde{m} = \dot{m}$. This has the strong advantage that we can make direct use of the equilibrium mass balance $\overline{m}(t^*)$ computed earlier, which satisfies $\int \overline{m} = 0$ by construction. q is then obtained by integrating the equilibrium mass balance $\overline{m}$ along the flowline(s). The tributaries will have a positive flux at their last grid point: this mass surplus is then transferred to the downstream line, normally distributed around the 9 grid

points centred at the flowlines' junction. By construction, q starts at zero and increases along the major flowline, reaches its maximum at the equilibrium line altitude (ELA) and decreases towards zero at the tongue (for glaciers without frontal ablation).

Equation 2.2 turns out to be a polynomial of degree 5 in h with only one root in R_+, easily computable for each grid point. Singularities due to flat areas are avoided since the constructed flowlines are not allowed to have a local slope α below a certain threshold (default: 1.5°, see Sect. 2.3.2). The equation varies by a factor of 2/3 if one assumes a parabolic ($S = \frac{2}{3}hw$, with w the glacier width) or rectangular ($S = hw$) bed shape. The default in OGGM is to use a parabolic bed shape, unless the section touches a neighbouring catchment (see Fig. 2.2c), neighbouring glacier (ice divides, computed from the RGI), or at the terminus of a calving glacier. In these cases the bed shape is rectangular. Optionally, OGGM can also compute the effect of lateral bed stresses (Cuffey and Paterson, 2010) following a parameterization and tabular correction factors developed by Adhikari and Marshall (2012b).

Figure 2.5 displays some examples taken from the OGGM test suite, where the automated inversion procedure is applied on idealized glaciers generated with OGGM's flowline model (see Sect. 2.3.5). In the equilibrium cases (Fig. 2.5a to c), the inverted topography is nearly perfect. Differences arise at strong surface gradients, mostly because of numerical differences (the inversion method uses a second order central difference which tends to smooth the slope). The transient case (Fig. 2.5d) illustrates the consequences of the steady-state assumption: although the glacier is retreating, the constraint $\int \widetilde{m} = 0$ leads to a lowered ELA and, even with a perfectly known mass balance gradient, leads to an overestimated ice thickness (in this case, 25%). This effect is visible everywhere, but is strongest at the tongue. The importance of the steady state assumption on ice thickness estimates has been studied with numerical experiments (e.g. Adhikari and Marshall, 2012a) and is often compensated by calibration in real world applications.

The sensitivity of the inversion procedure to various parameters is illustrated with the example of the Hintereisferner glacier (Fig. 2.6). The total volume (and the local thickness) is very sensitive to the choice of the creep parameter A, varied from a factor 1/10 to 10 times the default value of 2.4×10^{-24} s^{-1} Pa^{-3} (Cuffey and Paterson, 2010). With a smaller A, the ice is stiffer and the glacier gets thicker (A is expected to get smaller by one or more orders of magnitude

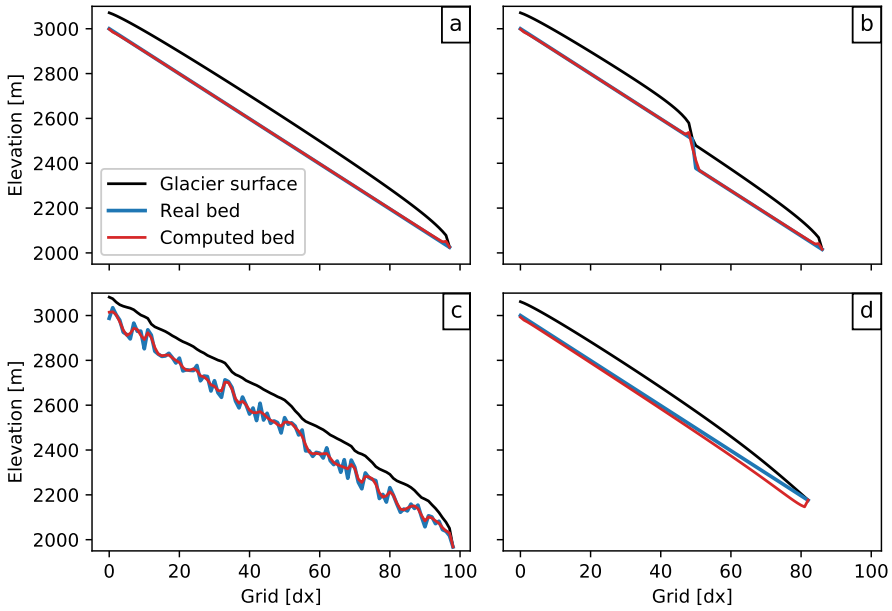

Figure 2.5: Idealized inversion experiments: we compute the bed topography out of the surface elevation obtained from a flowline model applied to a predefined bed topography. (**a**), (**b**) and (**c**): glacier grown to equilibrium with different bed topographies (flat, cliff, random). (**d**): transient experiment with a shrinking glacier. The same mass balance profile is used for all experiments (linear gradient of 3 mm w.e. m^{-1}, ELA altitude of 2600 m a.s.l.). For (d), the glacier is first grown to equilibrium then shrunk for 60 years after an ELA shift of +200 m.

with colder ice temperatures). Inversely, softer ice leads to a thinner glacier. The shape of the curve is proportional to the fifth root of the fraction $1/A$, explaining why the volume gets very sensitive to small values of A. Adding sliding reduces the original thickness significantly for the same reasons as an increasing A, since both sliding and ice rheology (A) have a strong influence on the computed ice flux q. Inversely, adding lateral bed stresses reduces ice velocity and increases the computed ice volume. Changing from a rectangular to a parabolic bed shape yields a volume loss of exactly 1/3: this is expected from geometrical considerations. The mixed parabolic/rectangular bed shape model implemented by default therefore lies in between.

The total precipitation amount, by acting on the mass balance gradient and

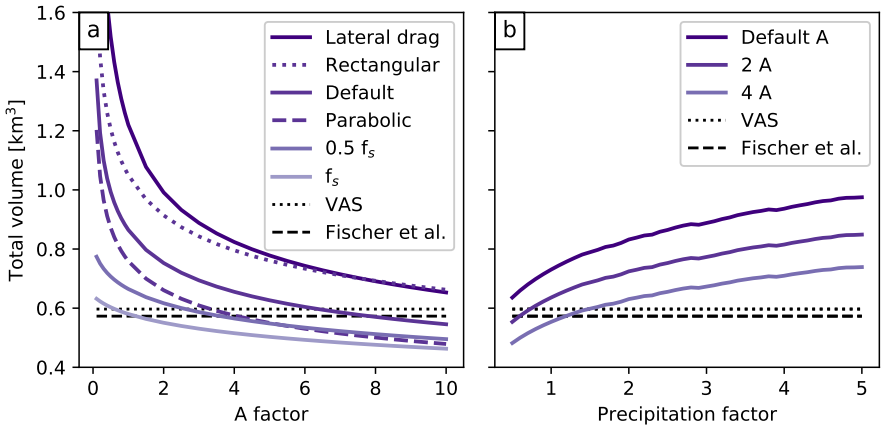

Figure 2.6: Total volume of the Hintereisferner glacier computed with (**a**) varying factors for the default creep parameter A, and (**b**) varying precipitation factors. The dotted and dashed black lines display the total volume estimated with volume-area scaling (VAS, Bahr et al., 1997, 2015) and based on point observations (Fischer and Kuhn, 2013). For (**a**), additional sensitivities are computed with an additional sliding velocity (Oerlemans, 1997) and his sliding parameter f_s. For (**b**), additional sensitivities are computed with a varying creep parameter A.

therefore on the ice flux q will also play a non-negligible role for the ice thickness (Fig. 2.6b). The effect is small in comparison to the influence of A, but it is noticeable: glaciers located in maritime climates (with high values of accumulation) will be thicker on average than similar glaciers in drier conditions.

This example shows that one can always find an optimum (and non-unique) set of parameters leading to the correct total volume. In practice, however, calibrating the model for accurate global glacier volume estimates is a major challenge for global glaciological models and will be the topic of a separate study. The IACS Working Group on Glacier Ice Thickness Estimation[5] is working towards this goal: OGGM participated in the first Ice Thickness Models Intercomparison eXperiment (ITMIX, Farinotti et al., 2017), ranking amongst the best models with limited data requirements.

[5] `http://www.cryosphericsciences.org/wg_glacierIceThickEst.html`

2.3.5 Ice dynamics

At this stage of the processing workflow, the ice-dynamics module is straightforward to implement. Provided with the mass balance, slope, width w and bed topography along the flowline, we solve the equation:

$$\frac{\partial S}{\partial t} = w\,\dot{m} - \nabla \cdot uS \tag{2.7}$$

numerically with a forward finite difference approximation scheme on a staggered grid. Numerical stability is ensured by the use of an adaptive time stepping scheme following the Courant-Friedrichs-Lewy (CFL) condition $\Delta t = \gamma \frac{\Delta x}{max(u)}$ with γ as the dimensionless Courant number chosen between zero and one. Unlike many solvers of the shallow-ice equation, we do not transform Eq. 2.7 to become a diffusivity equation in h, but solve it as it is formulated here. This has the advantage that the numerical solver is the same regardless of the shape of the bed (parabolic, trapezoidal or rectangular). The new section S at time $t + \Delta t$ allows to compute $h(t + \Delta t)$ according to the local bed geometry. Therefore, it is possible to have changing bed geometries along a single flowline using the same numerical solver. The drawback of our approach is that we cannot take advantage of the diffusivity equation solvers already available elsewhere. We tested our solution against the robust and and mass-conservative solver presented by Jarosch et al. (2013): our model yields accurate (and faster) results in most cases, but fails to ensure mass-conservation for very steep slopes like most other solvers to date. While a flowline version of the solver presented by Jarosch et al. (2013) is available in OGGM, it is not used operationally since it cannot yet handle varying bed shapes and multiple flowlines – it will become the default solver when these elements are implemented.

At a junction between a tributary and its downstream line, an artificial grid point is added to the tributary line. This grid point has the same section area S and thickness h as the previous one, but the surface slope is computed from the difference in elevation between tributary and descendant flowline. This is necessary to ensure a dynamical connection between the two lines: when the main flowline is at a higher elevation than its tributary, no mass exchange occurs and the tributary will build up mass until enough ice is available. At a junction point, Eq. 2.7 therefore contains an additional mass flux term from the tributary.

Before the actual run, a final task merges the output of all preprocessing steps and initialises the flowline glacier for the model. For the glaciers to be allowed

to grow, a downstream flowline is computed using a least cost routing algorithm leading the glacier towards the domain boundaries (this algorithm is similar to the algorithm used to compute the glacier centerlines). The bed geometries along the downstream line are computed by fitting a parabola to the actual topography profile. In case of bad fit, the values are interpolated or a default parabola is used. Along the glacier, where the bed geometries are unknown before the inversion, the bed geometries are either rectangular (ice divides and junctions) or parabolic. Very flat parabolic shapes can happen occasionally, for wide sections with a shallow ice thickness. These geometries are unrealistically sensitive to changes in h. They create a strong positive feedback (the thickening of ice leading to a highly widening glacier) and are therefore prevented: when the parabola parameter falls below a certain threshold, the geometry is assumed to be trapezoidal instead.

The coupling between the mass-balance and ice dynamics modules is a user choice. The spatially distributed mass-balance used by the dynamical model can be updated: (i) at each time-step of the dynamical model's computation, (ii) each month, (iii) each mass-balance year (the default), or (iv) only once (for testing and feedback sensitivity investigations). In practice, this does not make much difference for the yearly averages of glacier change (except for option iv), and the choice of a yearly update is mostly driven by performance considerations. Note that the mass-balance model can compute the mass-balance at shorter time intervals if required by the physical parameterizations: the interface between the model elements simply requires the mass-balance model to integrate the mass-balance over a year before giving it to the dynamical model.

The results of two idealized simulations with an advancing and a shrinking scenario are shown in Fig. 2.7. When put under the cold and wet climate of the beginning of the 20th century, Hintereisferner would grow about 2/3 larger than it is today. Inversely, the glacier is in strong disequilibrium with today's climate: it would lose about 2/3 of it's volume if the climate remained as it was during the past 31 years. The response time of the glacier is approximately twice as fast in the shrinking case, and the natural random variations of the glacier are much smaller than for a large glacier with more inertia and a longer response time.

The previous results were obtained with the default set-up of OGGM. In Fig. 2.8 we assess the sensitivity of the dynamical model to changes in the creep parameters A and to the addition of lateral drag and basal sliding velocity. As expected, these dynamical parameters affect the equilibrium volume and the

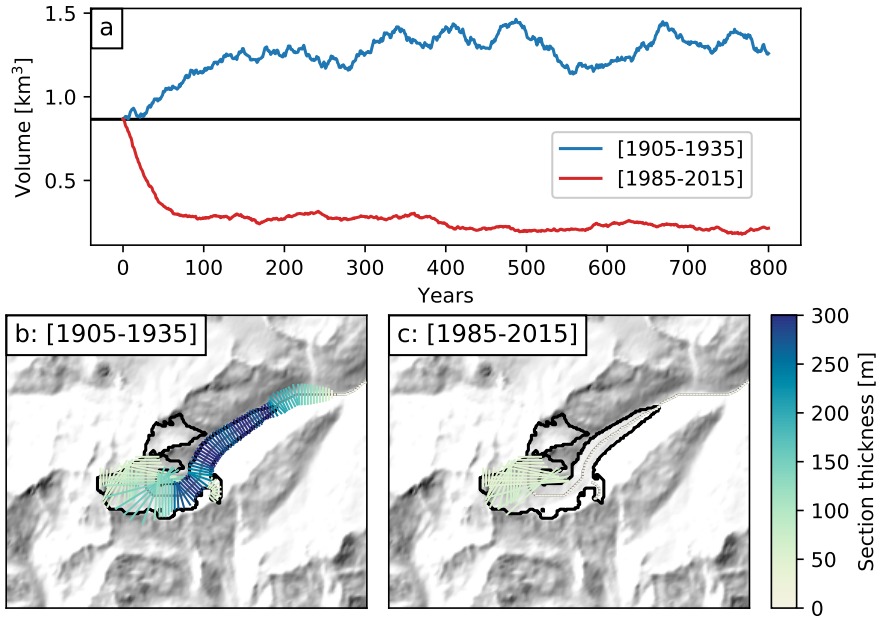

Figure 2.7: Evolution of the Hintereisferner under two random forcing scenarios and for the default parameter set. For each scenario, the "climate years" during a 31-yr period are shuffled randomly, therefore creating a realistic climate representative for a given period. (**a**): the glacier volume evolution for each scenario (the black line marks the initial computed glacier volume). (**b**) and (**c**): the glacier shape at the end of the 800 yrs simulation for each case.

response time of the glacier (faster ice leading to a thinner glacier, and inversely). Because of the mass-balance elevation feedback, the stiffer and therefore thicker glacier is also larger and longer, but its response to climate variability is smaller in amplitude than that of the fast moving sliding glacier.

A and f_s depend on many factors such as ice temperature or basal characteristics and they cannot be assumed to be globally constant. They are considered as calibration parameters in OGGM, and will be tuned towards observations of ice thickness or glacier length changes. In this study we only calibrate the mass-balance model while the ice dynamics parameters are set to their default values ($\mathrm{A} = 2.4 \times 10^{-24}$ s^{-1} Pa^{-3}, $f_s = 0$, no lateral drag). Nevertheless, we discuss the model sensitivity to these dynamical parameters for individual glaciers (Fig. 2.8) or global runs (Fig. 2.10).

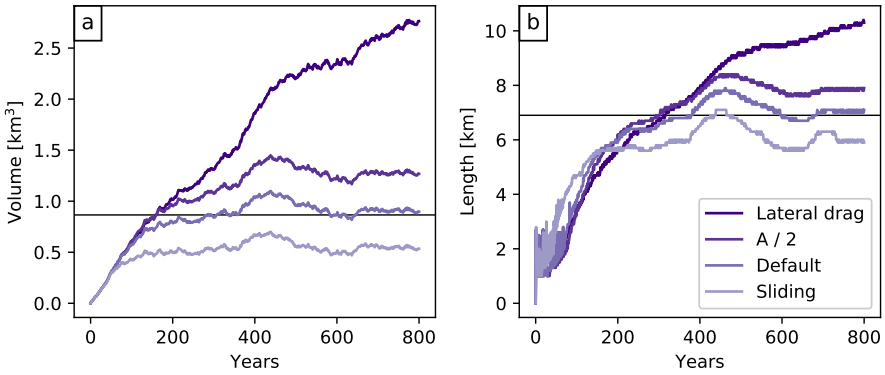

Figure 2.8: Evolution of volume (a) and length (b) of the Hintereisferner glacier under a random climate forcing generated by shuffling the "climate years" representative for the 31-yr period centred on t*. The glacier is reset to zero for each simulation, and the bed topography is obtained with the default parameters. The sensitivity to the addition of a sliding velocity or to a halving of the creep parameter A are also shown. The noisy patterns of the length time series are due to the fact that the length of a glacier on a discrete grid is sensitive to small interannual variations.

2.3.6 Special cases and model limitations

The previous experiments demonstrate that the OGGM model is capable of simulating the dynamics of glaciers in a fully automated manner. In this section we describe the implications of the flowline approximation in the special cases of water-terminating glaciers and ice caps, and discuss some examples of glaciers with a less trivial geometry.

Water-terminating glaciers

Glaciers are defined as "water-terminating" in OGGM when their RGI terminus attribute is either flagged as marine-terminating or lake-terminating. The major difference between a water-terminating glacier and a valley glacier is the additional mass-loss that occurs at the glacier front (frontal ablation). This has implications for the bed thickness inversion which currently assumes that the mass-flux at the front is zero (by setting $\int \widetilde{m} = 0$, see Sect. 2.3.4) and for the dynamics of the glacier. The current treatment of water-terminating glaciers in

OGGM is very simple but explicit: we do not take frontal ablation into account for the bed inversion (i.e. the original glacier front has a thickness of zero), but we do have a basic parametrisation in the ice dynamics module. We add a grid point behind the glacier front which is reset to zero ice thickness at each time step: the ice mass suppressed this way is the frontal ablation flux, that we store. This parametrisation has the advantage of preventing water-terminating glaciers from advancing while still allowing them to retreat (in which case they stop calving). We are working on a more advanced frontal ablation parametrisation for both the ice dynamics and the ice thickness inversion (Recinos et al., 2019).

Ice caps and ice fields

Ice caps and ice fields in the RGI are divided in single dynamical entities separated by their ice divide (Fig. 2.9). However, the entities that belong to an ice cap are classified as such in the RGI: currently, the only special treatment for these entities in OGGM is that only one major flowline is computed (without tributaries). Indeed, the geometry of ice caps is often non trivial and it is not clear whether tributaries would really improve the model results. An example of an ice cap is shown in Fig. 2.9: while the general behaviour of the ice cap is reasonably simulated by the flowline model (e.g. at the outlet glaciers), other features appear to be unrealistic (e.g. close to the ice-divides). Moreover, the mass-conservation inversion method is probably underestimating the real ice-thickness at the location of the ice-divide, where other processes related to the past history of the ice cap are at play. A possible way forward would be to run a distributed shallow-ice model instead of the flowline representation, and it is part of our long-terms plans to do so.

Glacier complexes

Single glaciers can be defined as the smallest dynamically independent entity, i.e. the boundaries between two glaciers should approximately follow the ice divides or hydrological basin boundaries. The flowline assumption strongly relies on this condition being true, and indeed most of the RGI glaciers are properly outlined. Unfortunately there are notable exceptions, for three main reasons:

- human decision: some well known glaciers have historical boundaries that the inventory provider wanted to keep, although the glacier is now disin-

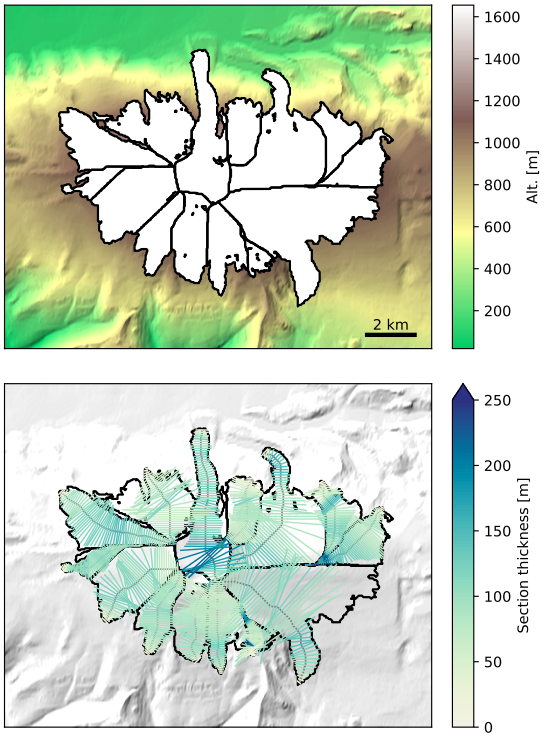

Figure 2.9: OGGM inversion workflow applied to the RGI entities of the Eyjafjallajökull ice cap, Iceland. **Upper panel**: outlines and topography. **Lower panel**: glacier thickness.

tegrated in smaller entities. A good example is the Hintereisferner glacier (Fig. 2.7), which should have three outlines instead of one.

- uncertainties in the topography: the inventories are often generated using both automated processes and manual editing. There is no guarantee that we use the same DEM as the original inventory, and therefore OGGM and RGI might disagree on the ideal position of an ice divide.

- unavailable data: some remote glaciers and ice caps are outlined in the RGI, but not divided at all. These are the most problematic cases, and should be a matter of concern for all RGI users. For example, the largest glacier in RGI (an ice cap in north-eastern Greenland with id RGI60-05.10315 and area 7537 km^2) is wrongly outlined and should be separated in at least a dozen of smaller entities.

Most of the small errors are filtered out by OGGM with algorithms based on surface slope thresholds (see Sect. 2.3.2), but the latter group of glaciers should be handled upstream. We have developed an open source tool to automatically compute glacier divides (`https://github.com/OGGM/partitioning`, based on Kienholz et al., 2013), but do not use it here. This issue is a large source of uncertainty for ice thickness estimates and dynamical modelling of glaciers in general, and could be the subject of a dedicated study.

Glacier centric modelling

Like most global glacier models, OGGM simulates each glacier individually. This has evident practical advantages, and is also a strong asset for our mass balance model calibration algorithm. However, this has two major drawbacks: (i) neighbouring glaciers won't merge although they grow together, and (ii) we can only simulate glaciers which are already inventoried, while uncharted glaciers are simply ignored. Both errors are a source of uncertainty for long or past simulations but less for short term projections in a warming world. The most obvious way to deal with this issue is to use distributed models (e.g. Clarke et al., 2015), with their own drawbacks (mostly: computational costs and the need for distributed mass balance fields). Another way would be to allow the dynamical merging of neighbour flowline glaciers at run time. While both are viable options for the OGGM workflow, they represent a considerable increase in complexity and are not available yet. Like other fundamental issues described in this paper (such as missing topographical data or wrongly outlined glaciers), this problem will affect other glacier models as well. We hope that some of the tools we introduce here will help to solve some of these issues upstream, and that the community will soon be able to put pressure on commercial data providers for better data availability.

2.4 Global simulations

Thanks to its automated workflow, OGGM is able to apply all processes described in the previous section to all glaciers of the globe with the exception of Antarctica, where no CRU data is available (see Appendix A.3 for an overview of the RGI regions). No special model setup is needed, we use all model default settings without any calibration (this is not strictly true for the μ^* calibration,

which is an automated process and cannot be tuned or turned off). In the following analyses the focus is put on the model behaviour and not on the quantitative results. However, as we are going to see our results are close to expectations even without calibration, indicating a realistic model behaviour.

2.4.1 Hardware requirements and performance

Thanks to the computational efficiency of the flowline model, OGGM runs quickly enough to be used on a personal computer for up to a hundred glaciers. At the global scale a high performance computing environment is required. For these global simulations we used a small-sized cluster comprising two nodes with 16 quad-core processors each, resulting in 128 parallel threads. With this configuration, the model preprocessing chain (including the ice thickness inversion) takes about 7 hours to complete (without data download). The total size of the (compressed) preprocessed output is 122G, an amount which can be reduced by deleting intermediate computing steps. The amount of required storage increases with each dynamical run; here again it is possible to reduce the data amounts by storing only diagnostic variables such as volume, area, length, ELA instead of the full model output. The dynamical runs are the most expensive computations: running five 300-yr long global runs takes about 24 hours on our small cluster, a very satisfying performance. It is interesting to note that because of the adaptive time-step, glacier shrinkage scenarios run faster than growing ones.

2.4.2 Invalid glaciers

Due to uncertainties in the input data (topography, outlines, climate), a certain number of glaciers fail to be modelled by OGGM. The statistics of these invalid glaciers are summarized in Table 2.1. The largest amount of errors (2.6% of the total area) is due to invalid climate series. Errors occur mostly when the climate is too cold for melt to happen or, inversely, too warm or too dry for accumulation to happen. While some of these errors are directly due to incorrect climate data, some can also be attributed to missing processes in the OGGM mass balance model: sublimation and frontal ablation, both leading to mass-loss even at cold temperatures. The least problematic source of error (0.2% of the total area) is due to failures during the actual dynamical run. The large majority of dynamical failures (751 out of 772) happen because the glacier exceeded the

domain boundaries at run time. Some of these errors could be mitigated by increasing the domain size (at the cost of computational efficiency). Only 21 glaciers fail due to numerical instabilities. Finally, there is a number of other errors (0.3% of the total area) happening at other stages of the model chain. Examples include errors in processing the geometries or failures in computing certain topographical properties due to invalid DEMs. Altogether, 7084 glaciers (3.1% of the total area) cannot be modelled by OGGM. There are strong regional differences, remote low and high latitude regions accounting for most of the errors.

2.4.3 Volume inversion

A summary of the volume inversion results is presented in Fig. 2.10. As expected from theory (Bahr et al., 1997, 2015), our glacier volume estimates approximately follow a power law relationship with the glacier area ($V = c\,S^{\gamma}$). The coefficients obtained by a linear fit in log space are close, but not equal to the coefficients computed by Bahr et al. (1997). In particular, the OGGM fit is slightly flatter than the theoretical value (Fig. 2.10, upper panel), in accordance with empirical coefficients (e.g. Bahr et al., 2015; Grinsted, 2013). This is an encouraging result, especially because it was reached with the OGGM default settings and without calibration.

The global volume estimates are particularly sensitive to the choice of the ice dynamics parameters, as shown in Fig. 2.10 (lower panel). As for individual glaciers, the total volume follows an inverse polynomial curve as expected from the equations of ice flow. Changing from a rectangular to a parabolic bed shape yields a volume loss of exactly 1/3 (see Sect. 2.3.4). Adding lateral drag yields a volume very close to the rectangular case: although this is fortuitous (individual glaciers can show different results, see Fig. 2.6), it matches nicely the original purpose of the parametrization, which is to compute a more realistic ice flow for parabolic bed shapes. The three independent estimates plotted as straight dotted lines (VAS; Grinsted, 2013; Huss and Farinotti, 2012) illustrate that A is a relatively straightforward parameter to act upon in order to fit the model to observations. The effect of A, however, is going to be the same on all glaciers and therefore will be a poor measure of performance (see also Bahr et al., 2015, Sect. 8.11). In fact, the added value of OGGM is more likely to be found in the *deviations* from the scaling law (Fig. 2.10, lower panel). The deviations are the result of a range of possible factors such as slope, total accumulation, or altitude

Table 2.1: Statistics of the model errors for each RGI region. The column names indicate which processing step produces an error, the value is the number of invalid glaciers and (in parentheses) the percentage of regional area they represent.

	N	Area (km2)	Climate	Dynamics	Others	All
01: Alaska	27108	86725	166 (0.1%)	1 (0.0%)	19 (0.1%)	186 (0.3%)
02: Western Canada and US	18855	14524	4 (0.0%)	7 (0.0%)	50 (0.5%)	61 (0.6%)
03: Arctic Canada North	4556	105111	155 (2.1%)		16 (0.1%)	171 (2.2%)
04: Arctic Canada South	7415	40888	58 (0.0%)	8 (0.0%)	11 (0.2%)	77 (0.2%)
05: Greenland	20261	130071	4422 (8.4%)	531 (0.7%)	33 (0.2%)	4986 (9.3%)
06: Iceland	568	11060				
07: Svalbard	1615	33959			6 (0.1%)	6 (0.1%)
08: Scandinavia	3417	2949		3 (0.0%)	4 (0.1%)	7 (0.1%)
09: Russian Arctic	1069	51592		2 (0.0%)	4 (0.2%)	6 (0.2%)
10: North Asia	5151	2410	55 (1.3%)	1 (0.0%)	15 (2.6%)	71 (3.9%)
11: Central Europe	3927	2092	30 (0.1%)		7 (0.0%)	37 (0.1%)
12: Caucasus and Middle East	1888	1307			2 (0.0%)	2 (0.0%)
13: Central Asia	54429	49303	59 (0.1%)	121 (0.6%)	23 (0.6%)	203 (1.3%)
14: South Asia West	27988	33568	110 (0.1%)	34 (0.1%)	31 (0.9%)	175 (1.1%)
15: South Asia East	13119	14734	178 (0.6%)	37 (0.1%)	10 (0.3%)	225 (1.0%)
16: Low Latitudes	2939	2341	383 (8.4%)	5 (0.2%)	10 (0.5%)	398 (9.1%)
17: Southern Andes	15908	29429	375 (8.4%)	21 (0.1%)	60 (0.4%)	456 (8.9%)
18: New Zealand	3537	1162	5 (0.0%)	1 (0.1%)	11 (0.1%)	17 (0.2%)
TOTAL	213750	613226	6000 (2.6%)	772 (0.2%)	312 (0.3%)	7084 (3.1%)

area distribution. With accurate boundary conditions, OGGM should be able to provide more accurate estimates, within the limits of the assumptions and

simplifications behind the model equations. The calibration and validation of the OGGM inversion model will be the topic of a subsequent study.

2.4.4 Dynamical runs

We test the model behaviour by running several 300-yr long global simulations under various climate "scenarios". In the first simulations (Fig. 2.11), we run the model under the climate of the past 31 years. In order to keep the forcing realistic, we create a pseudo-random climate by shuffling the years infinitely. We also run two additional simulations with a 0.5°C positive and negative bias. The unbiased simulation illustrates the committed glacier mass-loss, i.e. the ice mass which is not sustainable under the current climate. Figure 2.11 shows that all regions will continue to lose ice even if the climate remains constant. The regions with the largest committed mass loss relative to the initial volume are Western Canada and US (02), Svalbard (07), and the three High Mountain Asia regions (13, 14, 15). Inversely, the regions Arctic Canada South (04), Greenland (05) and Iceland (06) are least affected. The reasons for these regional differences are complex: they are due to the climate itself of course, but also to glacier properties such as size, slope, and continentality. The regions that are far from equilibrium also tend to be less sensitive to the temperature bias experiments, although this should not be over-interpreted (indeed, the range of the y-axes can hide differences which appear small in comparison to the large regional glacier loss).

In general, the model behaviour looks reasonable and the regional differences are in qualitative agreement with other global studies (e.g. Huss and Hock, 2015, where the regions with a stronger response to 21st century climate change are the same as the ones listed above). Also our global estimate of the committed mass loss (approx. 33% at the end of the 300-yr simulation, probably more at equilibrium) is in agreement with other studies (27±5%, 38±16%, and 36±8% for Bahr et al., 2009; Marzeion et al., 2018; Mernild et al., 2013, respectively).

A further model test is presented in Fig. 2.12. Here, we apply a new climate scenario: the climate at t^* which, for each glacier individually, represents a theoretical equilibrium climate. In addition to the global response to these scenarios, we separate between the majority group of smaller glaciers and the much smaller group of very large glaciers. Both groups are selected so that they sum up to one quarter of the total glacier volume. A striking feature of the runs is that

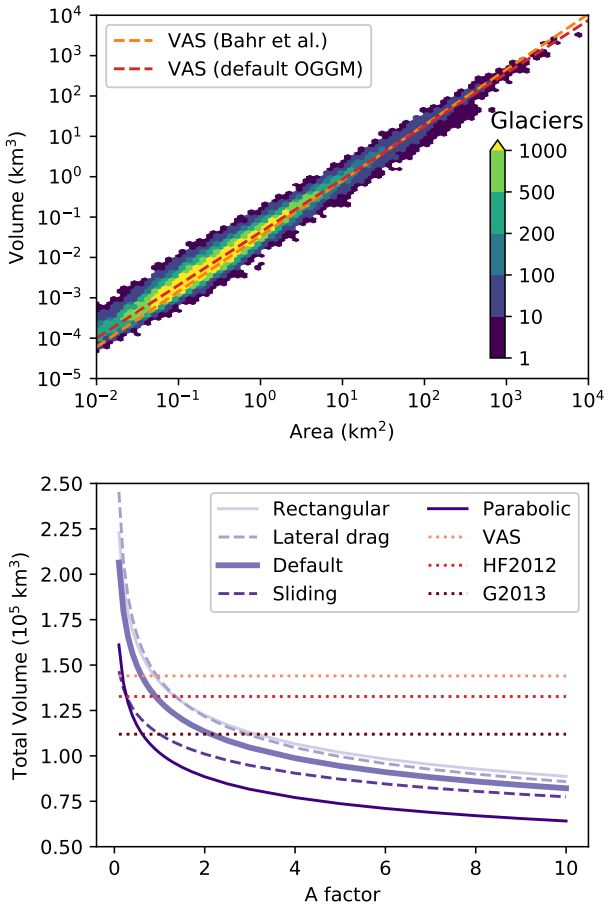

Figure 2.10: Global glacier volume modelling. **Upper panel**: binned scatter plot of volume versus area for all valid glaciers (N=207,438) with the default OGGM setup. Color shading indicates the number of glaciers in each bin. Note the logarithmic scale of the axes and the irregular color scale levels. The dashed lines indicates the volume area scaling relationship with either the theoretical parameters from Bahr et al. (1997) ($V = 0.034\,S^{1.375}$) or fitted on our own data ($V = 0.042\,S^{1.313}$). **Lower panel**: global volume estimates as a function of the multiplication factor applied to the ice creep parameter A, with five different set-ups: defaults, with sliding velocity, with lateral drag, and with rectangular and parabolic bed shapes only (instead of the default mixed parabolic/rectangular). In addition, we plotted the estimates from standard volume area scaling (VAS, $V = 0.034\,S^{1.375}$), Huss and Farinotti (2012) (HF2012) and Grinsted (2013) (G2013). The two latter estimates are provided for indication only since they are based on a different glacier inventory.

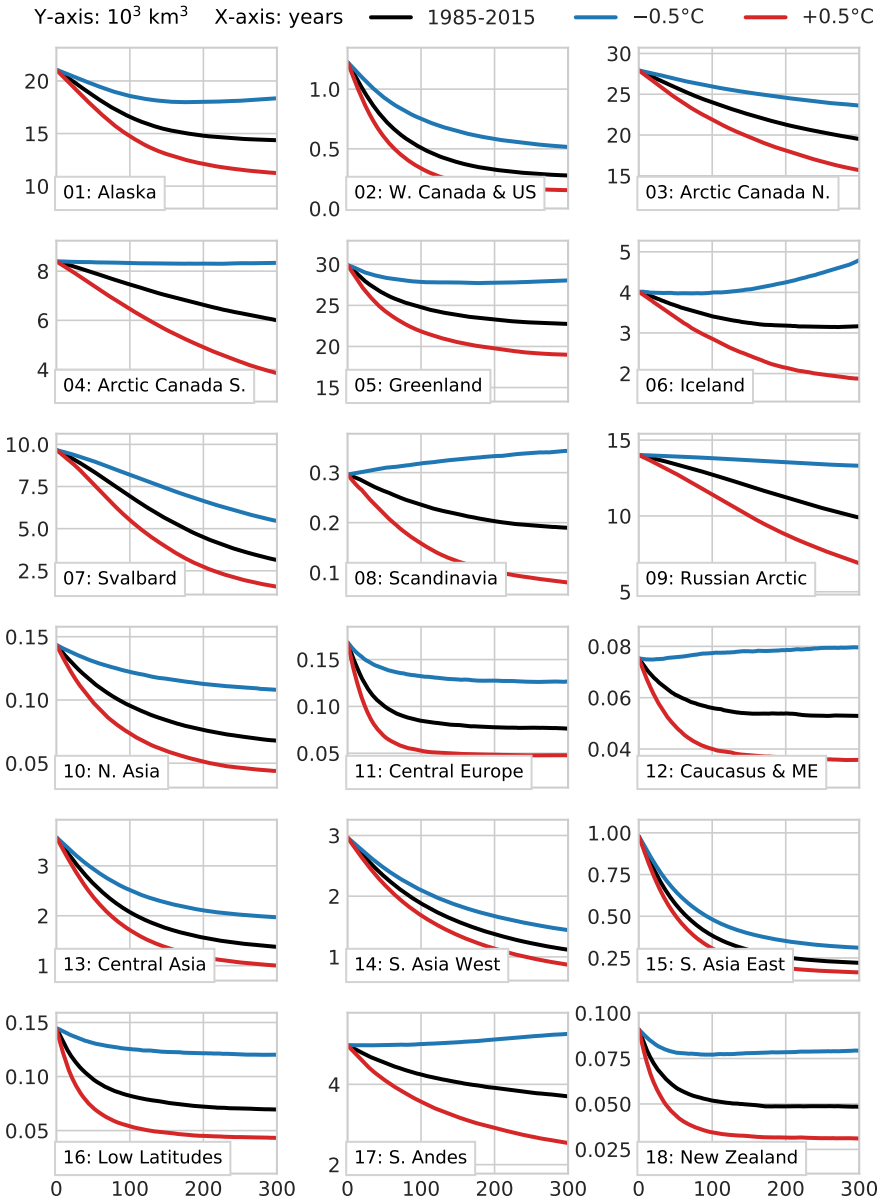

Figure 2.11: Regional glacier volume change under the 1985-2015 climate (randomized) with three temperature biases (−0.5°, 0°, +0.5°). Note the units of the y-axes (10^3 km^3) and the marked regional differences.

the glaciers tend to grow under the artificial t* climate: the growth is slow at first and accelerates with time, hinting towards a positive feedback. This feedback is driven by two factors: first, a higher surface elevation leads to a positive change in mass balance (mass balance-elevation feedback); second, because of the parabolic and trapezoidal bed shapes, a larger ice thickness leads to a wider accumulation area above the ELA and to a wider ablation area below the ELA. It appears that the positive width-accumulation feedback is stronger than the negative width-ablation feedback. This can be explained by the larger accumulation area of glaciers in an equilibrium climate: the average accumulation area ratio at t* in OGGM is 51%. In order to test which of these feedbacks is stronger, we run a simulation with rectangular bed shapes exclusively (dotted light purple line in Fig. 2.12), therefore eliminating the width-accumulation but keeping the mass balance-elevation feedback. The results show that for the vast majority of glaciers the feedback almost disappears, while the very large glaciers still show a weak and delayed altitude feedback.

It is unclear whether this is a bug or a feature. On the one hand, this behaviour is not really desirable since one would expect glaciers to remain constant under a theoretical equilibrium climate. On the other hand, t* is just a vehicle to calibrate the model and was not supposed to yield a particular insight (for example, many glaciers can only have an equilibrium t* climate after the application of a bias to the operational mass balance model). There are many reasons why small initial perturbations such as numerical noise or the differences between the bed inversion and forward model numerical schemes might lead to a different equilibrium. It must also be noted that this feedback is slow to appear, and will only have a notable influence on the largest glaciers for long term simulations in a cooler climate (the global volume change after 100 years due to the feedback is 2.4% for the default and 1% for the all rectangular cases). The very simple definition of an "equilibrium climate" for these very large glaciers is problematic anyway: large glaciers have a very slow but potentially large response to the smallest changes in climate. At the global scale, most of the 300-yr volume loss is due to the small glaciers, which respond faster and stronger than larger ones.

2.5 Conclusions

We present a new model of global glacier evolution, the Open Global Glacier Model (OGGM, v1.1). The panoply of tools available to compute past and

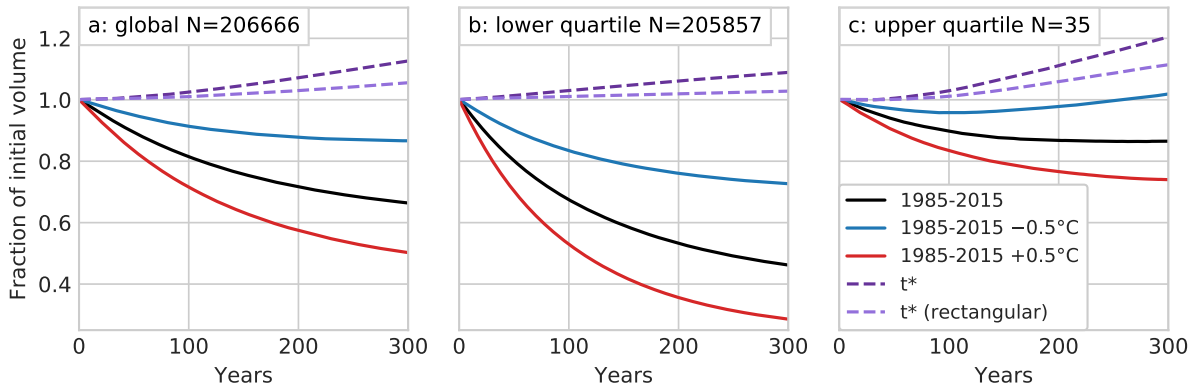

Figure 2.12: **a**: global glacier volume change under various climate scenarios (1985-2015 climate with three temperature biases and climate at t* which, for each glacier individually, represents a theoretical equilibrium climate) and model configurations (rectangular bed instead of the mixed default), plotted as a fraction of the initial volume. **b** and **c**: volume changes of all glaciers making up for the first and last quartile of the sorted cumulative total volume.

future glacier change range from simple box models (e.g. Harrison, 2013) to more complex, geometry aware models (Huss and Hock, 2015, to cite the most recent in date). OGGM undoubtedly belongs to the complex side of this scale. Different model complexities are justified by different problem settings, taking into account the model-specific merits and drawbacks. Instead of endorsing one approach over the other, OGGM aims to provide a framework which allows one to switch between models and allows objective intercomparisons. In fact, the ice dynamics module represents only a small fraction of the OGGM codebase: a huge amount of work has been invested to provide a series of tools which will help others in their own modelling endeavours. Any interested person can download, install, and run these tools at no cost. This includes the automated download of topographic and climate data for any location on the globe, the collation of glacier attributes, the automated computation of glacier centerlines, or the delineation of glacier dynamical entities. While some of these tools have been described elsewhere, the added value of OGGM is that they are now centralised, documented, and available for public review via the open-source model.

In the future, we will continue to encourage external contributions in several ways. First, it must be as easy as possible for a new user to detect where and

how a contribution can be implemented: here, documentation is key. Then, the model must be able to cope with different ways to simulate a considered process: every single task in the OGGM workflow can be replaced or enhanced, as long as the format of the input and output files is agreed beforehand. Perfect modularity will be hard to achieve, but the recent implementation of alternative numerical solvers show that modularity is possible. Finally, we need to ensure attribution to the original contribution (e.g. a scientific publication) in order to engage the wider community. For this purpose, we developed a template repository for external OGGM modules: `https://github.com/OGGM/oggmcontrib`. This development model will ensure that users importing OGGM extensions will be aware of the source of each module they are using and will be able to refer to the original contribution appropriately. We hope that this development model will foster new collaborations.

We cannot (and do not want to) demonstrate that OGGM will provide more accurate estimates of future sea-level rise than earlier attempts. However, OGGM allows new studies which weren't possible before. The dynamical representation of glacier advances and retreat enables studies of glacier evolution at long (paleo-) time scales, where ice dynamics and geometrical attributes such as the accumulation area ratio play an important role (e.g. Mackintosh et al., 2017). First OGGM simulations over the last millennium show very promising results (Goosse et al., 2018). The modular framework allows one to compare the performance of various parametrisations such as the mass balance and downscaling algorithms. It may be argued that the amount of available data is not enough to constrain modelling studies such as ours at the global scale: OGGM can now be used to test this argument by allowing simpler modules to be added to the codebase and test the added value of increased complexity.

Planned and envisioned future developments for the model follow the general guidelines of modularity and extendability. While some of the authors are working on adding even more complexity to the model (for example by improving the frontal ablation and mass balance parametrisations or by implementing a distributed ice dynamics module), it is part of our plans to implement simpler approaches such as the original Marzeion et al. (2012b) model or the Huss and Farinotti (2012) approach to ice thickness estimation. A considerable amount of work will be needed to correctly assess the uncertainties associated with the model chain: here, Monte Carlo and Bayesian approaches might be the way to follow.

The non-linear dynamical behaviour of glaciers raises a wide range of very interesting inverse problems. For example, how to deal with the transient climate issue in the ice thickness inversion algorithm? How much information about past climate can be extracted from moraine proxies and today's glacier extent? What are the uncertainties associated with global sea-level rise estimates, and where do they originate? How much complexity is just right? These are all questions the authors hope will be easier to address through the publication of OGGM.

2.6 Code availability, testing, and software requirements

The OGGM software is coded in the Python language and licensed under the GPLV3 free software license. The latest version of the code is available on Github (`https://github.com/OGGM/oggm`), the documentation is hosted on ReadTheDocs (`http://docs.oggm.org`), and the project webpage for communication and dissemination can be found at `http://oggm.org`. Past and intermediate versions are available in a permanent DOI repository (`https://zenodo.org/badge/latestdoi/43965645`). The software ships with an extensive test suite which can be used by the users to test their configuration. The tests are triggered automatically at each new code addition, reducing the risk of introducing new bugs (`https://travis-ci.org/OGGM/oggm`). The suite contains unit tests (for example for the numerical core) and integration tests based on sets of real glaciers. At the time of writing, 85% of all relevant lines of code are covered by the tests (i.e. called at least once by the test suite). The remaining 15% are challenging to monitor because they mostly concern the automated downloading tools which are used in production and cannot be tested automatically.

The following open-source libraries have to be installed in order to run OGGM: `numpy` / `scipy` (van der Walt et al., 2011), `scikit-image` (van der Walt et al., 2014), `shapely` (Gillies, 2007), `rasterio` (Gillies, 2013), `pandas` (McKinney, 2010), `geopandas`, `xarray` (Hoyer and Hamman, 2017), `pyproj`, `matplotlib` (Hunter, 2007), and `salem` (Maussion et al., 2017). OGGM runs on all major platforms (Windows, Mac, Linux) but we recommend using Linux as this is the platform it is most tested on. The code and data used to generate all figures and analyses of this paper can be found at `https://github.com/OGGM/gmd_paper_2018`.

2.7 Acknowledgements

BM, JL, and CW were supported by the Austrian Science Fund (FWF), grant P25362. BM, AB, and JE were supported by the German Research Foundation, grant MA 6966/1-1. AV and BR were supported by the DFG through the International Research Training Group IRTG 1904 ArcTrain. KF was supported by the ENS Paris-Saclay. NC was funded by the German Federal Ministry of Education and Research (grant 01LS1602A). The computations were realised partly on resources provided by Amazon Web Services Cloud Computing (sponsored by Amazon) and on the computing facilities of the Institute of Geography, University of Bremen.

3

Paper II: Impact of frontal ablation on the ice thickness estimation of marine-terminating glaciers in Alaska

Recinos, B., Maussion, F., Rothenpieler, T., and Marzeion, B.

Abstract

Frontal ablation is a major component of the mass budget of calving glaciers, strongly affecting their dynamics. Most global scale ice volume estimates to date still suffer from considerable uncertainties related to i) the implemented frontal ablation parameterisation or ii) not accounting for frontal ablation at all in the glacier model. To improve estimates of the ice thickness distribution of glaciers, it is thus important to identify and test low-cost and robust parameterisations of this process. By implementing such parameterisation into the ice-thickness estimation module of the Open Global Glacier Model (OGGM v1.1.2), we conduct a first assessment of the impact of accounting for frontal ablation on the estimate of ice stored in glaciers in Alaska. We find that inversion methods based on mass conservation systematically underestimate the mass turnover, and therefore the thickness of tidewater glaciers when neglecting frontal ablation. This underestimation can amount to up to 19 % on a regional scale and up to 30 % for individual glaciers. The effect is independent of the size of the glacier. Addi-

tionally, we perform different sensitivity experiments to study the influence of i) a constant of proportionality (k) used in the frontal ablation parameterisation, ii) Glen's temperature-dependent creep parameter (A) and iii) a sliding velocity parameter (f_s) on the regional dynamics of Alaska tidewater glaciers. OGGM is able to reproduce previous regional frontal ablation estimates applying a number of combinations of values for k, Glen's A and f_s. Our sensitivity studies also show that differences in thickness between accounting for and not accounting for frontal ablation occur mainly at the lower parts of the glacier, both above and below sea level. This indicates that not accounting for frontal ablation will have an impact on the estimate of the glaciers' potential contribution to sea-level rise. Introducing frontal ablation increases the volume estimate of Alaska marine-terminating glaciers from 9.18 ± 0.62 to 10.61 ± 0.75 mm SLE, of which 1.52 ± 0.31 mm SLE (0.59 ± 0.08 mm SLE when ignoring frontal ablation) are found to be below sea level.

3.1 Introduction

Estimates of the spatial distribution of ice thickness are needed as initial conditions for glacier models, for attempting to understand how glaciers respond to climate change, and for quantifying their contribution to sea-level rise. Despite this importance, ice thickness measurements around the globe are scarce, performed only in approx. 600 glaciers (Gärtner-Roer et al., 2014) out of more than 200,000 identified in the latest Randolph Glacier Inventory (RGI v6.0, RGI Consortium, 2017). In order to overcome this under-sampling problem, a number of methods have been developed to infer the total volume and/or the ice thickness distribution of glaciers from characteristics of the glacier surface properties. Some of these methods rely on scaling approaches relating the length, slope and area of the glacier to its total volume (e.g. Bahr et al., 1997; Grinsted, 2013; Lüthi, 2009; Radić and Hock, 2011). Others rely on parameterisations of basal shear stress (e.g. Frey et al., 2014; Linsbauer et al., 2012; Paul and Linsbauer, 2012), on observed surface velocities (e.g. Gantayat et al., 2014), or on applying the shallow-ice approximation (e.g. Cuffey and Paterson, 2010; Oerlemans, 1997) and/or an integrated form of Glen's flow law (see Farinotti et al. (2017), for a review of all these methods and Farinotti et al. (2019), for a global-scale

intercomparison).

One method presented by Farinotti et al. (2009) and successfully applied several times since then (e.g. Clarke et al., 2013; Huss and Farinotti, 2012; Maussion et al., 2019; Morlighem et al., 2011), combines ice flow dynamics and mass conservation principles to constrain mass fluxes through given glacier cross-sections. The method infers ice thickness from estimates of ice fluxes derived from the assumption that ice fluxes balance the surface mass budget (Farinotti et al., 2009). The results are thus sensitive to the spatial distribution of the mass flux and the mass balance. For calving glaciers, the surface mass budget cannot be considered balanced, even assuming equilibrium between glacier and climate. The derived ice thickness estimate for these glaciers hence depends on estimates of frontal ablation.

Frontal ablation (mass loss by calving and frontal melting Pope, 2012), is an efficient process to deliver ice from glaciers and ice sheets into the ocean. It has contributed substantially to sea-level rise in the past and played an important role in the stability of ice sheets and tidewater glaciers during the Pleistocene (Benn et al., 2007b). Calving is strongly coupled with dynamical processes inside the glacier. An increase in the ice flux can trigger a calving event and in turn this event can accelerate the movement of the ice. External aspects like ocean temperature, fjord bathymetry and, in polar areas, sea-ice concentration along the calving front can also influence the discharge of solid ice to the ocean (Straneo et al., 2013). As a consequence of the diverse nature of calving processes, the development of parameterisations of frontal ablation in numerical ice sheet and glacier models remains an important challenge. There is a wide spectrum of approaches that vary in scale and complexity, justified through the diversity of intended applications of the models (Price et al., 2015).

There have been many successful efforts to represent frontal ablation for individual glaciers (e.g. Åström et al., 2014; Nick et al., 2010; Oerlemans et al., 2011; Todd and Christoffersen, 2014; Ultee and Bassis, 2016). While these achieve encouraging results, it is unlikely that they can be implemented in a global glacier model anytime soon, because of the amount and quality of data needed to constrain this type of model. The crevasse-depth criterion proposed by Nick et al. (2010) for example, requires knowledge of surface melt and refreeze rates at the crevasses of the glacier tongue, and crevasse depth observations to calibrate and validate these rates. These kinds of observations are hard to obtain for entire glaciated regions: e.g., the 198 calving glaciers in Alaska investigated here, or

the 3,222 glaciers classified as calving (marine- and lake- terminating) glaciers in the RGI v6.0. Other recent calving models that use discrete particles or a full-Stokes model approach (e.g. Åström et al., 2014; Todd and Christoffersen, 2014; Todd et al., 2018) are too computationally expensive to be included in global glacier models that seek to consistently simulate past and future global scale glacier changes.

At the regional and global scale, very few estimates of frontal ablation fluxes of glaciers outside the ice sheets exist (Blaszczyk et al., 2009; Burgess et al., 2013; Huss and Hock, 2015; McNabb et al., 2015). From all the global glacier models published in the last decade, only Huss and Hock (2015) account for frontal ablation of marine-terminating glaciers. However, this model, along with the rest of ice thickness inversion methods, still suffers from considerable uncertainty associated with the uncertainty of the frontal ablation parameterisation.

For improving ice thickness distribution estimates at the global scale, it is thus important to identify and test low-cost and robust parameterisations of frontal ablation that might not resolve all the dynamical processes at the calving front (e.g. subaqueous frontal melting, subaerial frontal melting and sublimation), but that can estimate the amount of ice passing through the terminus of the glacier during a mass balance year. Using the ice-thickness estimation module of the Open Global Glacier Model (OGGM v1.1.2), we assess the impact of frontal ablation on the estimate of ice stored in Alaska glaciers classified as marine-terminating in the RGI v6.0 (also referred to tidewater glaciers in this study).

Alaska glaciers cover approximately 12 % of the global glacier area outside of the ice sheets (Kienholz et al., 2015). In the RGI (v6) there are 27109 glaciers in the region occupying an area of 86776.6 km^2, including adjacent glaciers in the Yukon and in British Columbia. From these glaciers, 51 have been classified as marine-terminating (74 km of tidewater margin) and 147 as lake- and river-terminating glaciers (420 km of lake/river margin) occupying an area of 11962.4 km^2 and 16720.6 km^2, respectively. Calving glaciers (marine- and lake- terminating) occupy approximately 33 % of the Alaska glacier area (Fig. 3.1; Kienholz et al., 2015; RGI Consortium, 2017).

The glaciers are divided into six subregions in the RGI. Subregions 1 and 3 contain only land terminating glaciers. Calving glaciers are mostly concentrated in the subregions 4, 5, and 6, along the mountain ranges of the southern Alaska coast (Fig. 3.1), an area characterised by maritime climate and topography reaching $>$ 5000 ma.s.l (Kienholz et al., 2015). Glaciers contained in the RGI in

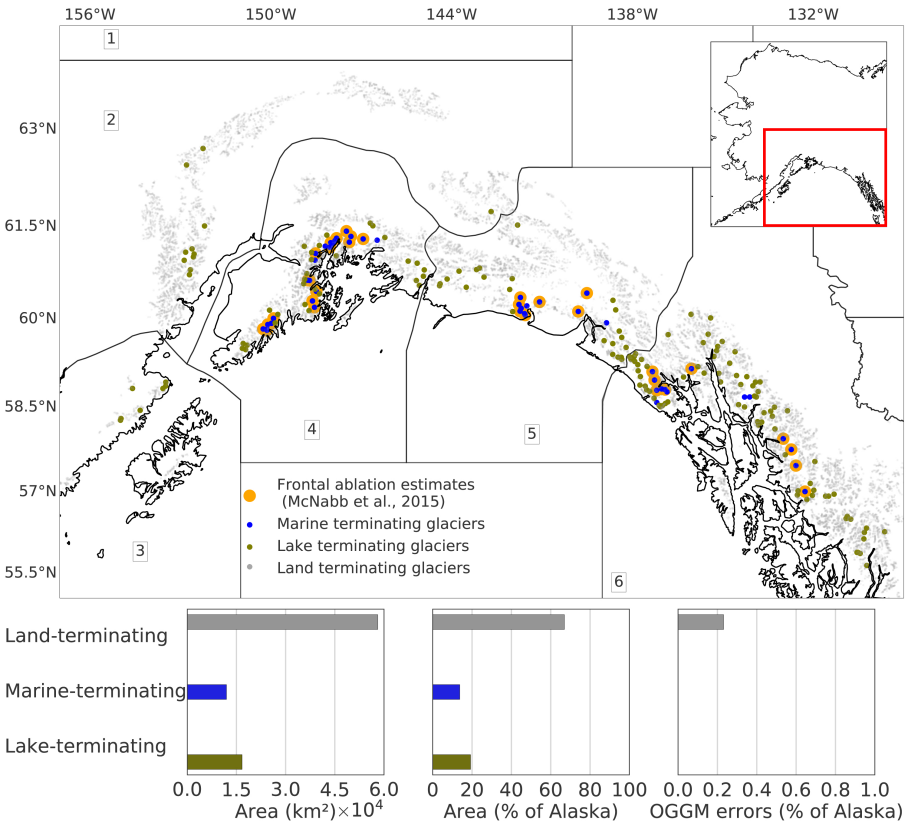

Figure 3.1: **Upper panel:** map of the RGI sub-regions of Alaska; the dots indicate the location of glaciers classified as land- (grey dots), lake- (olive dots) and marine- (blue dots) terminating in the Randolph Glacier Inventory (RGI v6). Yellow dots indicate the location of the glaciers from which there are frontal ablation estimates (McNabb et al., 2015). **Lower panel:** regional glacier types and basic statistics of the database (area of glaciers per terminus type, regional contribution to the Alaska area in percent, and percentage of the regional area which cannot be modelled by OGGM).

this region range in size from a few square kilometres (Ogive Glacier, 2.8 km^2) to many thousands of square kilometres (Hubbard Glacier, 3400 km^2; McNabb and Hock, 2014).

The subregions 4 and 5 are well studied glacierised areas of Alaska. McNabb et al. (2015) presented a 28 year record (1985 - 2013) of frontal ablation for a sub-

set of marine-terminating glaciers that includes the 27 most dominant tidewater glaciers of the region. They represent 96 % of the total tidewater glacier area in the gulf of Alaska. The total mean rate of frontal ablation was estimated to be 15.11 ± 3.63 Gt yr^{-1} (16.48 ± 3.96 km^3 yr^{-1}), over the period 1985 - 2013. Other studies also reported similar values (e.g. Larsen et al., 2007). Frontal ablation in this region is heavily dominated by two glaciers in particular: Hubbard and Columbia Glaciers (McNabb et al., 2015). Additionally, McNabb et al. (2015) identified 36 actively calving tidewater glaciers in Alaska; 27 of those were used to estimate the total mean rate of frontal ablation presented in McNabb et al. (2015).

We implement a simple parametrisation of frontal ablation in OGGM, following the approaches proposed by Oerlemans and Nick (2005) and Huss and Hock (2015). By performing sensitivity studies on the model, we i) investigate the effect of accounting for frontal ablation on the ice thickness estimation of OGGM and on the ice volume estimate for these glaciers, and ii) study the impact of varying several OGGM parameters (the calving constant of proportionality k, Glen's temperature-dependent creep parameter A, and sliding velocity parameter f_s) on the regional frontal ablation rates of Alaska.

3.2 Input data and pre-processing

3.2.1 Glacier outlines and local topography

The glacier outlines used in this study are those defined in the region 1 of the RGIv6. Four glaciers (Columbia, Grand Pacific, Hubbard and Sawyer Glacier) were merged with their respective pair branches (West Columbia, Ferris, Valerie and West Sawyer Glacier) into a single outline. A local map projection is defined for each glacier in the inventory following the methods described in Maussion et al. (2019). A Transverse Mercator projection is used, centred on the glacier in order to conserve distances, area and angles. Then, topographical data is chosen automatically depending on the glacier's location and interpolated to the local grid. For this study we used a combination of the Shuttle Radar Topography Mission (SRTM) 90 m Digital Elevation Database v4.1 (Jarvis et al., 2008) for all latitudes below 60°N and the Viewfinder Panoramas DEM3 product (90 m, `http://viewfinderpanoramas.org/dem3.html`) for higher latitudes. For Columbia Glacier, we used the DEM from the Ice Thickness Models Inter-

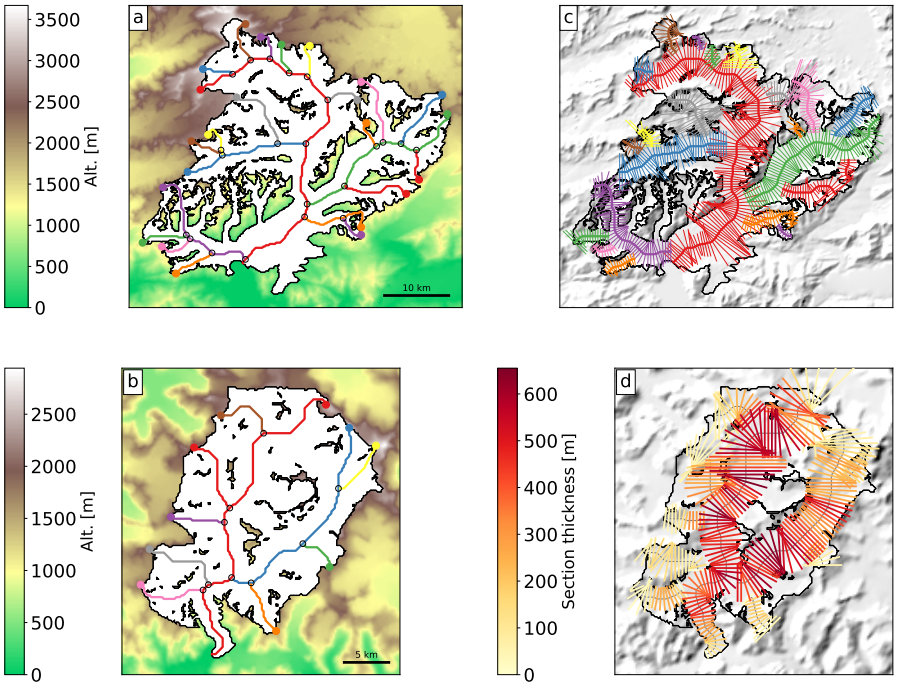

Figure 3.2: Columbia and LeConte Glacier model workflow; **a and b:** topographical data preprocessing and computation of the flowlines; **c:** width correction according to catchment areas and altitude-area distribution; **d:** thickness distribution before accounting for frontal ablation.

comparison eXperiment (Farinotti et al., 2017, ITMIX) instead [1]. All datasets are re-sampled to a resolution depending on glacier size (Maussion et al., 2019) and smoothed with a Gaussian filter of 250 m radius.

3.2.2 Glacier flowlines, catchment areas and widths

The glacier centrelines are computed following an automated method based on the approach of Kienholz et al. (2014). Fig. 4.3a illustrates an example of this geometrical algorithm applied to the Columbia Glacier. The centrelines are then filtered and slightly adapted to represent glacier flowlines with a fixed grid

[1] See Sect. 3.5 for a discussion about the importance of reliable topographic data for the frontal ablation estimate.

spacing (Fig. 4.3c). The geometrical widths along the flowlines are obtained by intersecting the normals at each grid point with the glacier outlines and the tributaries' catchment areas. Each tributary and the main flowline has a catchment area, which is then used to correct the geometrical widths. This process assures that the flowline representation of the glacier is in close accordance with the actual altitude-area distribution of the glacier. The width of the calving front, therefore, is obtained from a geometric first guess multiplied by a correction factor. This may lead to uncertainties in the frontal ablation computations, as discussed in Sect. 3.5.

3.2.3 Regional frontal ablation estimates

Frontal ablation for 27 marine-terminating glaciers presented by McNabb et al. (2015) are used to compare the results of the model and calibrate the calving constant of proportionality k. These estimates were calculated from satellite-derived ice velocities and modeled estimates of glacier ice thickness.

3.2.4 Climate data and mass balance

The mass balance (MB) model implemented in OGGM uses monthly time series of temperature and precipitation. The current default is to use the gridded time-series dataset CRU TS v4.01 (Harris et al., 2014), which covers the period of 1901-2015 with a 0.5° resolution. This raw, coarse dataset is downscaled to a higher resolution grid (CRU CL v2.0 at 10' resolution, New et al., 2002), following the anomaly mapping approach described in Maussion et al. (2019), allowing OGGM to have an elevation-dependent climate dataset from which the temperature and precipitation at each elevation of the glacier are computed, and then converted to the local temperature according to a temperature gradient (default: 6.5 K km^{-1}). No vertical gradient is applied to precipitation, but a correction factor p_f =2.5 is applied to the original CRU time series (see Maussion et al., 2019, appendix A for more information). The MB model (see Sect. 3.3.2) is calibrated with direct observations of the annual surface mass balance (SMB). For this, OGGM uses reference mass-balance data from the World Glacier Monitoring Service (WGMS, 2017) and the links to the respective RGI polygons assembled by Maussion (2017).

3.3 Open Global Glacier Model (OGGM) and frontal ablation parameterisation

For this study, a simple frontal ablation parametrisation is implemented into the Open Global Glacier Model (OGGM v1.1.2). OGGM is developed to provide a global scale, modular and open source numerical model framework for consistently simulating past and future global scale glacier change. The mathematical framework of the model and its capabilities have been explained in detail by Maussion et al. (2019). In this section, we will only describe the modifications done to the mass-balance and ice thickness inversion modules, together with the frontal ablation parametrisation implemented in order to improve the initialisation of the model for marine-terminating glaciers. Sect. 3.3.3 provides details on the limitation of applying the parameterisation to lake-terminating glaciers.

3.3.1 Ice thickness

The method of estimating ice thickness from mass turnover and principles of ice-flow dynamics in glaciers go back to Budd and Allison (1975) and Rasmussen (1988), whose ideas were further developed by Fastook et al. (1995) and Farinotti et al. (2009). The later aims to estimate ice thickness distribution from a given glacier surface topography, which can be achieved assuming that the mass-balance distribution should be balanced by the ice-flux divergence. This method has been modified in OGGM in order to implement a new ice thickness inversion procedure physically consistent with the flowline representation of the glaciers and taking advantage of the mass-balance calibration procedure of OGGM (see below).

The flux of ice q ($m^3\ s^{-1}$) through a glacier cross-section of area S (m^2) is defined as:

$$q = \bar{u}S \tag{3.1}$$

with $\bar{u}$ being the average cross-section velocity ($m\ s^{-1}$). By applying the well known shallow-ice approximation (Cuffey and Paterson, 2010; Hutter, 1981, 1983; Oerlemans, 1997) and making use of the Glen's ice flow law, we compute the depth-integrated centerline velocity u of the cross-section with:

$$u = \frac{2A}{n+2} h_0 \tau^n \tag{3.2}$$

with A being the ice creep parameter (which has a default value of 2.4×10^{-24} s^{-1} Pa^{-3}), n the exponent of Glen's flow law (default: n=3), h_0 the centerline ice thickness (m), and τ the basal shear stress defined as:

$$\tau = \rho g h_0 \alpha \tag{3.3}$$

with ρ the ice density (900 kg m^{-3}), g the gravitational acceleration (9.81 m s^{-2}) and α the surface slope (computed along the centerline). Optionally, a sliding velocity u_s can be added to the deformation velocity to account for basal sliding, using the following parametrisation (Budd et al., 1979b; Oerlemans, 1997):

$$u_s = \frac{f_s \tau^n}{h_0} \tag{3.4}$$

with f_s a sliding parameter (default: 5.7×10^{-20} $m^{-2}s^{-1}$ Pa^{-3}). We then assume that the centerline velocity is equal to the average section velocity ($\bar{u} \approx u$), which in absence of lateral drag is correct for a rectangular bed shape but isn't in the parabolic case, where we neglect the variations of the shear stress (and u) along the parabola. In the parabolic case and with N=3, this results in a section velocity overestimation of a factor 315 / 128 (approx 2.46) in comparison to the section velocity obtained by integrating the shallow-ice velocity over the parabola. We proceed with this approximation because (i) this factor cannot be computed analytically for any other non-integer value of Glen N or for other bed shapes (e.g. trapezoidal) and (ii) the uncertainties about the true shape of the bed would make the model very sensitive to this choice. The computed flux in OGGM however does vary by a factor 2/3 depending on whether one assumes a parabolic ($S = \frac{2}{3}hw$) or rectangular ($S = hw$, with w being the glacier width) bed shape. The default in OGGM is to use a parabolic bed shape, unless the section touches a neighbouring catchment or neighbouring glacier (ice divides, computed from the RGI). For the last five grid points of tidewater glaciers, the bed shape is also assumed to be rectangular. Singularities with flat areas are avoided since the constructed flowlines are not allowed to have a local slope α below a certain threshold (default: 1.5°, see Maussion et al., 2019).

Following the approach described in Maussion et al. (2019), q can be estimated from the mass-balance field of a glacier. If u and q are known, S and the local ice thickness h (m) can also be computed by making some assumptions about the geometry of the bed and by solving Eq. 4.1. This equation becomes

a polynomial in h of degree 5 with only one root in R_+, easily computable for each grid point.

3.3.2 Mass-balance and ice flux *q*

OGGM's mass balance model is an extension of the model proposed by Marzeion et al. (2012b) and adapted in Maussion et al. (2019), to calculate the mass balance of each flowline grid point for every month, using the CRU climatological series as boundary condition. The equation governing the mass-balance is that of a traditional temperature index melt model. The monthly mass-balance m_i (kg m^{-2} s^{-1}) at elevation z is computed as:

$$m_i(z) = p_f P_i^{\text{solid}}(z) - \mu^* \, max\left(T_i(z) - T_{\text{melt}}, 0\right) \tag{3.5}$$

where P_i^{solid} is the monthly solid precipitation, p_f a global precipitation correction factor, T_i the monthly temperature and T_{melt} is the monthly mean air temperature above which ice melt is assumed to occur (default: -1°C). Solid precipitation is computed as a fraction of the total precipitation: 100 % solid if T_i <= T_{solid} (default: 0°C), 0 % if T_i >= T_{liquid} (default: 2°C), and linearly interpolated in between. The parameter μ^* indicates the temperature sensitivity of the glacier, and it needs to be calibrated: in a nutshell, the MB calibration consists of searching a 31-year climate period in the past during which the glacier would have been in equilibrium while keeping its modern-time geometry, implying that the mass balance of the glacier during that period in time $m_{31}(t)$ is equal to zero, with $m_{31}(t)$ being the glacier integrated mass-balance computed for a 31 yr period centred around the year t (e.g. $t^* = 1962$ for most glaciers in Alaska) and for a constant glacier geometry fixed at the RGI outline's date (e.g. 2009 for the Columbia Glacier). It should be noted that the mass balance calibration in OGGM excludes MB measurements from tidewater glaciers as reference data, for reasons described below.

This "equilibrium mass-balance" ($m_{31}(t)$) is then assumed to be equal to the "apparent mass-balance" ($\tilde{m} = \dot{m} - \rho\frac{\partial h}{\partial t}$) as defined by Farinotti et al. (2009), where the flux of ice q through a glacier catchment area (Ω) is defined as:

$$q = \int_\Omega (\dot{m} - \rho\frac{\partial h}{\partial t}) dA = \int_\Omega m_{31} dA \tag{3.6}$$

If the glacier is land-terminating, $\int m_{31} = 0$ by construction (a property which is used to calibrate μ^* in Eq. 4.2). q is then obtained by integrating the equilibrium mass-balance m_{31} along the flowline(s). q starts at zero and increases along the major flowline, reaches it's maximum at the equilibrium line altitude (ELA) and decreases towards zero at the tongue (Maussion et al., 2019).

However, this assumption does not hold for tidewater glaciers, where a steady state implies that:

$$\int m_{31} = \frac{q_{calving}\ \rho}{A_{RGI}} \tag{3.7}$$

Where $q_{calving}$ is the frontal ablation flux of the glacier ($m^3\ yr^{-1}$). This flux is then converted to units of specific MB ($kg\ m^{-2}\ yr^{-1}$) by multiplying with the ice density ($900\ kg\ m^{-3}$) and dividing by the total glacier area as given by the RGI. A more precise definition would be that $q_{calving}$ is the average amount of ice that passes through the glacier terminus in a year for a glacier in equilibrium with the climate forcing. This has direct consequences for the calibration of the temperature sensitivity parameter μ^*. With all other things kept equal, two otherwise identical glaciers (one calving, one non-calving) will have to have different temperature sensitivities μ^*: the calving glacier will have a lower μ^*, resulting in a lowered Equilibrium Line Altitude (ELA), a positive surface mass budget, and finally to a mass flux through the terminus. The objective here is to allow the model to have a non-zero calving flux, with the goal of improving the glacier thickness inversion computed by OGGM.

3.3.3 Frontal ablation parameterisation

Calving law

To account for frontal ablation of marine-terminating glaciers we employ a calving law proposed by Oerlemans and Nick (2005) and that has already been applied at a large scale by Huss and Hock (2015). The annual frontal ablation flux $q_{calving}$ ($km^3\ yr^{-1}$) is computed as a function of the height *(h_f)*, width *(w)* and estimated water depth *(d)* of the calving front as:

$$q_{calving} = max(0; kdh_f) \cdot w \tag{3.8}$$

k is a calibration parameter (which has a default value of $2.4\ yr^{-1}$ in this study). The water depth (d) is estimated from free-board, using elevation, and

ice thickness (h_f) data obtained from the model output:

$$d = h_f - E_t + z_w \tag{3.9}$$

Where E_t is the elevation of the glacier surface at the terminus and z_w is the elevation of the water body with respect to sea level. The water depth (d) is estimated using the terminus elevation (E_t) obtained by projecting the RGI outline onto the DEM (i.e., the terminus elevation is the top of the cliff). We follow the same definition as Oerlemans and Nick (2005) where d is the bed elevation with respect to sea level. For lake-terminating glaciers, we are not able to estimate a water depth since one would need to know the free-board of the glacier terminus, i.e. the elevation of the glacier lake surface. For this reason, most of our experiments and results focus on marine-terminating glaciers only (z_w is set of 0 m a.s.l.), with the exception of the experiment presented in section 4.2.

Unlike Huss and Hock (2015), who estimated the thickness of the calving front *(h_f)* by scaling approaches, we solve for the ice thickness by prescribing that the amount of ice calved ($q_{calving}$) must be equal to the amount of ice delivered to the terminus by OGGM (q, computed from ice deformation and sliding in Section 3.3.1):

$$q_{calving} = q \tag{3.10}$$

$q_{calving}$ varies with h_f as a polynomial of degree 2. q is a polynomial in h_f of degree 5 (with n = 3 in Eq. 3.2), with an extra term in degree 3 if we account for a sliding velocity (see Eq. 3.4). Eq. 4.6 is therefore a polynomial that can be solved for h_f.

Illustration of the method

We use the LeConte Glacier (see Fig. 4.3b and d) as a test case to illustrate our solution method. Fig 4.3d shows the result of the model's default ice thickness inversion procedure, which assumes an ice flux of zero at the terminus ($q_{calving} = 0$). Note that by default, the ice thickness at the glacier front h_f is zero.

First we examine how the frontal ablation flux ($q_{calving}$) from the calving law would change if we increase the terminus ice thickness of the glacier, while keeping the free-board fixed (E_t is the only variable known in Eq. 4.5 "with certainty", from the DEM surface elevation at the terminus). Fig. 3.3a shows that the flux

remains equal to zero as long as h_f is not thick enough to reach water, after which the water depth is positive and calving occurs. At this point, we are unaware of the real frontal ablation flux for this glacier, but we make some very coarse assumptions:

- Oerlemans and Nick (2005) calving law is perfectly exact
- the tuning parameter k is known
- our glacier is in equilibrium with climate (we assume mass-conservation inversion in OGGM)
- ice deformation at the glacier terminus follows Glen's flow law

Under these assumptions, we set up an experiment where we compute a frontal ablation flux (from the calving law, Eq.4.4) for a range of prescribed frontal ice thicknesses (see Fig. 3.3b, blue line), then give this flux back to the inversion model which computes a frontal ice thickness according to the physics of ice flow (Fig. 3.3b, green and orange lines). As shown in Fig. 3.3b, both curves meet at a frontal thickness value which complies with both the calving law ($q_{calving}$) and the ice thickness inversion model of OGGM (q). Note that changing Glen's deformation parameter A or adding sliding does not change the problem qualitatively: we will still solve a polynomial degree 5 in OGGM, with a new term in degree 3.

Fig. 3.3c displays the same data as Fig. 3.3b (here as a function of the prescribed water depth), showing more clearly that there are two locations where the zero line is crossed and the condition of Eq. 4.6 is met. However, only one solution (the larger one) provides a realistic water depth, and therefore a realistic frontal ablation flux.

Implementation

We solve the polynomial in Eq. 4.6 numerically, via bound-constrained minimisation methods (algorithm provided by SciPy Jones et al., 2001), which leads to a quick convergence. The advantage over an analytical solution is that numerical solvers have the flexibility to be applied to any other formulation of $q_{calving}$ and q, i.e. that this method will still be applicable if a lateral drag parameterisation or another formulation for the calving law is added to OGGM in the future.

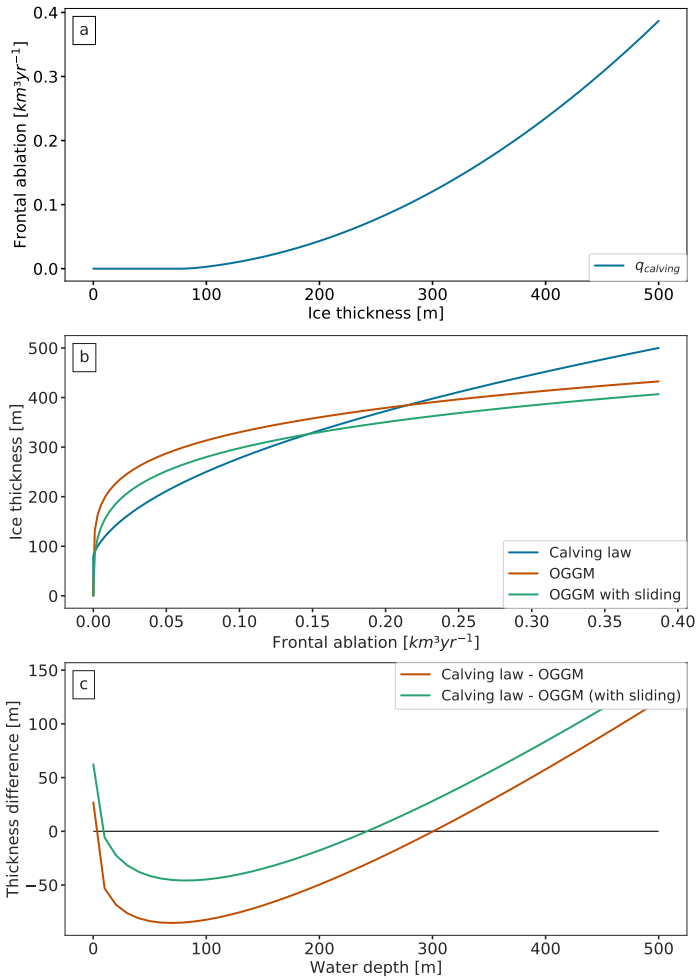

Figure 3.3: Idealised experiments applied to the LeConte Glacier. **a:** Frontal ablation flux computed by the calving law when prescribing a terminus thickness, with h_f ranging from 0 to 500 m. **b:** terminus ice thickness per frontal ablation flux obtained; i) by the calving law (blue curve, same as **a**), ii) by OGGM using ice deformation (orange curve) and iii) by OGGM using ice deformation and adding a sliding velocity (green curve). **c:** illustration of the ice thickness function from Eq. 4.6 for a given range of water depth values; i) without a sliding velocity (orange curve), ii) with a sliding velocity (green curve).

After finding the solution for the frontal ice thickness (h_f) and the corresponding frontal ablation flux ($q_{calving}$), we give this flux back to the mass balance model (Eq. 4.3), adjust the temperature sensitivity of the glacier μ^*, and invert for a new ice thickness distribution for the entire glacier (see Sect. 3.4.1 for results). This always results in a adjustment of μ^* towards lower values in order to lower the ELA and unbalancing the steady-state surface mass-budget for a frontal ablation flux to exist. Note that this adjustment of mass-balance is always necessary (regardless of the choice of model parameters such as k or Glen's A) in order to ensure mass-conservation and the update of upstream ice thickness.

However, sometimes the flux estimated by the calving law (Eq. 4.4) is too large to be sustained by the surface mass-balance. Even without glacier melt ($\mu^* = 0$), the total accumulation over the glacier is too small to close the frontal mass budget. This can be due to several factors: frontal ablation is overestimated, or solid precipitation is underestimated. The frontal ablation can be overestimated if k and/or the calving law does not represents the dynamics of that particular glacier, or if h_f is overestimated. In most cases (see results), it is possible to find a realistic μ^* compatible with a frontal ablation flux, but when this is not possible μ^* is fixed to zero and the frontal ablation flux $q_{calving}$ is obtained by closing the mass-budget instead of using the calving law.

3.4 Results

We apply this frontal ablation parameterisation to all marine-terminating glaciers in Alaska. We study the impact of including this parameterisation on the estimated glacier thickness, volume and ice flow velocity. The following sections describe different sensitivity experiments: i) varying the frontal ablation flux added to the MB model and assessing the impact on glacier volume, ii) varying several model parameters (Glen's flow law ice creep parameter A, a sliding parameter f_s, and the calving constant of proportionality k) and assessing each parameter's impact to the regional frontal ablation of Alaska, and iii) show the impact of different model configurations (obtained from the sensitivity experiments of sect. 3.4.4) to the total volume of Alaska marine-terminating glaciers. The parameter set up for each configuration can be found in Table 3.1.

3.4.1 Case study: Columbia Glacier

The Columbia Glacier located in south-central Alaska, is one of the most studied tidewater glacier in the world. With a detailed record of its retreat since 1976, it is the single largest contributor of the Alaska glaciers to sea-level rise (Berthier et al., 2010; Larsen et al., 2015). The ice flow, ice discharge and tidewater retreat of the glacier are all extensively documented, providing rich insight into the underlying processes that modulate tidewater glacier behaviour and stability (Mcnabb et al., 2012). These reasons motivated the selection of the Columbia Glacier as an exemplary study site to illustrate our results for an individual glacier, while the goal of our approach is the ability to improve the model representation of any calving glacier.

Following the process described in section 3.3.3, we calculate a virtual frontal ablation for the Columbia Glacier of 2.98 km^3 yr^{-1} (2.73 Gt yr^{-1}). This flux represents the estimated amount of ice passing through the terminus of the glacier, if the glacier was in equilibrium with the climate for a constant glacier geometry fixed at the RGI outline's date (e.g. 2009 for this glacier). This estimate was obtained using the model's default values for the parameters k, A and f_s. McNabb et al. (2015) estimated a mean frontal ablation of 3.53 $\pm$ 0.85 Gt yr^{-1} during 1982–2007, with previous studies estimating 5.5 Gt yr^{-1} for the same period (Rasmussen et al., 2011). Fig. 3.4 shows the difference between not accounting for frontal ablation in the mass balance ($q_{calving} = 0$ in Eq. 4.3) and accounting for frontal ablation, adding the frontal ablation flux calculated to the MB module ($q_{calving} = 2.98$ km^3 yr^{-1} in Eq. 4.3). If $q_{calving} = 0$ (Fig. 3.4a), we estimate the total volume of the Columbia Glacier to be 270.40 km^3, 29.21% less than the volume calculated if the frontal ablation is added (Fig. 3.4b), which results in a volume of 349.39 km^3.

When computing the ice thickness distribution map of the glacier, the impact of accounting for frontal ablation is mainly reflected in the two adjacent branches of the Columbia Glacier (Fig. 3.4b) and at the glacier terminus (Fig. 3.4c). An overview of the glacier main centreline profile is shown in Fig. 3.4c, together with the 2007 thickness map published by Mcnabb et al. (2012) (green dotted line), a study that provided a reconstructed bed topography and ice thickness, based on velocity observations of the Columbia Glacier and mass conservation. Fig. 3.4c also includes the result of the "consensus estimate" for the Columbia glacier ice thickness from Farinotti et al. (2019). OGGM's glacier bed estimation without accounting for frontal ablation (grey line) as well as the composite solution from

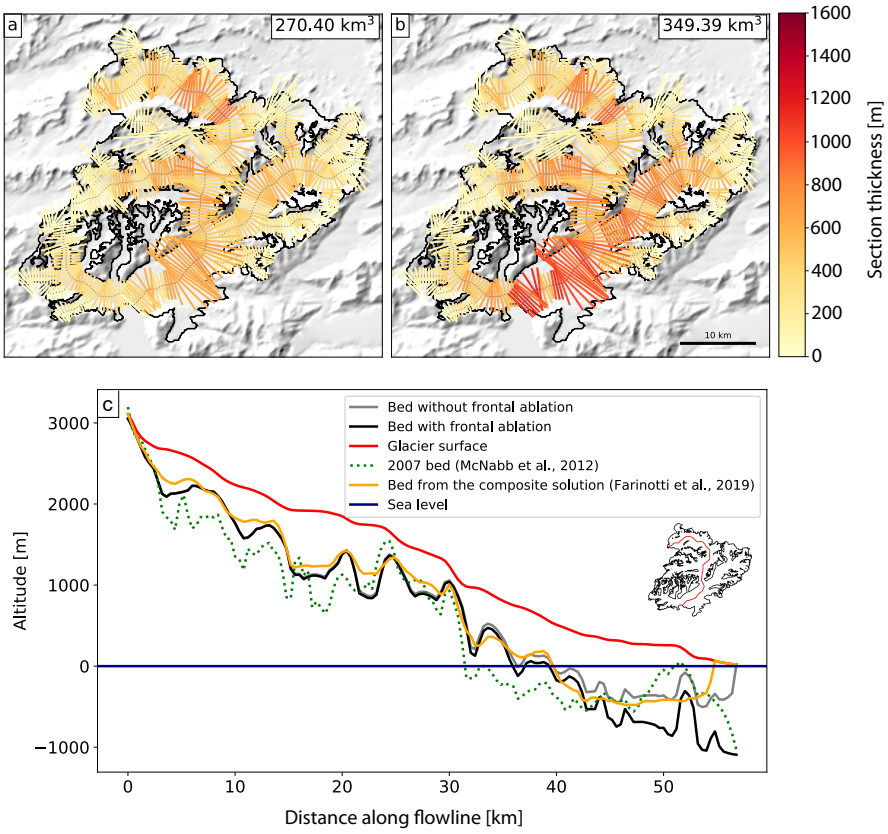

Figure 3.4: Ice thickness inversion results for the Columbia Glacier; **a:** thickness distribution before accounting for frontal ablation; **b:** thickness distribution after accounting for frontal ablation, with a frontal ablation flux computed by the model of 2.98 km^3 y^{-1}; **c:** Columbia Glacier main centreline profile, comparison between the 2007 estimated bed map (green doted line) from Mcnabb et al. (2012), the consensus estimate from Farinotti et al. (2019) (orange line) and model output before accounting for frontal ablation (grey line) and after accounting for frontal ablation (black line).

Farinotti et al. (2019) (yellow line) estimate zero thickness at the calving front.

By accounting for frontal ablation in OGGM's MB and thickness inversion modules, we can compute a bedrock profile closer to the 2007 bed map, especially close to those points located at the terminus of the glacier. The frontal ablation parameterisation allows OGGM to grow a thick calving front at the glacier terminus. Additionally, we observe that both bed estimations from OGGM (grey

and black lines, Fig. 3.4c) diverge primarily below sea level.

3.4.2 Frontal ablation and glacier volume

In this experiment, we assign a frontal ablation flux ranging from 0 - 5 $km^3\ yr^{-1}$ to each glacier classified as potentially calving in the RGI v6.0, keeping the model's default values for the parameters A and f_s. The aim is to calculate the changes in volume for each glacier as a function of the frontal ablation value, while keeping the rest of the aspects that control the volume of the glacier fixed to the default values (e.g. solid precipitation, outline, topography, ice parameters). As a result of the automated workflow of OGGM, we are able to calculate the changes in volume of all 198 calving glaciers in Alaska[2], for each value in the frontal ablation flux range.

The results of this experiment are shown in Fig. 3.5, where the frontal ablation fluxes are expressed as a fraction of the annual accumulation ($p_f P_i^{Solid}(z)$) over each individual glacier. This fraction is de facto normalised to a maximum of 1, since the calving flux cannot exceed the total accumulation. Large glaciers (green and red lines in Fig. 3.5) won't reach this value in the prescribed calving range of 0 - 5 $km^3\ yr^{-1}$. Eq. 4.2 and 4.3 indicate that a temperature sensitivity $\mu^* \leq 0$ would imply that the glacier is producing a frontal ablation larger than its annual accumulation. When this happens, OGGM clips the temperature sensitivity μ^* to zero, setting a physical limit to the frontal ablation of each individual calving glacier.

Fig. 3.5a shows that the effect of frontal ablation on the glacier volume is systematic, in that accounting for frontal ablation in the MB will always result in an increase of the glacier volume. Even if the frontal ablation fraction is only 0.14 of the total accumulation, a glacier volume can be underestimated by up to 20% if we ignore this extra source of ablation. However, there is a wide range of sensitivities of the estimated glacier volume to the calving flux, and no simple relation to e.g. glacier size was found. Other glacier specific parameters likely to play a role are the slope, the accumulation area ratio and the total precipitation.

[2] Only in this section we include lake-terminating glaciers in the experiments, because we are not calculating a frontal ablation flux but assigning a specific value to the mass-balance equation (Eq. 4.3).

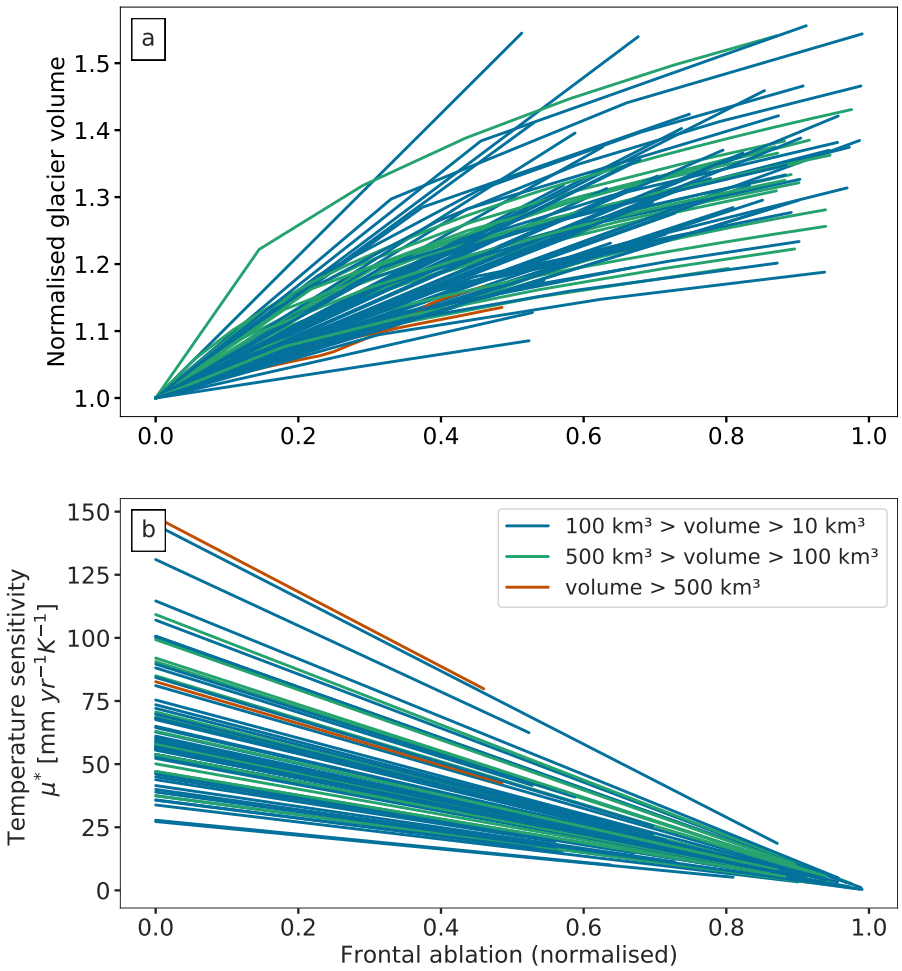

Figure 3.5: **a:** Normalised glacier volume and **b:** temperature sensitivity (μ^*) of individual glaciers, as a function of the prescribed frontal ablation fluxes normalised by the total accumulation over each glacier. The different colors represents different glacier classes.

3.4.3 Effect of frontal ablation on ice velocity

To analyse the effect of frontal ablation on ice velocity, we keep the same model configuration (default values of k, A and f_s) and calculate the average ice velocity along the main flowline for all marine-terminating glaciers that produced a frontal ablation flux. Fig. 3.6 shows the difference between the average velocity output of the model when accounting for frontal ablation and without accounting for frontal ablation. When taking frontal ablation into account, the glaciers

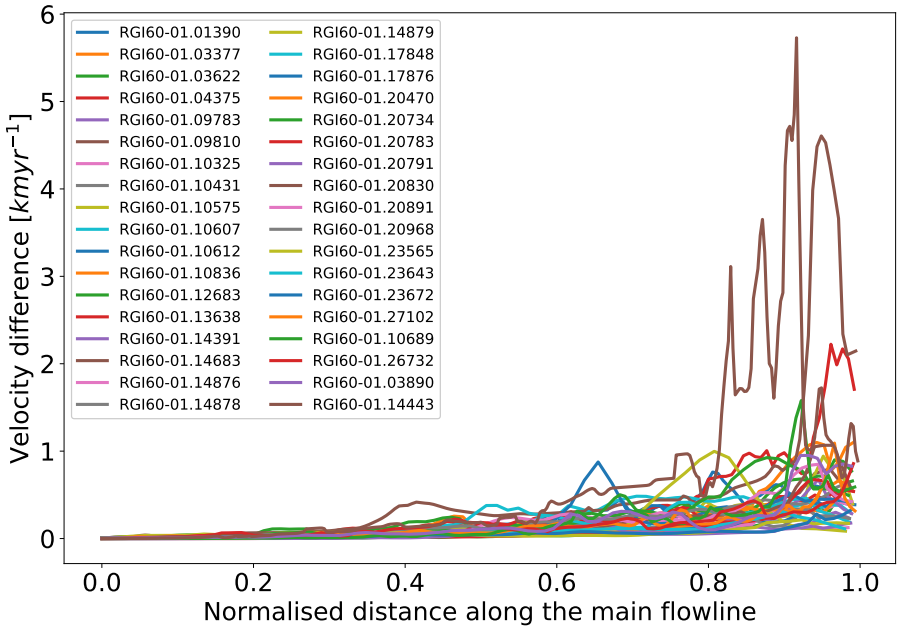

Figure 3.6: Glacier average velocity differences between the two outputs of the model for a subset of marine-terminating glaciers. The differences are between the model output before accounting for frontal ablation and after accounting for frontal ablation in points along the main flowline. The x-axis has been normalised.

experience an increase in ice velocity towards the terminus. This increase of velocities is due to an increase of the mass flux (and therefore ice thickness) when we account for frontal ablation.

These results highlight the importance of applying a frontal ablation parameterisation at the initialisation stages of the model in order to recreate a realistic tidewater glacier behaviour. Without this extra term on the mass balance, velocities and ice thicknesses go to zero towards the terminus. This is not only a problem for the inversion procedure: these unrealistic features will also affect the dynamical runs realised with the forward model, i.e. any calving parameterisation applicable in the future will rely on a realistic bedrock to work properly.

Note that these velocities are not surface velocities but average section velocities. Annual surface velocities would have to be estimated from these values and the vertical profile of velocity in order to be compared to observations. Furthermore, since we run OGGM under an equilibrium assumption, the results

presented here will not reflect the transient states that appear in observations. The usefulness of any comparison to other data (observed or modeled) is therefore limited. Additionally, some of the velocity maps in Alaska previously published (e.g. Burgess et al., 2013) are computed with many glaciers undergoing significant interannual velocity variability over the observation interval and only one velocity snapshot is included in the maps. Velocities might thus not represent long term average. However, comparing surface velocities derived from OGGM with observations might be useful when no previous estimates of frontal ablation fluxes exist in a RGI region (e.g. Greenland), providing another way of calibrating OGGM parameters.

3.4.4 Sensitivity studies in Alaska marine-terminating glaciers

We perform different sensitivity experiments to study the influence of i) the calving constant of proportionality k, ii) Glen's temperature-dependent creep parameter A and iii) sliding velocity parameter, on the regional frontal ablation of Alaska. The results of these experiments are shown in Fig. 3.7. In the first experiment we vary the calving constant of proportionality k in a range of 0.24 - 2.52 yr^{-1} and used the model default values for Glen A and sliding parameter. Fig. 3.7a shows that our estimate for the regional frontal ablation matches the regional estimate by McNabb et al. (2015) if k has an approximated value of 0.63 yr^{-1}, in the case of excluding sliding ($f_s = 0$), or if k is equal to 0.67 yr^{-1} in the case of including a sliding velocity (with $f_s = 5.7{\times}10^{-20}$ s^{-1} Pa^{-3}). It is important to emphasize that the regional frontal ablation from McNabb et al. (2015) only comprises 27 glaciers but that they represent an estimated 96% of the total frontal ablation of Alaska.

We then keep these two values of k and vary the values of Glen A creep parameter and sliding parameter (f_s). The results are shown in Fig. 3.7 b and c. It is well known that ice flow models are sensitive to the values chosen for parameters describing ice rheology and basal friction (e.g. Brondex et al., 2017; Enderlin et al., 2013a). As expected, our frontal ablation estimates are also sensitive to different values of Glen A and sliding parameter, but highly dependent on different values of k, at least for the first part of the k values range (0.24 - 0.80 yr^{-1}). The linear relationship between $q_{calving}$ and k at the start of the curve in Fig. 3.7a is mainly a consequence of the calving law used in the parameterisation. For larger k values ($\geq$ 0.8 yr^{-1}) the shape of the curve is due to OGGM's physical constraint of clipping μ^* to zero and calculating the

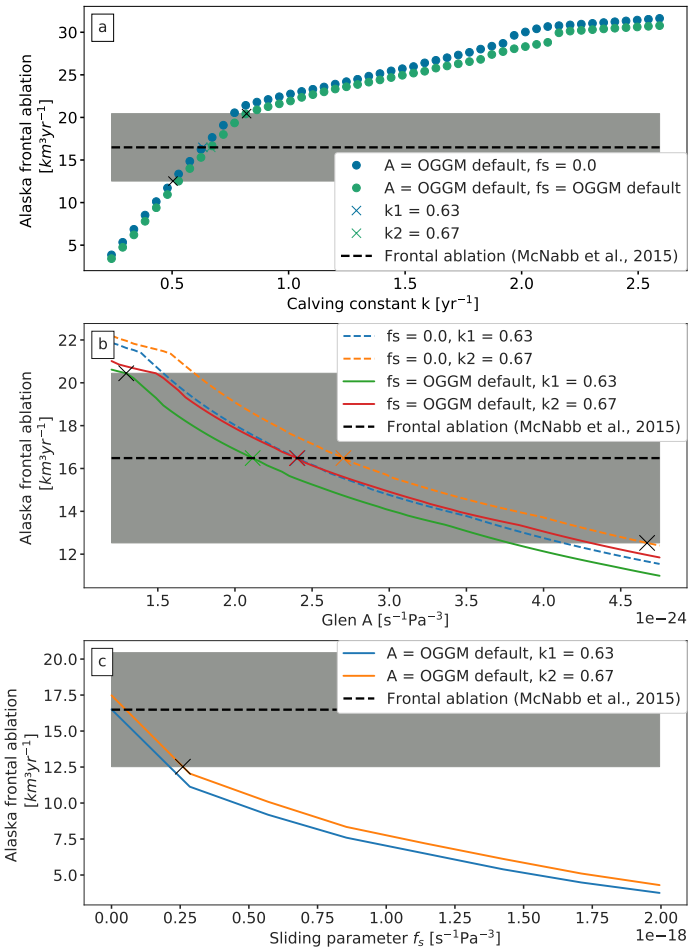

Figure 3.7: Total frontal ablation of Alaska marine-terminating glaciers computed with varying OGGM parameters. The dashed dark line indicates the Alaska regional frontal ablation calculated by McNabb et al. (2015), light gray shading indicating the standard errors as provided in the study. **a:** sensitivity on calving constant of proportionality (k); **b:** sensitivity on Glen's A parameter, the coloured dashed lines represent zero sliding; **c:** sensitivity on sliding parameter (f_s). Crosses in all plots represent the intercepts between OGGM frontal ablation estimates and McNabb et al. (2015). Note the different y-axis ranges.

maximum $q_{calving}$ allowed by the local climate (see Sect.3.3.3).

Maussion et al. (2019) showed that both sliding and ice rheology (A) have

a strong influence on OGGM's computed ice volume, hence a strong influence on the thickness of the glacier and in this case the frontal ablation estimate. Like in Maussion et al. (2019); Fig. 3.7 shows that one could always find an optimum combination of Glen A and sliding parameters that lead to (in this case) previously calculated frontal ablation estimates. Enderlin et al. (2013a) also showed that when such flowline models are applied to a tidewater glacier, there is a non-unique combination of these parameter values that can produce similar stable glacier configurations, making k, Glen A and f_s parameters highly dependent on observations of either frontal ablation, ice velocity or glacier ice thickness.

3.4.5 Regional volume of marine-terminating glaciers for different model configurations

Finally, we compute the total volume of marine-terminating glaciers for different "equally good" parameter sets based on the results of Fig. 3.7 a, b and c. Each configuration is constructed by finding the intercepts between the model frontal ablation estimates and the regional estimate from McNabb et al. (2015), including the intercepts to the lower and upper error (see Fig. 3.7). A summary of the different parameter sets used for each model run can be found in Table 3.1 and the results of each configuration are shown in Fig. 3.8. Each configuration was run twice: once setting $q_{calving} = 0$, then a second time accounting for frontal ablation.

Similarly to the results shown in sections 3.4.1 and 3.4.2, Fig. 3.8 shows that there are significant differences between total volume estimates without and with accounting for frontal ablation. Volume estimates after accounting for frontal ablation are 11.7 to 19.7% higher than the volume estimates ignoring frontal ablation, considering all model configurations shown in Table 3.1, indicating a robust relationship. We find that there are no significant differences between the resulting volumes for different k values and that the differences in volume estimates between configurations are mainly due to adding or ignoring a sliding velocity or varying the value of the Glen A creep parameter.

Additionally, we also calculate the regional ice volume below sea level. The results for Columbia Glacier discussed in section 3.4.1 might create the impression that the differences in thickness along the main centerline, with and without accounting for frontal ablation, are not relevant for the potential glacier contri-

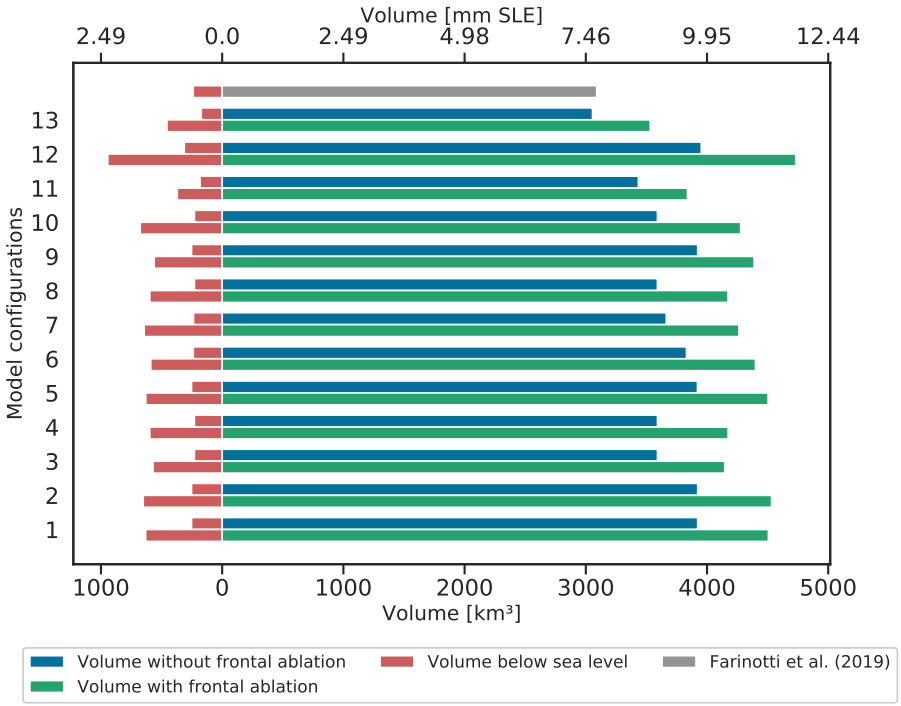

Figure 3.8: Total volume of Alaskan marine-terminating glaciers before (blue) and after (green) accounting for frontal ablation, and the total volume below sea level (red) before and after accounting for frontal ablation. The light shading color bars represent configurations obtained from finding the intercepts between OGGM frontal ablation estimates and the lower and upper error provided by McNabb et al. (2015). The grey bar represent the consensus estimate for these glaciers obtained by Farinotti et al. (2019). The descriptions for each configuration can be found in Table 3.1.

bution to sea-level rise, since most of the differences in thickness (grey and black line in Fig. 3.4c) are found below sea level. However, Fig. 3.8 shows that considering the whole region, a significant fraction of the total volume difference is found above sea level, implying that accounting for frontal ablation will directly impact the estimate of these glacier's potential contribution to sea-level rise. By introducing frontal ablation, the volume estimate of marine-terminating glaciers in Alaska is increased from 9.18 ± 0.62 to an average of 10.61 ± 0.75 mm SLE, of which 1.52 ± 0.31 mm SLE are found to be below sea level (instead of only 0.59 ± 0.08 without). The uncertainties presented here are the standard deviation

Table 3.1: Different model configurations applied to marine-terminating glaciers of Alaska. OGGM default values for Glen A = 2.4×10^{-24} s^{-1} Pa^{-3} and f_s = 5.7×10^{-20} s^{-1} Pa^{-3}. The experiments below the line represent configurations obtained from finding the intercepts between OGGM frontal ablation estimates and the lower and upper error provided by McNabb et al. (2015).

Experiment	Calving constant k [yr^{-1}]	Glen A creep parameter [s^{-1} Pa^{-3}]	Sliding parameter f_s [s^{-1} Pa^{-3}]
1	0.63	default	$f_s = 0.0$
2	0.67	default	$f_s = 0.0$
3	0.63	default	default
4	0.67	default	default
5	0.63	2.41×10^{-24}	$f_s = 0.0$
6	0.67	2.70×10^{-24}	$f_s = 0.0$
7	0.63	2.11×10^{-24}	default
8	0.67	2.40×10^{-24}	default
9	0.50	default	$f_s = 0.0$
10	0.82	default	default
11	0.67	4.67×10^{-24}	$f_s = 0.0$
12	0.63	1.29×10^{-24}	default
13	0.67	default	2.59×10^{-19}

of the model configurations shown in Tab. 3.1. The consensus estimate from Farinotti et al. (2019) for these glaciers is 7.68 mm SLE, 27.58% lower than our average estimate of 10.61 ± 0.75 mm SLE.

3.5 Discussion

We have shown that the model is capable of computing regional frontal ablation estimates by tuning model parameters with published regional-scale esti-

mates of frontal ablation, but the question of model performance for individual glaciers still remains open. In areas with no observational data or previous knowledge of frontal ablation, OGGM could make use of physical constraints (e.g. that μ^* must be greater than zero) as well as bathymetry and terminus width estimates to calibrate the model at the glacier scale. In the following section, we will explain such calibrations, discuss other parameters that affect frontal ablation estimates and discuss these estimates for individual glaciers.

In all previous model runs, we used the standard OGGM terminus geometry computation without correcting the width and water depth at the glacier front using potentially known values from other sources. As a result, not all of the glaciers classified as marine-terminating glaciers in the RGI produce a frontal ablation flux in OGGM (6 glaciers). This is mainly due to a wrong estimation of the water depth from free-board. These glaciers typically have a high terminus elevation (e.g. $E_t = 151.96$ m. a.s.l for the Chenega Glacier, RGI60-01.09639), for which the only possible value of $q_{calving}$ that complies with both the calving law and the ice thickness inversion model of OGGM is a $q_{calving} = 0$, since there is not enough mass turnover to grow a calving front under our mass conservation assumptions (see Sect. 3.3.3). The wrong water depth estimation can thus be best explained by a poor surface altitude estimation at the calving front (E_t). The problematic surface altitude estimation in turn can probably be explained by a mismatch between the acquisition dates of the DEM and the glacier outline.

Maussion et al. (2019) noted that a number of glaciers will suffer from poor topographic information, especially those located in the high latitudes. Most marine-terminating glaciers are located in regions where cloud free satellite measurements are rare. Therefore, the DEM of these regions might present errors (e.g. A wrong elevation at the terminus and/or a date of data acquisition which does not match that of the RGI outlines) that will spread to water depth estimations from free-board (see Eq. 4.5). The possibility of using higher resolution DEM's such as the ArcticDEM was explored during this study but was quickly eliminated because of large data voids present on the data, especially for big glaciers (e.g. Hubbard Glacier). However, new data sets such as the TanDEM-X (Wessel et al., 2018) are currently being explored for future versions of OGGM.

For 36 marine-terminating glaciers, we assess the model performance in comparison to the estimates by McNabb et al. (2015), with and without corrections for these errors (Fig. 3.9a). Calving front widths were corrected with the Alaska Tidewater Glacier Terminus Positions database (McNabb and Hock, 2014). The

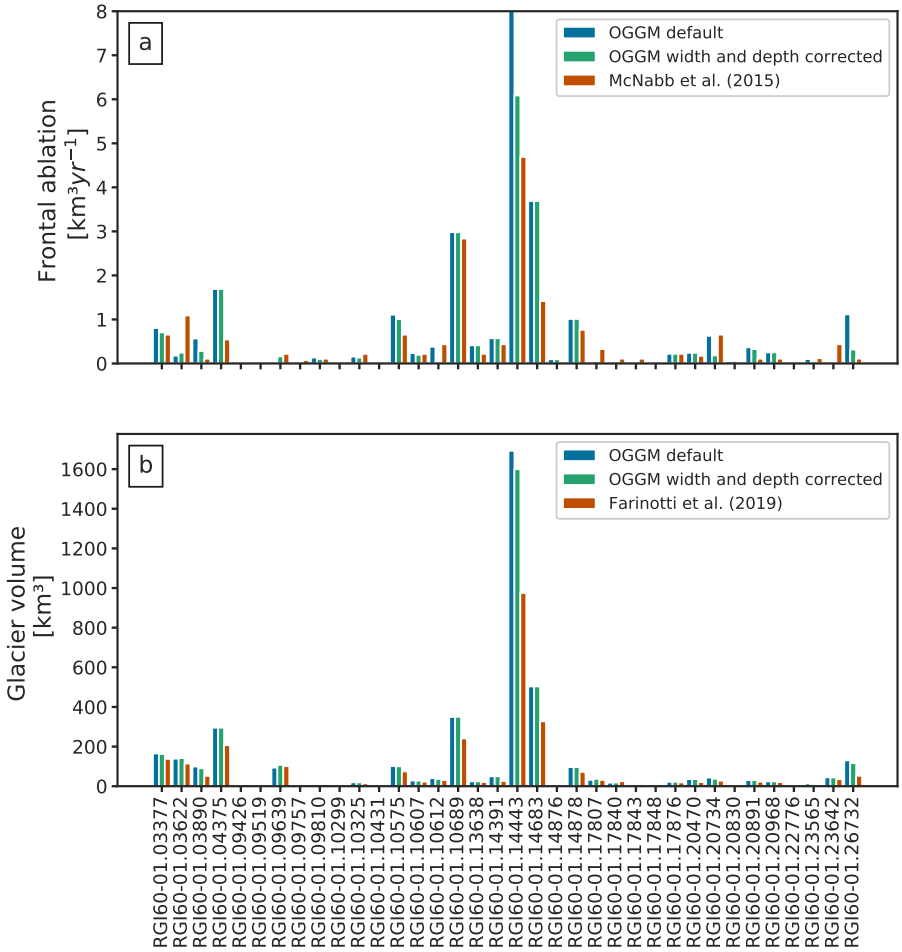

Figure 3.9: Comparison of OGGM (blue and green) $q_{calving}$ and volume estimates for 36 glaciers to **a:** frontal ablation estimates computed by McNabb et al. (2015) and **b:** volume estimates from Farinotti et al. (2019) (red bars). Both OGGM estimates were calculated using default values of k, A and f_s (blue) and correcting the width and water depth at the calving front (green). Note that in a, the Hubbard Glacier (RGI60-01.14443) is off scales if no correction is applied to the width and depth of the calving front (blue).

database contains terminus positions for 49 marine-terminating glaciers. Since three of these glaciers (Grand Pacific, Hubbard and Sawyer Glacier) were merged with their respective pair branches (Ferris, Valerie and Sawyer western Glacier), we are left with a total of 46 glacier terminus widths. The widths are computed

by selecting the terminus positions closest to the glacier's RGI outline and by averaging the widths that resulted from the projection of the vector lines selected. These widths are used to correct OGGM's flowline width at the calving front in the cases where the model is not able to represent the real calving front width. The last flowline width at the front of the glacier is then clipped to the width value estimated from the database. To smooth the transition between the clipped value and OGGM's flowline width, we linearly interpolate between the clipped value and 5 pixels upstream on the flowline. We then correct the modified widths to preserve the same glacier area than the RGI's. By doing this, we slightly modify the altitude-area distribution of the glacier.

Additionally, multi-beam bathymetry data from NOAA National Centers for Environmental Information (2004) was used to estimate the water depth in front of the glacier terminus. This data was used only for glaciers where the DEM resolution would not allow an estimate of the water depth from elevation data and ice thickness (free-board). The bathymetry data was compiled into a raster format and provided to us by Robert McNabb (pers. comm.). Both corrections were used for Fig. 3.9 only.

Fig. 3.9a demonstrates that without calibrating any OGGM parameter (only using the model default values for Glen A, f_s and k), but making use of additional data (e.g. terminus positions and bathymetry), we are able to estimate a frontal ablation flux for individual glaciers within the same order of magnitude as those estimated by McNabb et al. (2015). The model root mean square error (RMSE) is reduced from 1.08 km^3 yr^{-1} (mean deviation of 0.28) to 0.53 km^3 yr^{-1} (mean deviation of 0.11). Even though part of these errors may arise from the fact that glaciers are in a disequilibrium state at the time of the McNabb et al. (2015) estimate, errors in boundary conditions (e.g., topography date not coinciding with the glacier outline date and uncertainties in the frontal width) and plain model errors also contribute. By using bathymetry and real terminus width estimates we improve the boundary conditions of the parameterisation that are highly dependent on the DEM quality.

When these corrections (terminus width and water depth) are not implemented and errors occur while estimating the real terminus geometry, OGGM has to rely on clipping μ^* to be larger than or equal to zero, setting a physical limit where the frontal ablation flux for each individual tidewater glacier cannot be larger than its annual accumulation ($p_f P_i^{Solid}(z)$). This is not ideal, because it implies that all of the glacier's ablation in an equilibrium setting is due to frontal

ablation and no surface melt occurs, which is unrealistic in the climate conditions of Alaska. For applications on the global scale, bathymetry data and terminus mapping will be very valuable in regions with poor topographic resolution and where no observations of frontal ablation exist.

Additionally, we compare our final glacier volume estimates with the default configuration and by correcting the terminus geometry. These results are shown in figure Fig. 3.9b, together with the consensus volume estimate for each glacier from Farinotti et al. (2019). Fig. 3.9b shows that even if these corrections to the glacier terminus might have a large effect on the frontal ablation flux for some glaciers (e.g. Hubbard glacier), the effect is not as big as if we do not account for frontal ablation at all. This is the case of the consensus estimate from Farinotti et al. (2019) (red bars in Fig. 3.9b), where the models used do not account (or crudely account) for this extra lost of mass when inverting for the ice thickness.

3.6 Conclusions

We have implemented a frontal ablation parameterisation into OGGM and shown that inversion methods ignoring frontal ablation systematically underestimate the mass flux and thereby the thickness of calving glaciers. Accounting for frontal ablation in ice thickness inversion methods based on mass conservation (as listed in Farinotti et al., 2017) increases estimates of the regional ice mass stored in marine-terminating glaciers by approximately 11 to 19 %. While for individual glaciers, ice volume may be underestimated by up to 30% when ignoring the impact of frontal ablation, the effect is independent of the size of the glacier. Implementing a frontal ablation parameterisation allows OGGM to represent a non-zero thickness calving front, which is necessarily the case when no ice flux is assumed to cross the glacier terminus. This parameterisation is key for initialising the glacier's thickness in the model.

The model was able to reproduce previously calculated regional frontal ablation estimates by finding the best combination of values for k, Glen's A and the sliding parameters. Note that this comparison is limited by the equilibrium condition imposed on OGGM during initialisation, which is not the case in observations. The best-performing parameter set for transient runs of OGGM may be different.

Our sensitivity studies also show that the differences in thickness, between

adding or not frontal ablation to the MB model, occur mainly at the lower parts of the glacier, but often above sea level. This indicates that not accounting for frontal ablation will have an impact on the estimate of this glacier's potential contribution to sea-level rise.

Additionally, our experiments highlight the need for bathymetry data and terminus mapping, as they may constrain model parameters when the DEM quality is not sufficient to provide a realistic estimate of the terminus geometry.

3.7 Code availability

The OGGM software together with the frontal ablation parameterisation module are coded in the Python language and licensed under the GPLV3 free software license. The latest version of the OGGM code is available on Github (`https://github.com/OGGM/oggm`), the documentation is hosted on ReadTheDocs (`http://oggm.readthedocs.io`), and the project webpage for communication and dissemination can be found at `http://oggm.org`. The code and data used to generate all figures and analyses of this paper can be found at `https://github.com/bearecinos/cryo_calving_2019`. The OGGM version used for this study is available in a permanent DOI repository (`https://doi.org/10.5281/zenodo.2580277`).

3.8 Acknowledgements

BR was supported by the DFG through the International Research Training Group IRTG 1904 ArcTrain. We would like to thank Robert McNabb for providing the Columbia Glacier thickness map and the bathymetry data which he compiled into raster formats. We also thank Chris Miele for discovering issues with the code and for helping extracting the water depth from the bathymetry raster files. We thank the editor Etienne Berthier, Douglas Brinkerhoff and an anonymous referee for their thoughtful reviews of this paper.

4

Paper III: Calibration of a frontal ablation parameterization applied to Greenland's peripheral calving glaciers.

Recinos, B., Maussion, F., Noël, B., Möller, M. and Marzeion, B.

Abstract

Greenland Peripheral Glaciers (PGs) are glaciers that are weakly or not connected to the Ice Sheet. Many are tidewater, losing mass via frontal ablation. Without regional observations or enough individual estimates of frontal ablation, constraining model parameters remains a challenging task. We present two independent methods to calibrate the calving parameterization implemented in the Open Global Glacier Model. We estimate an average regional frontal ablation flux for PGs of 8.17Gt yr^{-1} after calibrating the model with velocity observations, and of 1.63Gt yr^{-1} if the model is constrained using frontal ablation fluxes derived from independent modeled Surface Mass Balance (SMB) averaged over an equilibrium reference period. This second method is based on the assumption that most PGs during that time have an equilibrium between mass gain via SMB and mass loss via frontal ablation. This assumption can serve as a basis to assess the order of magnitude of dynamic mass loss of glaciers when compared to the SMB imbalance. Results show that by introducing frontal ablation and calibrat-

ing the model with velocity observations, volume estimates increased from 11.02 to 12.56mm SLE and to 11.29mm SLE when using the second method. These changes are also reflected in the volume below sea level.

4.1 Introduction

At its rapidly warming margins (Shepherd et al., 2020), the Greenland Ice Sheet (GrIS) is surrounded by (semi-) detached glaciated areas, commonly referred to in the literature as Peripheral Glacier and Ice caps (PGs) (Bjørk et al., 2018; Rastner et al., 2012). These are bodies of ice that are not dynamically coupled to the ice sheet, since they are either entirely detached, or separated from the ice sheet by well-defined ice divides. All PGs in Greenland including those strongly connected to the ice sheet cover an ice area of 89,720 ± 2,781 km^2 (Rastner et al., 2012), approximately 12% of the world's total glaciated area, playing an important role on Greenland's freshwater export. According to Bolch et al. (2013), all glaciers and ice caps (including those with strong but hydrologically separable connections) lost 40.9 ± 16.5 Gt yr^{-1} (0.12 ± 0.05 mm SLE). A significant fraction (up to 14 or 20%) of the reported overall mass loss of Greenland and up to 10% of the estimated contribution from the world's glaciers and ice caps to sea level rise (Bolch et al., 2013). For the same period Noël et al. (2017) estimated a mass loss of 40 ± 16 Gt yr^{-1}. In a scenario of continued global warming, Greenland's PGs may lose 19-28% (7.5 - 11 mm) of their volume by 2100 (Machguth et al., 2013).

Despite this significant contribution, their mass balance variability and overall thickness distribution have been difficult to quantify on multi-decal timescales, mainly due to an absence of long-term data (Bjørk et al., 2018). In general, most studies of the GrIS do not separate sea-level rise contributions between PGs and the ice sheet, making it difficult to differentiate if the PGs have already been included in reported global mean sea-level rise estimates (Bolch et al., 2013). This is probably related to issues of the ice sheet model grid scale and the size of the PGs. Noël et al. (2017) addressed this issue, separating the GrIS and all glaciers and ice caps mass loss contribution by using a 1 km surface mass balance product, evaluated against in situ and remote sensing data, and quantify the mass loss of all Greenland's glaciers and ice caps. However, in the study changes in solid ice

discharge are assumed to be negligible. The loss of mass from tidewater glaciers to the ocean through frontal ablation (i.e., calving, subaerial and subaqueous frontal melting) is a major component of the mass budget of the Greenland Ice Sheet (GrIS) (Cowton et al., 2018; King et al., 2018, 2020; Mankoff et al., 2019). The 2010 through 2019 average ice discharge through flux gates as estimated by Mankoff et al. (2019) is nearly 487 ± 49 Gt yr^{-1} with King et al. (2020) reporting similar values. Therefore, it is reasonable to assume that frontal ablation will also be a major component of the mass budget of PGs, strongly affecting their ice dynamics, and thus frontal ablation fluxes are substantial to assess the amount of ice stored in PGs and their potential contribution to sea-level rise.

While there are volume estimates from global glacier models for PGs (e.g. all models compared in Farinotti et al., 2019), some of the models used do not explicitly take frontal ablation processes into account. Other large regional studies (King et al., 2020; Mankoff et al., 2019) estimate ice sheet wide discharge focusing on outlet glaciers. Mankoff et al. (2019) presented a new dataset of flux gates and a 1986 through 2019 glacier-scale ice discharge estimate for the Greenland Ice Sheet and outlet glaciers, but most PGs are located outside the study region. PGs that are weakly or not connected to the ice sheet and slow moving glaciers (slower than 100 m yr^{-1}) are not included in the study ice discharge. There are no comprehensive regional observations or individual estimates of frontal ablation for PGs and little is known about their calving front geometry. Consequently, it is important to investigate not only the ice sheet but also these local glaciers most of which terminate in the ocean. That is approximately 25% of the total glaciated area in the region outside the main ice sheet as shown in Fig. 4.1.

Recinos et al. (2019) showed that when ignoring frontal ablation in ice thickness inversion methods based on mass conservation (as listed in Farinotti et al., 2017), most glacier models (including the volume consensus estimates from all glacier models compared in Farinotti et al., 2019) systematically underestimate the regional ice mass stored in tidewater glaciers by approximately 11 to 19% in the Alaska region. For individual glaciers ice volume may be underestimated by up to 30% when ignoring the impact of frontal ablation, independently of the size of the glacier.

In this study, we present a regional estimate of mass loss through frontal ablation for all PGs that are weakly connected to the Ice sheet (see study area Fig. 4.1b). We use the Open Global Glacier Model (OGGM v1.2.0 Maussion et al., 2019) and the calving parameterization described in Recinos et al. (2019) to

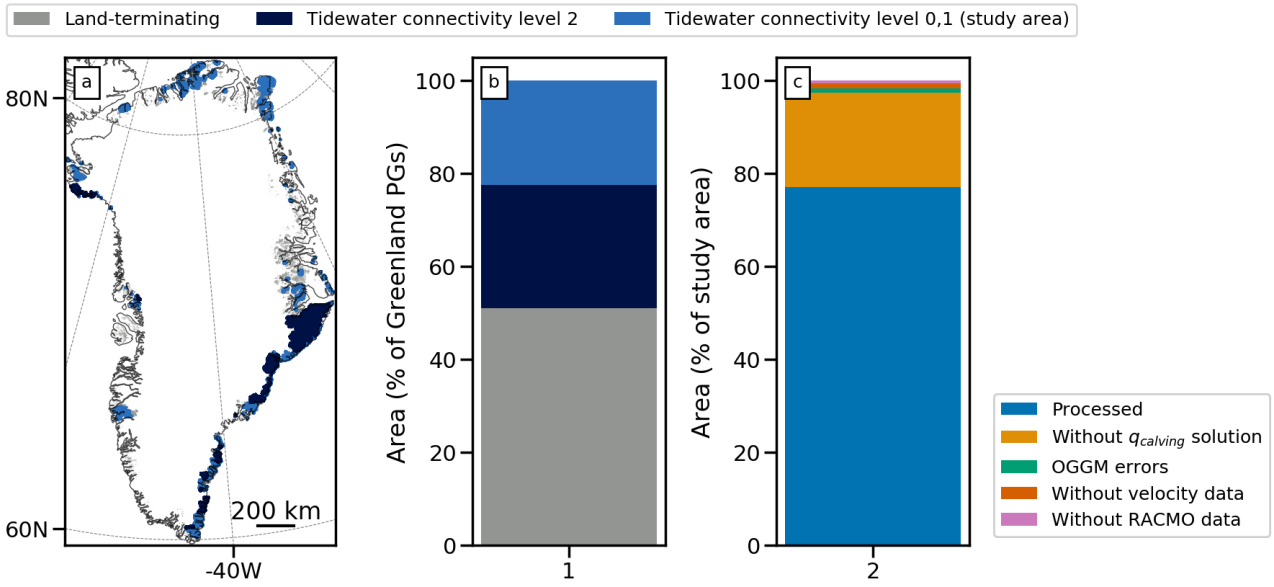

Figure 4.1: Study area overview. **a:** map with the PG distribution; the different colors indicate the outlines of the PGs classified as land-terminating (grey outlines) and marine-terminating glaciers (dark and light blue outlines) in the Randolph Glacier Inventory (RGI v6.0). Dark blue outlines indicate tidewater glaciers with connectivity level 2 and light blue outlines indicate tidewater glaciers with connectivity levels 0 and 1, which are the focus of this study. **b:** fraction of the ice sheet area covered by each glacier category in percent. **c:** percentage of the study area (light blue in b.) that can and cannot be modeled by OGGM due to preprocessing errors, gaps in observational data, or for which no calving value can be determined by the parameterization (more details in Sect. 4.5).

simulate frontal ablation fluxes for Greenland's tidewater PGs (also referred to as just PGs in this study) and compute their volume and ice thickness distribution. By accounting for frontal ablation estimates of each individual PG, we improve the first glacier thickness estimate and volume computed by OGGM and the overall improvement of bed-rock topography at the calving front for PGs.

The simple calving law implemented in OGGM by Recinos et al. (2019) was calibrated using regional and individual estimates of frontal ablation of 27 tidewater glaciers. However, these type of regional scale estimates do not exist for

Greenland. Here, we present two independent methods to calibrate the calving parameterization. The first method calibrates the parameterization using surface velocity fields derived from the MEaSUREs Multi-year Greenland Ice Sheet Velocity Mosaic (MEaSUREs v1.0 Joughin and Scambos., 2016). The second method uses Surface Mass Balance (SMB) estimates from the monthly output of the polar Regional Atmospheric Climate Model version 2.3p2 (RACMO2.3p2 Noël et al., 2019), statistically downscaled to 1 km resolution following Noël et al. (2016).

Both calibration methods make equilibrium assumptions for the ice dynamics and mass balance processes. We assume that the average amount of ice that passes through the glacier terminus in a mass balance year (average frontal ablation flux estimated by the calving law) must be equal to the amount of ice delivered to the terminus (ice flux estimated from the distribution of the mass). By assuming such equilibrium conditions, we estimate parameter values for each individual PG. We i) compare the difference of parameter values, frontal ablation and calving rate estimates between the two calibration methods, ii) investigate how the parameter values vary with glacier-specific characteristics (e.g. slope, width, average solid precipitation and temperature sensitivity) iii) quantify the effect of accounting for frontal ablation on the first ice thickness estimation of OGGM and on the ice volume and volume below sea level estimates for PGs. By using two independent calibration methods and comparing output of the model after calibration, we determine at which degree PGs have an equilibrium between their climatic mass balance and the dynamic discharge of ice into the ocean. If the results of both calibration methods were to be the same for a particular PG, we could assume that the glacier's solid ice discharge (best represented by calibrating the model with velocity observations) is in equilibrium with the glacier's climatic mass balance (best represented by the second method and the RACMO SMB data).

4.2 Input data and pre-processing

4.2.1 Glacier outlines and local topography

We use the glacier outlines defined in the region 5 of the Randolph Glacier Inventory (RGI v6.0, Pfeffer et al., 2014). We only include in our simulations glaciers that are classified as marine-terminating glaciers (also referred to as

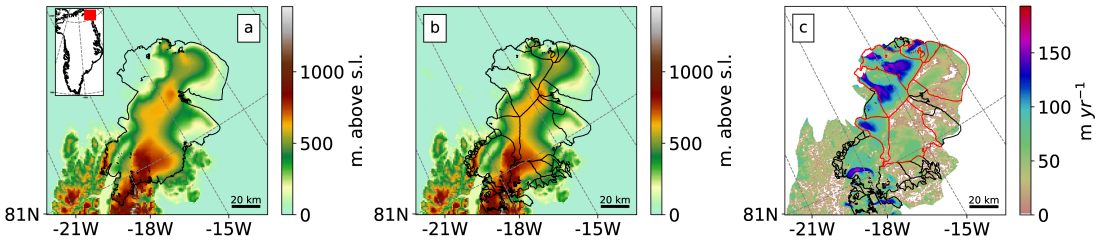

Figure 4.2: Flade Isblink Ice Cap outlines (black and red lines), topography and surface velocity (color maps). **a:** original outline from the RGIv6.0. (ID RGI60-05.10315) **b:** subdivided outline processed using ArticDEM data and velocity fields from the Greenland 250 m velocity mosaic (Joughin and Scambos., 2016). **c:** velocity fields over the ice cap. The tidewater basin outlines are highlighted in red.

tidewater glaciers in this study) with a weak or no connection to the ice sheet (see map in Fig. 4.1). Those are glaciers with a level of connectivity 0 and 1 in the RGI attributes (Rastner et al., 2012). From these outlines, only one entity has been manually modified. The Flade Isblink Ice Cap (ID no. RGI60-05.10315) is located in North-East Greenland (see Fig. 4.2a). In the RGI v6.0, this ice cap is a single glacier entity not subdivided into basins and is classified as a whole as marine-terminating (Fig. 4.2a). An improved outline was provided by Philipp Rastner (pers. comm.), containing individual drainage basins. It was processed using the ArcticDEM topograhic data (Porter et al., 2018) resampled to 25 m resolution (Fig. 4.2b). The tidewater basins were manually identified using velocity fields from the MEaSUREs Multi-year Greenland Ice Sheet Velocity Mosaic, v1.0 (Joughin and Scambos., 2016). The Flade Isblink Ice Cap features several water terminating basins 4.2c (red outlines) but according to velocity observations only five are active basins as shown in Fig. 4.2c.

In OGGM, a local map projection is defined for each glacier entity in the inventory following the methods described in Maussion et al. (2019). We use a Transverse Mercator projection centred on the glacier in order to conserve distances, area and angles. Then, topographical data is selected automatically and interpolated to the local grid. All DEM's are re-sampled to a resolution depending on the glacier size (Maussion et al., 2019) and smoothed with a Gaussian filter of 250 m radius.

For Greenland, OGGM uses the Greenland Mapping Project (GIMP) Digital Elevation Model (Howat et al., 2014) (data acquisition: 2003 to 2009). The possibility of using higher resolution DEM's such as the ArcticDEM was explored during this study but the velocity observations and the SMB data from RACMO utilise surface topography prescribed from a down-sampled version of GIMP (Joughin and Scambos., 2016; Noël et al., 2016; Noël et al., 2019). Therefore, we choose GIMP in order to maintain consistency. The velocity observations and RACMO SMB are both used to calibrate the calving constant of proportionality k in OGGM's calving law.

4.2.2 Glacier flowlines, catchment areas and widths

The glacier centrelines are computed following an automated method based on the approach of Kienholz et al. (2014). The centrelines are then filtered and interpolated to a constant grid spacing (see Fig. 4.3c). The geometrical widths along the flowlines are obtained by intersecting the normals at each grid point with the glacier outlines and the tributaries' catchment areas. Each tributary and the main flowline has a catchment area, which is then used to correct the geometrical widths (see Fig. 4.3d). This process assures that the flowline representation of the glacier is in close agreement with the actual altitude-area distribution of the glacier. The width of the calving front, therefore, is obtained from a geometric first guess, which may lead to uncertainties in the frontal ablation computations as shown in Recinos et al. (2019). Uncertainties in the terminus geometry can in this case be compensated by calibrating the k parameter with observations (see Sect. 4.4).

4.2.3 OGGM climate data and surface mass balance observations

The mass balance (MB) model implemented in OGGM uses monthly time series of temperature and precipitation. The current default is to use the gridded time-series dataset CRU TS v4.01 (Harris et al., 2014), which covers the period of 1901-2015 with a 0.5° resolution. This raw, coarse dataset is downscaled to a higher resolution grid (CRU CL v2.0 at 10' resolution, New et al., 2002), following the anomaly mapping approach described in Maussion et al. (2019). This provides OGGM with an elevation-dependent climate dataset from which the temperature and precipitation at each elevation of the glacier are computed,

and then converted to the local temperature according to a temperature gradient (default: 6.5 K km^{-1}). No vertical gradient is applied to precipitation, but a correction factor p_f =2.5 is applied to the original CRU time series . This correction factor can be seen as a large scale correction for orographic precipitation, avalanches, and wind-blown snow. It must be noted that this factor has little (if any) impact on the mass-balance model performance in terms of bias but might lead to larger uncertainties on mass-balance profiles, mass-turnover in the glacier and therefore also frontal ablation. The MB model (see Sect. 4.3.2) is calibrated with direct observations of the annual surface mass balance (SMB). For this, OGGM uses reference surface mass balance data from the World Glacier Monitoring Service (WGMS, 2017).

4.2.4 Glacier surface velocity observations

We use surface velocity fields derived from the MEaSUREs Multi-year Greenland Ice Sheet Velocity Mosaic, v1.0 (Joughin and Scambos., 2016) at 250 m resolution. The data was collected between 1995 and 2015 and covers most of Greenland, as shown in Fig. 4.3a. For each glacier, a subset of velocity estimates and their errors are computed by interpolating the main flowline coordinates onto the velocity raster grid using nearest-neighbor method. We calculate the mean surface velocity at the lowest one third section of the main flowline and use this value to compare with model derived velocities (see more in Sect. 4.4.1). We also extract from the uncertainty mosaics the mean velocity error for the same section of the flowline. We focus on the last one third of the flowline to ensure that even if there are data gaps right at the calving front, we still obtain a reasonable estimate of average velocity close to the front. Most of the study area is covered by the velocity mosaic, only 1.0% (287.35 km^2) has no data coverage (see Fig. 4.1c).

4.2.5 Surface mass balance from RACMO

We use output of RACMO2.3p2 at 5.5 km (Noël et al., 2019), statistically downscaled to 1 km resolution following Noël et al. (2016). In brief, the model covers the period 1958-2018, and incorporates the dynamical core of the High Resolution Limited Area Model and the physics from the European Centre for Medium-Range Weather Forecast - Integrated Forecast System (ECMWF-IFS

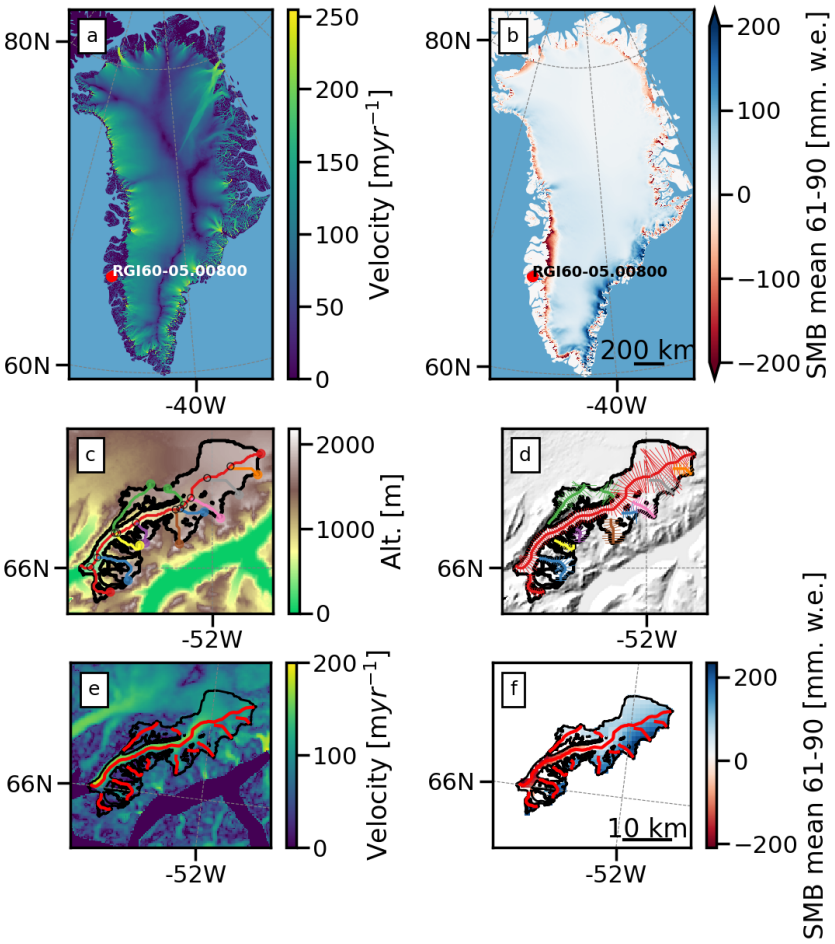

Figure 4.3: Input data and preprocessing steps using the glacier with ID RGI60-05.00800 as an example. **a:** Greenland 250 m velocity mosaic. **b:** OGGM topographical data preprocessing and computation of the flowlines. **c:** velocity data re-projected to the glacier grid. **d:** flowlines width correction according to the glacier catchment areas and altitude-area distribution. **e:** surface mass balance mean over 1960-1990, from the Regional Atmospheric Climate Model RACMO2.3p2, downscaled to 1 km and re-projected to the glacier grid. **f:** surface mass balance mean over 1960-1990, from the Regional Atmospheric Climate Model RACMO2.3p2, downscaled to 1 km.

cycle CY33r1). RACMO2.3p2 includes a multilayer snow module that simulates melt, water percolation, and retention in snow, refreezing, and runoff. The model also accounts for dry snow densification, and drifting snow erosion and sublimation. Snow albedo is calculated on the basis of snow grain size, cloud optical thickness, solar zenith angle, and impurity concentration in snow (Noël et al., 2019). RACMO2.3p2 is described in Noël et al. (2018), no model physics have been changed. However, increased horizontal resolution of the host model, i.e., 5.5 km instead of 11 km previously, better resolves gradients in SMB components over the topographically complex ice sheet margins and neighbouring peripheral glaciers and ice caps (Noël et al., 2019). RACMO does not estimate frontal ablation but provides and independent estimate of the PG's SMB. RACMO SMB has been extensively evaluated in Noël et al. (2019), by using accumulation measurements from stakes, firn pits, cores and airborne radar campaigns in the GrIS accumulation zone, as well as 1073 ablation measurements from 213 stake sites (see Noël et al. (2019) for more details). According to Noël et al. (2019), RACMO at 1 km resolution resolves SMB patterns over narrow glaciers and marginal ablation zones. As shown in Fig. 4.3b and f, the data covers the majority of PGs and its time resolution allows us to compute a glacier-wide SMB mean over several decades (e.g. 1960-1990). Only 0.61% of the study area (176.18 km^2) has no data coverage (see Fig. 4.1c). For each RGI entity, a glacier-wide SMB mean is estimated by generating a region of interest; all grid points outside the glacier outline are masked out as shown in Fig. 4.3f and a mean over all the pixels inside the glacier outline is computed. The SMB estimate is then used to calibrate the calving parameterization as explained in Sect. 4.4.2. In this study we use the state-of-the-art RACMO SMB for model calibration and evaluation.

4.3 Open Global Glacier Model (OGGM)

We use the Open Global Glacier Model (OGGM v1.2.0 Maussion et al., 2019) and the calving parameterization described in Recinos et al. (2019) to simulate frontal ablation fluxes for Greenland's tidewater PGs and compute their volume and ice thickness distribution. The mathematical framework of OGGM and the frontal ablation parameterization have been explained in detail by Maussion et al. (2019) and Recinos et al. (2019). However, in order to understand the calibration methods described in Sect. 4.4, we hereby summarize the ice thickness inversion, mass balance and frontal ablation modules.

4.3.1 Ice thickness

The ice thickness inversion scheme relies on a mass-conservation approach similar to that of Farinotti et al. (2009), and is fully automated. The ice thickness is computed from mass turnover and the shallow ice approximation along multiple flowlines.

The flux of ice q (m^3 s^{-1}) through a glacier cross-section of area S (m^2) is defined as:

$$q = \bar{u}S \tag{4.1}$$

with $\bar{u}$ being the average cross-section velocity (m s^{-1}). Following the approach described in Maussion et al. (2019), q can be estimated from the mass-balance field of a glacier. If u and q are known, S and the local ice thickness h (m) can also be computed by making some assumptions about the geometry of the bed and by solving Eq. 4.1. The default in OGGM is to use a parabolic bed shape for valley glaciers (unless the section touches a neighbouring catchment or neighbouring glacier via ice divides, computed from the RGI) and a rectangular bed shape for ice caps. For the last five grid points of tidewater glaciers, the bed shape is also assumed to be rectangular. Singularities with flat areas are avoided since the constructed flowlines are not allowed to have a local slope α below a certain threshold (default: 1.5°, see Maussion et al., 2019). Eq. 4.1 becomes a polynomial in h of degree 5 with only one root in R_+, easily computable for each grid point (see Maussion et al., 2019; Recinos et al., 2019, for more details).

4.3.2 Mass balance

OGGM's mass balance model is an extension of the model proposed by Marzeion et al. (2012b) and adapted in Maussion et al. (2019), to calculate the mass balance of each flowline grid point for every month, using the CRU climatological series as boundary condition. The equation governing the mass-balance is that of a traditional temperature index melt model. The monthly mass-balance m_i at elevation z is computed as:

$$m_i(z) = p_f P_i^{\text{solid}}(z) - \mu^* \, max\left(T_i(z) - T_{\text{melt}}, 0\right) \tag{4.2}$$

where P_i^{solid} is the monthly solid precipitation, p_f a global precipitation correction factor, T_i the monthly temperature and T_{melt} is the monthly mean air

temperature above which ice melt is assumed to occur (default: -1 $^{\circ}$C). Solid precipitation is computed as a fraction of the total precipitation: 100 % solid if $T_i <= T_{solid}$ (default: 0 $^{\circ}$C), 0 % if $T_i >= T_{\text{liquid}}$ (default: 2 $^{\circ}$C), and linearly interpolated in between. The parameter μ^* indicates the temperature sensitivity of the glacier, and it needs to be calibrated.

The MB calibration consists of searching a 31 year climate period in the past, during which the glacier would have been in equilibrium while keeping its modern-time geometry (a geometry fixed at the RGI outline's date), implying that the mass balance of the glacier during that period in time $m_{31}(t)$ is equal to zero.

By assuming $m_{31}(t) = 0$, OGGM calculates hypothetical μ candidates for each year t, following Eq. 4.2. For each $\mu(t)$ candidate, the model compares the MB observations and the model derived MB. A climatic period, centred at a year t^*, is determined where the bias of the modeled MB relative to observations is the smallest. t^* is then interpolated to nearby glaciers with no mass balance observations, to estimate their $\mu^* = \mu(t^*)$.

During the mass balance calibration of μ^*, only land-terminating glaciers are considered to find the correct climatic period t^*, since the approximation of a closed surface mass budget ($m_{31}(t^*) = 0$) cannot be extended to tidewater glaciers. For such glaciers, a steady state implies that:

$$\int m_{31}(t^*) = \frac{q_{calving}\ \rho}{A_{RGI}} \tag{4.3}$$

with $m_{31}(t^*)$ being the glacier-integrated mass-balance computed for a 31 yr period centred around the year t^* (e.g. $t^* = 1973$ for some glaciers in Greenland) and for a constant glacier geometry fixed at the RGI outline's date. $q_{calving}$ is the average amount of ice that passes through the glacier terminus in a year, for a glacier in equilibrium with the climate forcing. ρ is the ice density (900 kg m^{-3}) and A_{RGI} is the RGI glacier area. The steady state assumption of Eq.4.3 has direct consequences for the calibration of the temperature sensitivity parameter μ^* (for more information see sect 4.3.3 or referred to Recinos et al., 2019).

4.3.3 Calving law

The annual mean frontal ablation flux $q_{calving}$ (km^3 yr^{-1}) is computed as a function of the height *(h_f)*, width *(w)* and estimated water depth *(d)* of the

calving front, following the approach of Oerlemans and Nick (2005) and Huss and Hock (2015):

$$q_{calving} = max(0; kdh_f) \cdot w \tag{4.4}$$

k is a proportionality constant (which needs to be calibrated, see Sect. 4.4) with a default value of 2.4 yr^{-1} (Oerlemans and Nick, 2005; Recinos et al., 2019). The water depth (d) is estimated from the free-board, using elevation of the glacier surface at the terminus (E_t), and ice thickness (h_f) data obtained from the model output:

$$d = h_f - E_t + z_w \tag{4.5}$$

where z_w is the elevation of the water body with respect to sea level. The water depth (d) is estimated using the terminus elevation (E_t) obtained by projecting the RGI outline onto the DEM (i.e., the terminus elevation is assumed to be the top of the calving front). d is the bed elevation with respect to sea level and for tidewater glaciers, z_w is set to 0 m a.s.l. (for lake-terminating glaciers, it would be the level of the lake surface). In OGGM we solve for the ice thickness by prescribing that the amount of ice calved ($q_{calving}$) must be equal to the amount of ice delivered by ice deformation to the terminus calculated in Eq. 4.1 (see Recinos et al., 2019, for more details about the implementation and limits of the calving parameterization in OGGM):

$$q_{calving} = q_{deformation} \tag{4.6}$$

$q_{calving}$ varies with h_f as a polynomial of degree 2. $q_{deformation}$ is a polynomial in h_f of degree 5 (with Glen's flow law exponential constant $n = 3$), with an extra term in degree 3 if we account for a sliding velocity (see Sect. 4.4.1). Eq. 4.6 is therefore a polynomial that can be solved for h_f.

Implementation

We solve the polynomial in Eq. 4.6 numerically, via bound-constrained minimisation methods (algorithm provided by SciPy, Jones et al., 2001), which leads to a quick convergence. After finding the solution for the frontal ice thickness (h_f) and the corresponding frontal ablation flux ($q_{calving}$), we give this flux back to the mass balance model (Eq. 4.3), calibrate the temperature sensitivity of the glacier μ^* accordingly, and invert for a new ice thickness distribution for the entire glacier. This always results in a adjustment of μ^* towards lower values, thus

lowering the Equilibrium Line Altitude (ELA) and unbalancing the surface mass-budget, allowing a positive frontal ablation flux. Note that this re-calibration of the mass-balance model is always necessary (regardless of the choice of model parameters such as k or Glen's A) in order to reconcile mass-conservation and upstream ice thickness with frontal ablation.

For some glaciers, the flux estimated by the calving law (Eq. 4.4) is too large to be sustained by the modelled surface mass-balance: even without surface melt ($\mu^* = 0$), the total accumulation over the glacier is too small to close the frontal mass budget. This can be due to different factors, generally speaking either frontal ablation is overestimated, or solid precipitation is underestimated. The frontal ablation can be overestimated, e.g., if k and/or the calving law does not represent the dynamics of that particular glacier, or if h_f is overestimated. Only if no k value satisfies the mass balance condition of Eq. 4.6, μ^* is fixed to zero and the frontal ablation flux $q_{calving}$ is obtained by closing the mass budget instead of using the calving law (Recinos et al., 2019). However, in most cases (see Sect. 4.5.2) it is possible to find $\mu^* > 0$ compatible with a frontal ablation flux, by calibrating a glacier-specific k value.

4.4 Calibration of the calving parameterization

In the following sections, we present two methods for calibrating the k parameter in OGGM's calving parameterization. We do this by using two independent data products that focus on very different glacier processes: i) the ice dynamics and ii) the surface mass balance. We apply OGGM to all glaciers and ice caps in our study region (see Fig 4.1) and simulate frontal ablation fluxes and surface velocity estimates (see Sect. 4.4.1) by varying the k parameter (see Eq. 4.4) within a large range of values (0.01 - 3.0 yr^{-1}). For each k value, we compare the output of the model to i) satellite velocity observations and ii) frontal ablation fluxes derived from RACMO2.3p2 SMB means (see Sect. 4.4.2). This allows us to obtain a calibrated k value per method for each PGs.

The first method constrains the k parameter using velocity observations, thus frontal ablation fluxes will be consistent with satellite surface velocity observations and their uncertainty. Whereas the second method uses frontal ablation fluxes derived from RACMO2.3p2 SMB means over an equilibrium reference period to constrain k values, and is based on the strong assumption that most PGs during that time have a balanced budget (i.e. did not experience any mass loss

or gain).

According to Fettweis et al. (2017) the period between 1961-1990 has been considered as a period when the total mass balance of the GrIS was stable (Rignot and Kanagaratnam, 2006) and near zero. Results from all Modèle Atmosphérique Régional simulations (MAR, v3.5.2 Fettweis et al., 2017) indicate that the years from 1961 to 1990, commonly chosen as a stable reference period for Greenland SMB and ice dynamics, is actually a period of anomalously positive SMB ($\sim$ +40 Gtyr^{-1}) compared to 1900-2010. Reconstructions show that the SMB was particularly positive during those years (SMB was most positive from the 1970's to the middle of the 1990's), suggesting that a mass gain may well have occurred during this period, in agreement with results from Colgan et al. (2015). Noël et al. (2017) also estimate for the period of 1958-1996 a positive SMB trend ($\sim$ +1.11 $\pm$ 1.62 Gt yr^{-2}). The mass gain, according to Colgan et al. (2015), might have been only at a certain altitude a.s.l. due to mass being deposited there via ice dynamics (not directly gained via snowfall/accumulation).

Here we assume that most PGs also experienced the same equilibrium conditions and that their SMB should have also been positive, something that we can verify using RACMO SMB estimates (see sect. 4.4.2). More recent studies (e.g. Mouginot et al., 2019) suggest that PGs were in balance at the beginning of the seventies, and that the SMB of most of the GrIS was positive up until the year 2000. With the exceptions of the Northwest (NW) and Northeast (NE) sections where the SMB becomes slightly negative from 1972. Based on this literature research, we also consider the period from 1961-1990 as a stable reference period where we assume that the PGs in our study region were in equilibrium.

Considering an equilibrium between what the glacier gained and calved might not reflect real frontal ablation fluxes but such estimates serve as a base to estimate the dynamic mass loss of glaciers when combined with frontal ablation estimates constrained from velocity observations.

4.4.1 Method I: constraining k using velocity observations

For the first calibration method we compute modelled surface velocities along the main flowline after estimating a glacier thickness distribution per k value. OGGM relies on the shallow ice approximation (Cuffey and Paterson, 2010; Hutter, 1981, 1983; Oerlemans, 1997), thus assuming that the ice moves as a laminar flow, meaning that the z-component of the velocity equals zero. The creep rela-

tion can be written as Cuffey and Paterson (2010):

$$\frac{1}{2}\frac{du}{dz} = A\tau^n \tag{4.7}$$

with A being the ice creep parameter (which in OGGM has a default value of 2.4×10^{-24} s^{-1} Pa^{-3}), n the exponent of Glen's flow law (default: n=3) and τ the basal shear stress defined in OGGM as:

$$\tau = \rho g h_0 \alpha \tag{4.8}$$

with ρ the ice density (900 kg m^{-3}), g the gravitational acceleration (9.81 m s^{-2}), α the surface slope (computed along the flowlines) and h_0 the flowline ice thickness. For a constant ice density, the driving stress τ acting on a depth $h - h(z)$, within the glacier increases linearly from zero at the surface to τ_{basal} at the base. Then Eq. 4.7 can be written as:

$$u(z) = u_b + \frac{2A}{n+1}\tau^n h\,[1 - [1 - \frac{z}{h}]^{n+1}] \tag{4.9}$$

For velocities at the surface, Eq. 4.9 becomes:

$$u_s = u_b + \frac{2A}{n+1}\tau^n h \tag{4.10}$$

where u_b is the basal sliding velocity, estimated in OGGM using the following parametrization (Budd et al., 1979b; Oerlemans, 1997):

$$u_b = f_s \frac{\tau^n}{h} \tag{4.11}$$

with f_s a sliding parameter (default: 5.7×10^{-20} m^{-2} s^{-1} Pa^{-3}). We then estimate surface velocities following Eq. 4.10, for all the resultant glacier thicknesses h obtained with each k value (see sect. 4.3.1 and sect. 4.3.3 for detailed description of h estimation). Similar to the satellite observations, we calculate the model mean surface velocity u_s at the lowest one third section of the main flowline and use this value to compare with the satellite velocity estimate described in sect. 4.2.4. We then choose the k value that will result in both velocities (modeled and observed) being equal within a relative tolerance, given by the error in the satellite observation. We use the observational error to determine the maximum difference that we tolerate when comparing the model surface velocities with the satellite observations during the calibration.

However, there are cases where OGGM overestimates or underestimates the surface velocity (e.g. OGGM velocity is larger than upper bound limit of the observation) for all considered values of k. In this case we choose a k value that leads to the smallest difference between the model and either the upper or the lower bound of the observation (see sect. 4.6.1 for an overview of the model performance.)

4.4.2 Method II: constraining k values using SMB from RACMO

For the second calibration method we compute model frontal ablation fluxes for each k value and compare them with RACMO-derived frontal ablation fluxes. As explained at the beginning of this section, we consider the period from 1961-1990 as a stable reference period where the net mass change of the PGs was zero or close to zero and the PG SMB would have been positive. In a tidewater glacier, a closed mass budget will imply that the amount of ice being discharged from the glacier ($q_{calving}$ in Eq. 4.4) equals the amount of ice moved downhill via ice dynamic processes ($q_{deformation}$ in Eq. 4.1). According to the principles of mass conservation (Eq. 4.6 and 4.3), we can make the following assumption:

$$q_{calving,\ RACMO} = \frac{\bar{m}_{1961-1990} \cdot A_{RGI}}{\rho} \tag{4.12}$$

Where $\bar{m}_{1961-1990}$ is the RACMO SMB mean over the reference period, converted to flux units ($km^3\ yr^{-1}$) by multiplying by the RGI glacier area (A_{RGI}) and dividing by the ice density (ρ). We use RACMO-derived frontal ablation fluxes ($q_{calving,\ RACMO}$) as a reference and compare them with OGGM-derived frontal ablation fluxes ($q_{calving}$) computed while varying the k parameter. We select the k value that results in the smallest difference between both frontal ablation fluxes (model and RACMO derived).

Assuming that the RACMO SMB mean over the reference period equals the glacier mean frontal ablation flux is a meaningless approach if not compared with frontal ablation fluxes derived from constraining k values with velocity observations. The difference between the results from both calibration methods serves as an indication of how strong the dynamic imbalance might have been for PGs during that period in time.

4.5 Results

We adjust the calving constant of proportionality k in OGGM's calving parameterization to match satellite velocity observations and RACMO derived frontal ablation fluxes following the calibration methods described in sect 4.4. After adjusting the k parameter, we obtain a k value for each PG per calibration method and we simulate mean frontal ablation fluxes for tidewater glaciers in an equilibrium setting and compute their volume and ice thickness distribution. We are able to simulate between ∼77 to 78% of the glacierised area of interest (depending on the calibration method), approximately 3% of the glacierised area has data gaps in either one or both of the data sets used for calibration (RACMO2.3p2 and MEaSUREs) or present errors in the preprocessing stages of OGGM. The other 19% of the remaining area has no calving solution for Eq. 4.6 (see Fig. 4.1b and sect. 4.6.2 for an extended discussion regarding these glaciers).

In the following sections we describe the results of i) comparing k values, frontal ablation and calving rate estimates obtained by using the different calibration methods, ii) how the k parameter varies against glacier-specific characteristics (e.g. slope, width, average solid precipitation, and temperature sensitivity μ^*) and iii) the impact of accounting for frontal ablation on the ice volume estimate for PGs when using the different calibration methods.

4.5.1 Comparison between calibration methods

In this section, we only compare results of glaciers that have a valid k parameter value when using both calibration methods and glaciers for which a RACMO SMB mean over the reference period was not negative.

The calving constants of proportionality (k) and frontal ablation fluxes (after calibration) obtained using the velocity method (blue box plots in Fig. 4.4a and b) are larger in magnitude than those found using the RACMO method (orange box plots in Fig. 4.4a and b) this is independent of the glacier size as shown in Fig. 4.4.

However, when comparing the glacier-to-glacier output (see Fig. 4.5) there is a strong correlation among k values obtained by the different calibration methods ($r^2 = 0.78$ and p-value=$3.84e^{-40}$) but a weaker correlation among the resultant $q_{calving}$ estimates ($r^2 = 0.49$ and p-value=$4.90e^{-1}$). This suggests that even small changes in the k parameter will cause large differences on frontal ablation fluxes

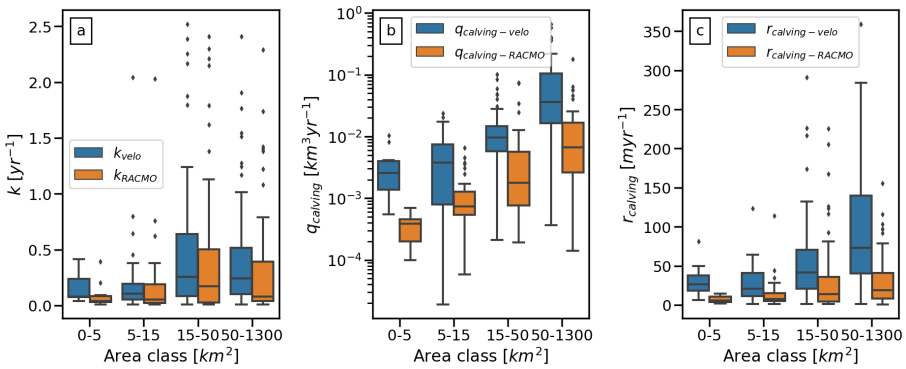

Figure 4.4: Difference between k values (**a**), frontal ablation fluxes (**b**) and calving rate (**c**) obtained by calibrating OGGM's calving parameterization with two independent methods: i) using velocities (blue) and ii) RACMO (orange). The x-axis is broken into different glacier size categories. The width of the boxes represents the inter quartile range (IQR) of the data values. The line dividing the boxes represents the median. The whiskers represent the range of values for 99.3% of the data. Points outside this range only contain 0.7% of the values distribution.

estimated after calibration (with the rest of the model parameters kept constant). Recinos et al. (2019) show that frontal ablation estimates are also sensitive to different values of Glen A and sliding parameter (here kept constant throughout the study), but highly dependent on different values of k, as it is also shown in Fig. 4.5d. This is a direct result of the calving law used in the parameterization which varies linearly with k (see Eq.4.4). The strong correlation between k values (see Fig. 4.5c) is due to how OGGM finds a frontal ablation flux (see 4.3.3). By default, the model constrains k to be of a specific magnitude, when it assumes that the amount of ice that passes through the glacier terminus in a mass balance year $q_{calving}$ must be balanced by the amount of ice delivered to the terminus $q_{deformation}$, in order to solve for the ice thickness (h_f) in Eq. 4.6 and compute a frontal ablation flux[1]. For a frontal ablation flux to exist, there should be a minimum value for the k parameter and the ice thickness (h_f) which ensures that a glacier calves (under that specific calving front geometry) and the balance between both fluxes in Eq. 4.6 is met. Differences in k values are then a

[1] Note that the water depth in Eq.4.4 is ultimately a function of h_f

result of constraining different parts of Eq. 4.6: i) choosing a k value for which model surface velocities match velocity observations and ii) choosing a k value for which model frontal ablation fluxes match RACMO derived frontal ablation estimates.

We also compare how frontal ablation fluxes computed after the k calibration vary against some glacier-specific characteristics (we only present here, those variables for which we find significant correlations). Frontal ablation fluxes are strongly correlated to the calving front width in both methods ($r^2 = 0.69$ and p-value=$1.29e^{-5}$ for the velocity method and $r^2 = 0.48$ and p-value=$3.88e^{-11}$ for the RACMO method). Fjord width is known to have a strong influence on glacier dynamics (Benn et al., 2007b; Carr et al., 2015, 2014; Enderlin et al., 2013b; Jamieson et al., 2012) and for that reason, we also estimate calving rates which are independent of the width for a better comparison between the output of both methods. Calving rates estimated after calibrating the k parameter with velocity observations are significantly larger in magnitude than those found using the RACMO method as shown in Fig. 4.4c.

OGGM frontal ablation fluxes derived with the RACMO calibration method do not present any significant correlation with the rest of the glacier-specific characteristics that should influence the frontal ablation flux estimate according to the calving law in Eq. 4.4 (e.g. water depth), which is not the case for frontal ablation fluxes estimated with the velocity method. This suggests that glacier processes are therefore not well represented if the model is only constrained based on the assumption of a closed budget, despite the fact that k values obtained with both calibration methods are very similar as shown in Fig. 4.5a. The low correlation between water depth and frontal ablation fluxes derived with the RACMO method highlights the need of velocity observations to constrain model parameters, and that such observations cannot well be replaced by surface mass balance estimates and a closed budget assumption. These last aspects are not sufficient to reproduce observed glacier dynamic behaviour (see 4.6.1 for more detail).

The "real" calving rate and frontal ablation flux of each glacier is probably best represented by the velocity calibration method. Satellite velocity measurements provide an insight into several ice dynamic components and reflect the ocean influence over the movement of the ice at the calving front. Whereas the second calibration method is based on mass balance data, and the equilibrium assumption that this is counterpoised by frontal ablation. Which is not the case

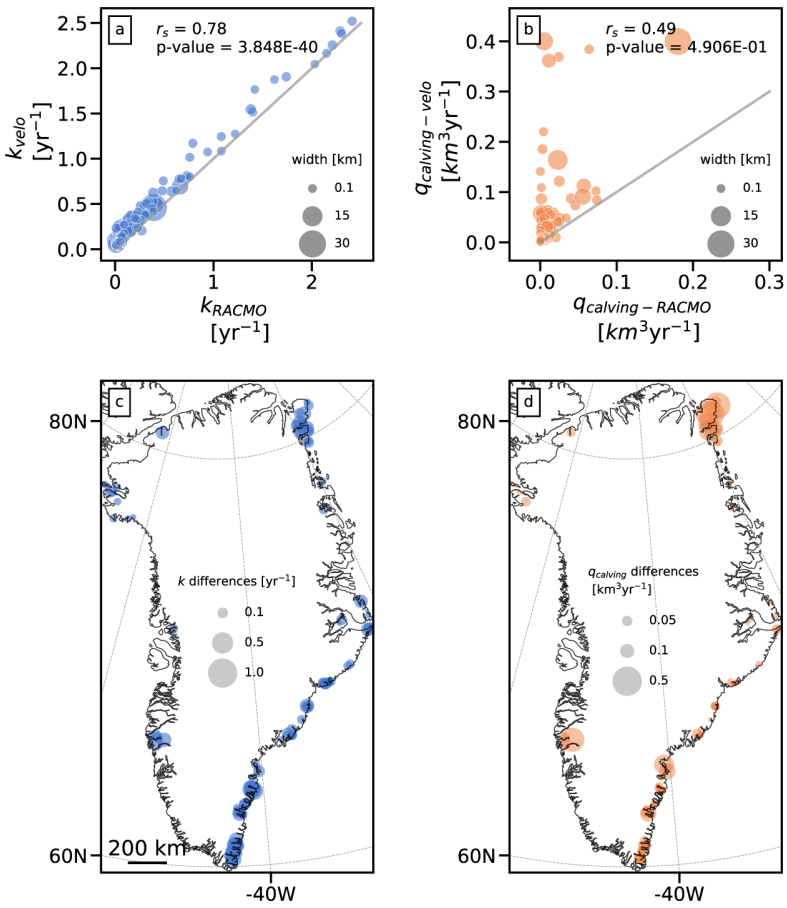

Figure 4.5: Comparison of k values (blue) and frontal ablation fluxes (orange) obtained by calibrating OGGM's calving parameterization with two independent methods: i) using velocities and ii) RACMO. **a:** scatter plot of k parameters. **b:** scatter plot of frontal ablation fluxes. Correlation coefficient and p-values are also given. The scatter points have different sizes based on the terminus width. Spatial overview of the difference between k values (**c**) and frontal ablation fluxes (**d**).

for most of the glaciers in the North-East of Greenland, where fluxes derived with the velocity method are significantly larger than those fluxes derived with the RACMO method ($q_{calving}$ differences > 0.5 km^3 yr^{-1}). Results shown in Fig. 4.5d demonstrate that all tidewater glaciers have considerable dynamic mass loss and

that in the North-East in particular, there is a significant imbalance between their climatic mass balance and ice dynamics.

4.5.2 Correlation between k values and glacier-specific characteristics

One of the major challenges to model tidewater glaciers at a global scale is the lack of frontal ablation observations or in situ glacier measurements (e.g. velocity fields, surface mass balance, mapping of terminus positions, etc.) required to calibrate the model parameters. Global glacier models ultimately seek to consistently simulate past and future global-scale glacier changes. Therefore, in order to make such long and expensive simulations, models not only require simple parameterizations but parameter values that can be approximated through other glacier-specific characteristics, for which data is already available on the global scale (e.g geometrical glacier characteristics derived from glacier outlines and DEM products). We compare k values found with both calibration methods to several glacier-specific characteristics, we only present here, those variables for which we find significant correlations (slope and freeboard at the calving front, average solid precipitation, and temperature sensitivity μ^*) in order to investigate possible proxies for the k parameter and model performance.

We find that the slope angle and freeboard at the calving front correlate well with k values (see Fig. 4.6a and b), with the slope angle presenting the strongest influence on the k parameter. Mercenier et al. (2018) investigated the effect of varying the calving front slope on the state of stress and flow regime for an idealized grounded ocean-terminating glacier. Their sensitivity studies show a strong relationship between the calving front slope and the stress state. An increase of a reclining slope strongly decreases the stresses and velocities in the vicinity of the terminus and hence has a stabilizing effect on the calving front. Fig. 4.6a shows how k values vary exponentially depending on the slope angle. This exponential relation is a result of the ice flux balance condition in Eq. 4.6 and the n exponent of Glen's flow law (default: n=3). The ice flux estimated via ice deformation by OGGM; $q_{deformation}$ is a polynomial in h_f of degree 5 with an extra term in degree 3 since we account for a sliding velocity, $q_{deformation}$ will push more mass towards the terminus with a lower thickness. The ice flux through the terminus estimated via the calving law changes with the ice thickness linearly ($q_{calving}$ varies with h_f as a polynomial of degree 2). To properly solve Eq. 4.6,

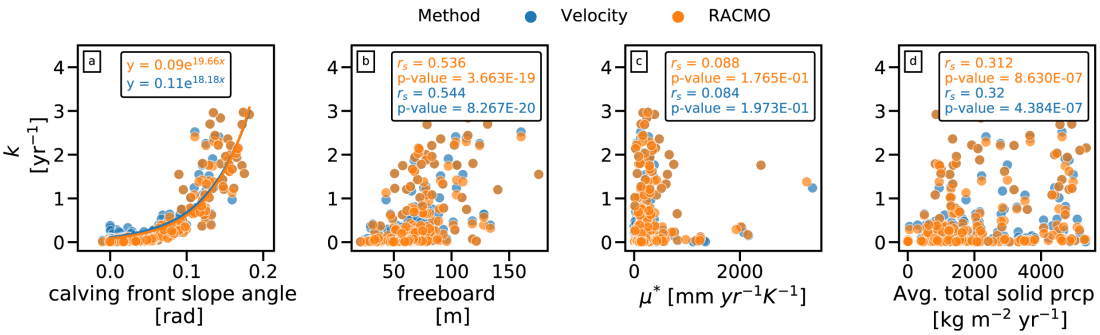

Figure 4.6: Correlation between k values and glacier-specific characteristics: (**a**) slope angle, (**b**) freeboard, (**c**) temperature sensitivity μ^* and (**d**) average total solid precipitation over the glacier. Blue dots represent k values calibrated using satellite velocities and orange dots represent k values calibrated using RACMO derived frontal ablation fluxes. The approximated exponential curves and pearson correlations between the k values and the glacier-specific characteristics are shown on each sub figure.

k has to increase when the slope angle at the calving front increases.

The rest of the parameters in Fig. 4.6 (the temperature sensitivity μ^* and average solid precipitation on the glacier, panel c and d) present weak linear relationships with k values estimated by both calibration methods. However, they provide information of how the frontal ablation fluxes feed back to the mass balance module.

Large frontal ablation fluxes (and large k values) lead to small temperature sensitivities μ^* as explained in sect. 4.3.3 and shown in Fig. 4.6c. For a frontal ablation flux to exist (independently of the k value found during the calibration), the model must adjust the surface mass balance and the amount of melt produced along the glacier in order to comply with mass conservation. This is done by modifying the only free unknown parameter in the mass balance equation: the temperature sensitivity μ^* (see Eq. 4.2). When calibrating k with velocity observations, 25% of PGs end up with a slightly smaller μ^* than if we calibrate k with the RACMO data. It is important to highlight that by calibrating k using both methods, frontal ablation fluxes are not overestimated and the model does not need to rely on suppressing surface melt by clipping μ^* to be equal to zero. There is no need for OGGM to enforce a physical limit where the frontal ablation flux

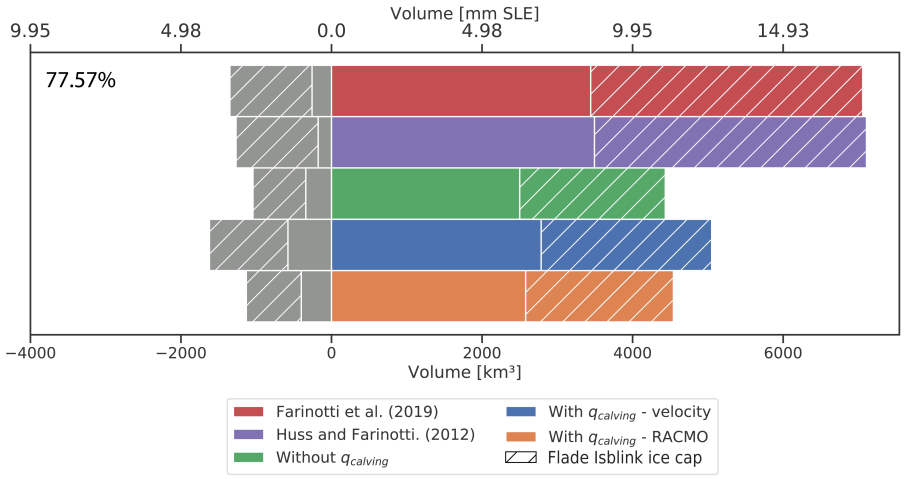

Figure 4.7: Total volume of Greenland's tidewater PGs before (green) and after accounting for frontal ablation (blue and orange), when calibrating the k parameter with velocity data (blue) and RACMO data (orange). The red bar represents the consensus estimate for these glaciers obtained by Farinotti et al. (2019). The purple bar represents Huss and Farinotti (2012) contribution to the consensus estimate (red bar). The grey bars represent the total volume below sea level for each volume estimate. The percentage in the top left is the percentage of the study area that has a k parameter in both calibration methods. The line pattern in the bars represent the volume estimate of The Flade Isblink Ice Cap.

for each PG cannot be larger than its annual accumulation ($p_f P_i^{Solid}(z)$). Calibrating k allows the glacier to lose mass via frontal ablation and via ice melting at the same time.

4.5.3 PGs frontal ablation, thickness and volume

Finally, we compute the average regional frontal ablation flux after calibrating the k parameter with both methods, and found an average flux of 8.92 km^3 yr^{-1} (8.17 Gt yr^{-1}) when k is constrained by velocity observations and 1.78 km^3 yr^{-1} (1.63 Gt yr^{-1}) if k is constrained using RACMO derived frontal ablation fluxes. The RACMO calibration method underestimates the amount of ice passing through the glacier terminus, consequently affecting the glacier volume

estimation as shown in Fig. 4.7 (see difference in orange and blue bar).

The velocity method allows us to find k values for 396 glaciers covering 77.93% of the study area and the RACMO method allows us to find k values for 330 glaciers covering 78.27%. For a better comparison between methods, we only compare in Fig. 4.7 results for glaciers that have a k parameter in both calibration methods, that is k values for 313 glaciers covering 77.57% of the study area (here we only report final numbers for this group of glaciers). The coloured bars in Fig. 4.7 correspond to different model configurations, one setting $q_{calving} = 0$ (green bars) and two accounting for frontal ablation and adjusting the k parameter according to the values found by each calibration method (blue and orange bars). Additionally we added another two bars to Fig. 4.7, showing the model consensus estimate from Farinotti et al. (2019) (red bar) and the model result of Huss and Farinotti (2012) (purple bar).

Results show that by introducing frontal ablation and calibrating k values volume estimates for Greenland's PGs increased from 11.02 to 12.56 mm SLE when using the velocity calibration method and to 11.29 mm SLE when using the RACMO calibration method. Regional volumes are underestimated by 2 to 14% if frontal ablation is ignored and up to 11% if the model relies only on surface mass balance estimates and the assumption of a closed budget to calibrate the calving constant of proportionality k. The consensus estimate from all models compared in Farinotti et al. (2019) for these glaciers is 17.55 mm SLE and 17.67 mm SLE for Huss and Farinotti (2012) model contribution, that is 28 to 36% higher than OGGM results for all model configurations. Note that the consensus estimate for Greenland's PGs is a composite mean of two models in particular Huss and Farinotti (2012) (purple bar in Fig. 4.7) and Frey et al. (2014). Only Huss and Farinotti (2012) prescribes a positive net flux at the glacier terminus by reducing the ELA that yields a balanced surface mass budget by a value $\Delta \mathrm{ELA}_{calving}$ which is separately defined for each RGI region and is not glacier-specific. Therefore, frontal ablation was not explicitly accounted for individual glaciers when estimating the glacier thickness distribution and volume (see Huss and Farinotti (2012) for more details). Thus the model consensus volume estimate for these glaciers still suffers from considerable uncertainties related to (i) the implemented frontal ablation parameterization or (ii) not accounting for frontal ablation at all in the glacier model as in the case of Frey et al. (2014) model contribution. The difference between the consensus estimate and OGGM's becomes smaller if we remove a single glacier entity from the results: the Flade Isblink Ice Cap, represented in Fig. 4.7 by the line pattern in each bar plot. In

Farinotti et al. (2019) and Huss and Farinotti (2012) the Flade Isblink Ice Cap remained as a single outline (as shown in Fig. 4.2a), subdividing the ice cap can contribute to significant differences in the ice thickness distribution and thus affect the final ice cap volume. As shown in Fig. 4.7, most of the regional volume can be attributed to the ice cap (see the line pattern in the bars).

Additionally, we also calculate the regional ice volume below sea level (grey bars in Fig. 4.7) and found that introducing frontal ablation increases the volume below sea level from 2.59 to 2.81 mm SLE when using the RACMO calibration method and up to 4.03 mm SLE when using velocity observations to constrain the k parameter (see Fig. 4.7). The volume below sea level reported by Farinotti et al. (2019) and Huss and Farinotti (2012) for these glaciers is 3.35 mm SLE and 3.15 mm SLE respectively. These results imply that not accounting for frontal ablation and/or only constraining the parameterization with surface mass balance estimates and a closed budget assumption will directly impact the estimate of these glacier's potential contribution to sea-level rise.

4.6 Discussion

4.6.1 Calibration methods performance

In the following section we analyse the model output after calibration by comparing modeled surface velocities to observations and modeled frontal ablation fluxes to RACMO derived frontal ablation estimates.

Figure 4.8a and b show the comparison between modeled (computed after calibration with both methods) and observed surface velocities. Figure 4.8a shows that for the velocity method (blue scatter plot) OGGM simulates approximately 40% of the velocity observations variability. The low coefficient of determination (r^2) is affected by large uncertainties in the satellite observations (e.g. relative tolerance > 0.80, see grey error bars in Fig. 4.8a), which weakly constrain the model. For most of the glaciers, OGGM is able to estimate a model surface velocity within the uncertainty limit of the observations. However, such large errors in the velocity observations will propagate as larger uncertainties in the k parameter. Figure 4.8b shows that for the RACMO method, OGGM simulates only 11% of the velocity observations variability. The discrepancy between the results among the two calibration methods, when compared to satellite obser-

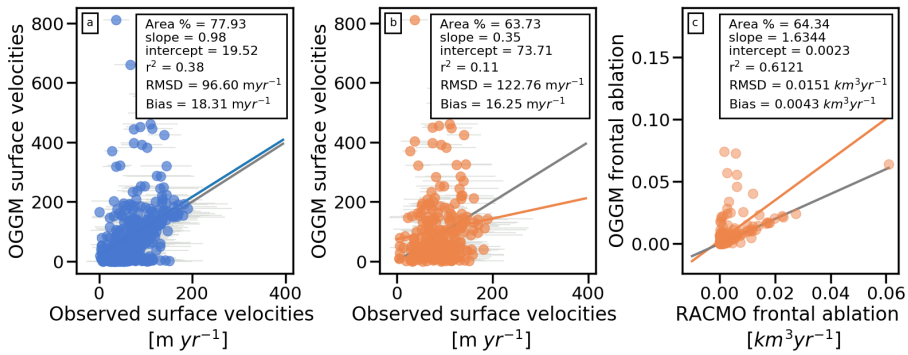

Figure 4.8: **a:** comparison of modeled (after calibrating k with the velocity method) and observed surface velocities. **b:** comparison of modeled (after calibrating k with the RACMO method) and observed surface velocities. Note in b that RACMO data and the velocity observations only have in common 63.7% of the study area. **c:** comparison of modeled (after calibrating k with the RACMO method) and RACMO-derived frontal ablation fluxes. The RACMO method is able to estimate k values for approximately 78% of the study area but 14 % of the study area has a RACMO SMB mean over the reference period that is below zero, which implies a $q_{calving}$ equal to zero. That 14% has been remove from the statistics in b and c. Regression lines (solid lines) and statistics are shown in the upper right corner, i.e. % of study area represented in the graph, regression slope, intercept, coefficient of determination (r^2), RMSD and bias. P-values are all smaller than 0.05. Grey solid lines represent slopes equal to 1 and intercepts equal to zero. Note that in (a and b) uncertainty bars for the velocity observations are plotted in light grey.

vations (Figure 4.8a and b), imply that the model fails to represent individual tidewater glacier dynamics by only constraining the k parameter with SMB estimates and the assumption of a closed budget, otherwise, there should be a better correspondence between the results of both calibration methods and the satellite observations.

Figure 4.8c shows the comparison between modeled and RACMO-derived frontal ablation fluxes. OGGM frontal ablation estimates after calibration explain approximately 62% of the variance of the RACMO-derived fluxes. The coef-

ficient of determination (r^2) between modeled ($q_{calving}$) and derived ($q_{calving-RACMO}$) frontal ablation fluxes is higher when using this calibration method. However, contrary to the satellite observations (see Fig. 4.8a), there are no uncertainty estimates for RACMO SMB data. Therefore, we are not able to assess with certainty if OGGM reproduces RACMO frontal ablation estimates within the RACMO uncertainty range. This method only allows to select a k parameter that will reproduce the smallest difference between both fluxes. With this method, we find a k value for ∼78% of the study area. It is important to note that 14% of this glacier area has a slightly negative RACMO SMB mean, indicating that for those glaciers, the equilibrium condition (defined in Eq. 4.12) is obviously problematic. For such glaciers we assign a k value (and a $q_{calving}$) equal to zero. This glaciers are not included in the study statistics and in Fig. 4.8.

4.6.2 Glaciers with no calving solution

The model does not produce a frontal ablation flux for ∼19% of the glacierised area of interest. These glaciers do not calve under any k value, from a range between 0.01 to 3.0 yr^{-1}. Recinos et al. (2019) showed that sometimes the flux estimated by the calving law Eq. 4.4 is too large to be sustained by the surface mass balance $q_{calving} \neq$ to $q_{deformation}$ (See Eq. 4.6). Even without glacier melt ($\mu^* = 0$), the total accumulation over the glacier is too small to close the frontal mass budget. This can be due to several factors: frontal ablation is overestimated by the calving law, or solid precipitation is underestimated by OGGM. The frontal ablation can be overestimated if k and/or the calving law does not represent the dynamics of that particular glacier, or due to errors estimating the calving front geometry. Further investigation is needed for these glaciers, to ensure the nature of the problem (input data errors or model concept errors). Such analysis requires more observations to constrain the model, such as mapping of terminus positions and/or bathymetric data. Unfortunately, this falls beyond the scope of this study but it will be addressed in future versions of OGGM. Finally large uncertainties might also arise from the fact that the calving parametrization implemented here is mostly representative of tidewater glaciers with a ground termini. PGs might also include extensive shelf ice areas, with floating parts, such a setting is not accounted for in the current frontal ablation parameterization of OGGM.

4.7 Conclusions

We have implemented two independent methods to calibrate the calving constant of proportionality k in OGGM's calving parameterization and are able to simulate average frontal ablation fluxes for the majority of Greenland PGs that terminate in the ocean. By comparing the model output after applying both calibration methods, we find that the model is not able to predict individual tidewater glacier dynamics if it relies only on SMB estimates and the assumption of a closed budget to constrain k values. Velocity observations are essential to constrain model parameters and estimate the dynamic mass loss of PGs. We estimate an average regional frontal ablation flux after calibrating the k parameter of 8.92 km^3 yr^{-1} (8.17 Gt yr^{-1}) when k is constrained by velocity observations and 1.78 km^3 yr^{-1} (1.63 Gt yr^{-1}) if k is constrained using RACMO derived frontal ablation fluxes. The RACMO calibration method, which is is based on mass balance data, and the equilibrium assumption that this is counterpoised by frontal ablation, underestimates the amount of ice passing through the glacier terminus, consequently affecting the regional glacier volume estimation and the models capacity to simulate the variance of the velocity observations. Results show that by introducing frontal ablation and calibrating k values, volume estimates for Greenland's PGs, increased from 11.02 to 12.56 mm SLE when using the velocity calibration method and to 11.29 mm SLE when using the RACMO calibration method. Regional volumes are underestimated by 2 to 14% if frontal ablation is ignored and up to 11% if the model only relies on surface mass balance estimates and the assumption of a closed budget to constrain the calving constant of proportionality k. This change in volume is also reflected on the regional volume below sea level where introducing frontal ablation increases the volume below sea level from 2.59 to 2.81 mm SLE when using the RACMO calibration method and up to 4.03 mm SLE when using the velocity method. Ignoring frontal ablation and the choice of calibration method impact the estimate of these glacier's potential contribution to sea-level rise. Velocity observations provide a different insight into the ice dynamic processes of each glacier, and to some extent, the influence that the ocean has over the movement of the ice at the calving front. RACMO SMB means (over a reference period 1961-1990) provides an insight into the energy balance of the glacier which is the result of long term climatic forcing. The discrepancy between the results among the two calibration methods imply that all PGs are losing mass and there is a significant imbalance between their climatic mass balance and ice dynamics, especially in

those glaciers located at the North-East of Greenland. When investigating how the k parameter values vary with glacier-specific characteristics, we find that the slope angle and freeboard at the calving front correlate well with k values in both methods, and that k values vary exponentially depending on the slope angle.

4.8 Acknowledgements

BR was supported by the DFG through the International Research Training Group IRTG 1904 ArcTrain. The computations were realized on the computing facilities of the Institute of Geography, University of Bremen. MM acknowledges support of the German Federal Ministry of Education and Research (BMBF) via grant no. 03F0778D. BN is funded by NWO VENI grant VI.Veni.192.019. The OGGM software together with the frontal ablation parameterization module are coded in the Python language and licensed under the BSD-3-Clause license. The latest version of the OGGM code is available on Github (`https://github.com/OGGM/oggm`), the documentation is hosted on ReadTheDocs (`http://oggm.readthedocs.io`), and the project webpage for communication and dissemination can be found at `http://oggm.org`. The code and data used to generate all figures and analyses of this paper can be found at `https://github.com/bearecinos/cryo_k_calibration_2020`. The OGGM version used for this study is available in a permanent DOI repository (`https://doi.org/10.5281/zenodo.3597756`).

5

Summary and outlook

5.1 Summary of the papers

5.1.1 Paper I: The Open Global Glacier Model (OGGM) v1.0

Maussion, F., Butenko, A., Champollion, N., Dusch, M., Eis, J., Fourteau, K., Gregor, P., Jarosch, A. H., Landmann, J., Oesterle, F., **Recinos, B.**, Rothenpieler, T., Vlug, A., Wild, C. T., and Marzeion, B.

Mountain glaciers are one of the few remaining subsystems of the global climate system for which no globally applicable community-driven model exists. In the recent past, great advances have been made in the global availability of data and methods relevant for glacier modeling; spanning glacier outlines, automatized glacier centerline identification, bed rock inversion methods, and global topographic data sets. Taken together, these advances now allow the ice dynamics of glaciers to be modeled on a global scale, provided that adequate modeling platforms are available.

This paper presents the Open Global Glacier Model (OGGM; `www.oggm.org`), developed to provide a modular and open-source numerical model framework for simulating past and future changes of any glacier in the world. To our knowledge, OGGM is the first global model to explicitly simulate glacier dynamics: the model relies on the shallow-ice approximation to compute the depth-integrated

flux of ice along multiple connected flow lines. In this study, we describe and illustrate each processing step by applying the model to a selection of glaciers before running global simulations under idealized climate forcings. Even without an in-depth calibration, the model shows very realistic behaviour. The model is able to reproduce earlier estimates of global glacier volume by varying the ice dynamical parameters within a range of plausible values.

Provided with the glacier outlines, topographical and climate data at reasonable resolution and accuracy, the model should be able to (i) provide a local map of the glacier including topography and hypsometry, (ii) estimate the glacier's total ice volume and compute a map of the bedrock topography, (iii) compute the surface climatic mass balance and (if applicable) at its front via frontal ablation, (iv) simulate the glacier's dynamical evolution under various climate forcings, and (v) provide an estimate of the uncertainties associated with the modelling chain. OGGM spans a wide range of applications, from ice-climate interaction studies at millennial timescales to estimates of the contribution of glaciers to past and future sea-level change.

Author contribution

BM and FM are the initiators of the OGGM project. FM is the main OGGM developer and wrote most of the paper. AB developed the downstream bed-shape estimation algorithm. NC wrote parts of the documentation. MD wrote the cross-validation monitoring webpage. JE developed the glacier partitioning tool. KF wrote parts of the bed inversion and dynamical cores. PG wrote the lateral drag parameterization. AJ provided a robust implementation of the dynamical core used for testing and contributed to the development of the operational scheme. JL provided the WGMS to RGI lookup table and contributed to the topographical data download tool. FO contributed to the AWS deployment tool. **BR developed the frontal ablation parametrisation tool (see Chap. 3) and made modification to the main OGGM code to improve the representation of water-terminating glaciers on the model (see sect. 2.3.6). BR modified the centerline code and the catchment area estimation module for calving glaciers, where the code is now able to automatically detect a flowline that reaches the center of the calving front and that assumes a rectangular bed shape for the last five pixels of the glacier terminus. Other contributions to the OGGM project and code have been done by BR, which includes documentation, tutorials for**

model users and small model additions that are not reflected in the text of this publication but that can be seen in the model code repository and documentation website: `https://github.com/OGGM/oggm`, `http://docs.oggm.org`. TR developed the download and parallelisation tools and is largely responsible for the successful deployment of OGGM on supercomputing environments. AV contributed to the climate and mass balance tools. CW provided the first implementation of the centerline determination algorithm. All authors continuously discussed the model development and the results together.

5.1.2 Paper II: Impact of frontal ablation on the ice thickness estimation of marine-terminating glaciers in Alaska

Recinos, B., Maussion, F., Rothenpieler, T., and Marzeion, B.

Glaciers have strongly contributed to sea-level rise during the past century, more than the Greenland and Antarctic ice sheets and will continue to be an important part of the sea-level budget during the twenty-first century. Therefore, accurate estimates of the glaciers volume and ice thickness will help narrow down uncertainties on the sea-level budget.

However, ice thickness measurements of glaciers and ice caps are hard to obtained, mainly due to the difficulties in measuring the ice thickness. To overcome this under-sampling problem, a number of methods have been developed to infer the total volume of glaciers, by using surface characteristics (see Farinotti et al. (2017), for a review of all these methods and Farinotti et al. (2019), for a global-scale intercomparison).

One method presented by Farinotti et al. (2009) and successfully applied several times since then (e.g. Clarke et al., 2013; Huss and Farinotti, 2012; Maussion et al., 2019; Morlighem et al., 2011), combines ice flow dynamics and mass conservation principles to constrain mass fluxes through given glacier cross-sections. The method infers ice thickness from estimates of ice fluxes derived from the assumption that ice fluxes balance the surface mass budget (Farinotti et al., 2009). The results are thus sensitive to the spatial distribution of the mass flux and the mass balance.

For calving glaciers, the surface mass budget cannot be considered balanced, even assuming equilibrium between glacier and climate. The derived ice thickness

estimate for these glaciers hence depends on estimates of frontal ablation.

In this study, our main goal is to implement a simple calving law in the Open Global Glacier Model (OGGM v1.1 Maussion et al., 2019) to improve the initial thickness estimation for this type of glaciers. We employ a calving law proposed by Oerlemans and Nick (2005) and that has already been applied at a large scale by Huss and Hock (2015). The annual frontal ablation flux $q_{calving}$ (km^3 yr^{-1}) is computed as a function of the height *(h_f)*, width *(w)* and estimated water depth *(d)* of the calving front. We applied this parameterisation to all the Marine terminating glaciers in Alaska, and use previously calculated frontal ablation estimates from McNabb et al. (2015), to asses and calibrate our results.

By implementing this calving law into OGGM, we show that inversion methods ignoring frontal ablation systematically underestimate the mass flux and thereby the thickness of calving glaciers. Accounting for frontal ablation in ice thickness inversion methods based on mass conservation (as listed in Farinotti et al., 2017) increases estimates of the regional ice mass stored in marine-terminating glaciers by approximately 11 to 19 %. While for individual glaciers, ice volume may be underestimated by up to 30% when ignoring the impact of frontal ablation, the effect is independent of the size of the glacier.

Our sensitivity studies also show that the differences in thickness (between adding or not frontal ablation to the MB model) occur mainly at the lower parts of the glacier, but often above sea-level. This indicates that not accounting for frontal ablation will have an impact on the estimate of this glacier's potential contribution to sea-level rise.

Author contribution

BM and FM are the initiators of the OGGM project and conceived this study. **BR is the main developer of the frontal ablation parameterisation module and wrote most of the paper, coded the runs for all the experiments and the scripts used to produced of all the images in this publication.** FM is the main OGGM developer and was largely involved with the development of the frontal ablation parameterisation module. TR made significant contributions to the OGGM code and the frontal ablation parameterisation module and is responsible for the successful deployment of the code on supercomputing environments.

5.1.3 Paper III: Calibration of a frontal ablation parameterization applied to Greenland's peripheral calving glaciers.

Recinos, B., Maussion, F., B. Noël, Möller, M. and Marzeion, B.

The Greenland Ice Sheet is surrounded by a large amount of Peripheral Glaciers (PG) covering approx. 12% of the world's total glaciated area, with most of them terminating in the ocean. Despite their importance in the global mean sea-level budget, there is no information of how much ice is discharge into the ocean from PG's and little is known about their calving front geometry. Which makes simulating their volume and ice thickness distribution a challenging tasks for ice sheet and global glacier models, with the main issue being the lack of observations to calibrate model parameters.

In this study, we present a regional estimate of mass loss through frontal ablation for all PG's that are weakly connected to the Ice sheet. We use the Open Global Glacier Model (OGGM v1.2.0 Maussion et al., 2019) and the calving parameterization described in Recinos et al. (2019) to simulate frontal ablation fluxes for Greenland's tidewater PG's and compute their volume and ice thickness distribution, by applying two independent methods to calibrate the calving parameterization.

The first method, constrains the calving constant of proportionality k in the parameterization, with surface velocity fields derived from the MEaSUREs Multi-year Greenland Ice Sheet Velocity Mosaic. Whereas the second method constrains the k parameter using frontal ablation fluxes, derived from Surface Mass Balance (SMB) means over an equilibrium reference period (1961-1990), obtained from the monthly output of the Polar Regional Climate Model RACMO, statistically downscaled to 1 km resolution. The second calibration method is based on the strong assumption that most PG's during that time have a balanced budget (i.e. did not experience any mass loss or gain). Considering an equilibrium between what the glacier gained and calved might not reflect real frontal ablation fluxes, but such estimates, serve as a base to asses the dynamic mass loss of glaciers when combined with frontal ablation estimates constrained from velocity observations. By comparing the model output after applying both calibration methods, we find that the model is not able to predict individual tidewater glacier dynamics, if it relies only on SMB estimates and the assumption of a closed budget to constrain k values. Velocity observations are essential to constrain model parameters and estimate the dynamic mass loss of PG's.

We estimate an average regional frontal ablation flux after calibrating the k parameter of 8.92 km^3 yr^{-1} (8.17 Gt yr^{-1}) when k is constrained by velocity observations and just 1.78 km^3 yr^{-1} (1.63 Gt yr^{-1}) if k is constrained using RACMO derived frontal ablation fluxes. The RACMO calibration method underestimates the amount of ice passing through the glacier terminus, consequently affecting the regional glacier volume estimation and the models capacity to simulate the variance of the velocity observations.

Author contribution

BM and FM are the initiators of the OGGM project and conceived this study. **BR is the main developer of the calibration methods and the frontal ablation parameterisation module. BR wrote most of the paper, coded the runs for all the experiments and the scripts used to produced the images in this publication.** FM is the main OGGM developer and was largely involved with the development of the frontal ablation parameterization module. BN provided the RACMO data used in the study. MM did the Flade Isblink Ice Cap tidewater basis identification and provide the insight to the velocity observations. All authors continuously discussed together the contents of the publication.

5.2 Main conclusions

The main conclusions of the papers constituting this thesis can be summarised as follows:

- A frontal ablation parameterisation has been implemented in the model, to account for a non-zero terminus flux, in the case of simulating calving glaciers. Failing to include this mechanism of mass loss in the model leads to an underestimation of the total glacier volume for this type of glaciers.
- Accounting for frontal ablation in ice thickness inversion methods based on mass conservation (e.g. such as the method use in OGGM and the methods listed in Farinotti et al., 2017) increases estimates of the regional ice mass stored in marine-terminating glaciers by approximately 11 to 19% in the region of Alaska and up to 14% in Greenland Peripheral Glaciers (PG). While for individual glaciers (e.g. Columbia Glacier in Alaska), ice volume

may be underestimated by up to 30% when ignoring the impact of frontal ablation, this effect is independent of the size of the glacier.

- Sensitivity studies show that the differences in thickness (between adding or not frontal ablation to the mass balance model) occur mainly at the lower parts of the glacier, but often above sea-level. This indicates that not accounting for frontal ablation will have an impact on the estimate of tidewater glacier's potential contribution to sea-level rise.

- Our experiments highlight the need for bathymetry data and terminus mapping, as they may constrain model parameters when the topographical Digital Elevation Model quality is not sufficient to provide a realistic estimate of the terminus geometry.

- By comparing the model output after applying two different calibration methods, we find that the model is not able to predict individual tidewater glacier dynamics if it relies only on surface mass balance estimates and the assumption of a closed budget to calibrate model parameters. Velocity observations are essential to constrain such parameters and estimate the dynamic mass loss of tidewater glaciers.

- We find that the slope angle and freeboard at the calving front correlate well with the calving constant of proportionality k in both calibration methods, with k values vary exponentially depending on the slope angle at the terminus of the glacier.

5.3 Discussion: model performance and future perspectives

5.3.1 OGGM global performance and limitations

Farinotti et al. (2017) summarizes the results of the Ice Thickness Models Intercomparison eXperiment (ITMIX). The ITMIX was the first coordinated intercomparison of approaches that estimate the ice thickness of glaciers and ice caps from surface characteristics. The goal was to assess model performance for cases in which no a priori information about the glacier ice thickness. OGGM participated in the experiment and ranked the highest on the category of being

able to simulate well the largest number of test cases. However, in the second ranking of the experiment based only on the average model performance, OGGM was ranked 11th out of 17. In contrast to the first ranking, the second does not consider the test cases individually and does not account for the number of considered test cases. A model considering only one test case but performing perfectly on it, for example, would score the highest (Farinotti et al., 2017). OGGM is penalized for having a large bias between the model results and the observations, primarily in the case of simulating ice caps. But perhaps the largest problem with all the models that participated in ITMIX, including that version of OGGM, is that none of them accounted for frontal ablation in their initial ice thickness inversion estimate for calving glaciers, hence significantly underestimating the ice volume of these type of glaciers their contribution to global mean sea-level.

The models that ranked the highest on the ITMIX were later compared globally in Farinotti et al. (2019) (OGGM included), where an ensemble of up to five models provided a consensus estimate for the ice thickness distribution of all the 215,000 glaciers in the globe outside the Greenland and Antarctic ice sheets. Recinos et al. (2019) showed that for the Alaska region that consensus underestimated the volume of tidewater glaciers by 27.58%, since the models used in the consensus did not account (or crudely accounted) for this extra lost of mass when inverting for the ice thickness.

Greenland is the most affected area since most of the peripheral glaciers in this region are marine-terminating ice caps. In Maussion et al. (2019) the Greenland region presented the largest percentage of the regional RGI area which cannot be modelled by OGGM. Most of the errors come from the fact that the version of the model described in Maussion et al. (2019) does not take frontal ablation into account for the bed inversion (i.e. the original glacier front has a thickness of zero) but it does count with a basic parametrisation in the ice dynamics module.

5.3.2 Frontal ablation parameterisation performance

To estimate the frontal ablation flux for marine-terminating glaciers in OGGM we solve for the ice thickness, by assuming that the total amount of ice calved is equal to the amount of ice delivered to the terminus; which is the ice flux estimated by OGGM using the physics of ice deformation and sliding velocity.

We solve for the ice thickness numerically using a bound constraint minimi-

sation method and finding the root of our resultant thickness equation in a given interval (see sect. 3.3.3). For the majority of glaciers we are able to find an optimal ice thickness that results in a frontal ablation flux compatible with the calving law implemented in OGGM and consistent with mass conservation.

However, for several tidewater glaciers in Alaska and Greenland, there is no thickness value which complies with the calving law and the ice dynamics in OGGM if a default parameters set up is used. This could be due to several reasons:

- the calving constant of proportionality k is over estimated or the solid precipitation on the glacier is underestimated.
- a difference > 0 between both fluxes in Eq. 4.6 corresponds to a glacier state outside of the equilibrium condition under this specific geometry (a glacier geometry fixed at the RGI outline's date).
- the calving law and the ice deformation equation do not represent well all the physical process affecting this particular glacier. Both processes are parametrized and therefore an approximation of reality.
- uncertain boundary conditions (e.g the wrong calving geometry) as explained in sect. 3.5.

Note that the number of glaciers where this happens in the Alaska region is only 6 and this number gets reduced to one, when we correct for observed water depths and frontal widths, indicating that uncertainties in the boundary conditions are the main problem in this region.

Limitations of the calibration methods applied for Greenland's peripheral calving glaciers.

The model does not produce a frontal ablation flux for ∼19.4% of the glacierised area of interest in Greenland. These glaciers do not calve under any k value, from a range between 0.01 to 3.0 yr^{-1}. Recinos et al. (2019) showed that sometimes the flux estimated by the calving law Eq. 4.4 even after calibration, is too large to be sustained by the surface mass-balance $q_{calving} \neq$ to q (See Eq. 4.6). Even without glacier melt ($\mu_* = 0$), the total accumulation over the glacier is too small to close the frontal mass budget. This can be due to several factors explained

in the previous sections. The frontal ablation can be overestimated if k and/or the calving law does not represent the dynamics of that particular glacier, or due to errors estimating the calving front geometry. Further investigation is needed for PG's in Greenland, to ensure the nature of the problem (input data errors or model concept errors). Such analysis requires more observations to constrain the model, such as mapping of terminus positions and/or bathymetric data. Unfortunately, this falls beyond the scope of this study but it will be addressed in future versions of OGGM. Finally large uncertainties might also arise from the fact that the calving parametrization implemented here is mostly representative of tidewater glaciers with a ground termini. PG's might also include extensive shelf ice areas, with floating parts, such a setting is not accounted for in the current frontal ablation parameterization of OGGM. Therefore, frontal ablation estimates provided in this thesis might still underestimate the amount of ice being lost via frontal ablation.

Limitations of the Frontal ablation parameterisation applied for lake-terminating glaciers.

Additionally, calving in lake-terminating glaciers are yet to be model by OGGM since for these glaciers, we are not able to estimate a water depth from freeboard. One would need to know the free-board of the glacier terminus, i.e. the elevation of the glacier lake surface (for the elevation of the ocean surface, we assume that it is 0 m a.s.l.).

Water bodies in a DEM can be either flattened or set to no data points. According to the Shuttle Radar Topography Mission (SRTM) and the Viewfinder Panoramas DEM3 product meta data (`http://viewfinderpanoramas.org/dem3.html`), the water bodies were flattened to a constant elevation. There may be a slight gradient on some smaller lakes, making it harder to select an elevation value but indeed this is possible. For a large number of glaciers, however, this will, require an automatic algorithm that is able to identify a constant elevation contour and assign that elevation to a lake corresponding to a given RGI glacier outline. While this seems possible to do, it would be impeded by the dynamic changes of glacier lakes over long periods in time.

Frontal ablation parameterisation for dynamical runs (past and future glacier states)

Simulating a calving flux and the position of the grounding line overtime is a challenging task for a flowline model like OGGM. The model relies in the Shallow Ice Approximation (SIA), which neglects longitudinal stress gradients and approximates the basal shear traction with the local driving stress. This may be a poor assumption, especially near the calving front of a tidewater glacier (Vieli et al., 2000). The SIA lacks boundary conditions at the grounding line (or the ice divide, where we require $\overline{u} = 0$). Therefore, a flotation condition must be applied at the grounding line for estimating the ice thickness (Pattyn et al., 2012).

In addition, a more complex sliding law needs to be implemented. Modelled glacier dynamics depend critically on the choice of sliding laws (Benn et al., 2007a). The current OGGM sliding parametrisation is simple and does not account for effective pressure. The effective pressure is the difference between ice overburden pressure and the basal water pressure. For a calving glacier where basal water flows towards the terminus, a minimum value for the basal water pressure is determined by the depth of the bed below sea-level (Benn et al., 2007a). OGGM could estimate this minimum value after the initialisation stages (after accounting for frontal ablation in the ice thickness estimation) and improve the basal sliding velocity estimation, which at the moment limits the implementation of any calving law in the dynamical model.

The calving treatment in the ice dynamics is very simple but explicit: We add a grid point behind the glacier front which is reset to zero ice thickness at each time step: the ice mass suppressed this way is the frontal ablation flux, that we store. This parametrisation allow glaciers to retreat but does not take into account advancing calving glaciers (e.g. Yahtse Glacier in Alaska).

The parametrisation and the calving law implemented in Chap. 3 are empirically based equations that do not simulate the actual physics of the calving process. Moreover, the calving law implemented in Chap. 3 has been tuned to match current observations and it will become less reliable under different climate conditions. Limiting its use for global projections under different climatic scenarios. Implementing a more physically based calving model into OGGM is therefore necessary if the model intends to predict global scale sea-level rise contribution of calving glaciers.

Another aspect to take into account for future developments is the implementation of conditions to simulate the transition between a calving glacier and a valley glacier, in the case of a grounding line in land retreat.

The main fact that we were able to quantify during this study, is that accounting for frontal ablation has a strong influence on the glacier thickness distribution and volume. Regional glaciers volumes are underestimated up to 19% and individual glacier volumes up to 30%. Modeling an in correct calving flux will impact the estimate of these glaciers contribution to sea-level rise.

A

Appendix

A.1 Climate data

The default climate dataset used by OGGM is the Climatic Research Unit (CRU) TS v4.01 Dataset (Harris et al., 2014, released 20.09.2017). It is a gridded dataset at 0.5° resolution covering the period 1901-2016. The dataset is obtained by interpolating station measurements and therefore does not cover the oceans and Antarctica. The TS dataset is further downscaled to the resolution of 10' by applying the 1961-1990 anomalies to the CRU CL v2.0 gridded climatology (New et al., 2002). This step is necessary because the TS datasets do not contain an altitude information, which is needed to compute the temperature at a given height on the glacier. To compute the annual mass balances we use the hydrological year convention (the year 2001 being October 2000 to September 2001 in the Northern Hemisphere, April 2000 to March 2001 in the Southern Hemisphere).

For each glacier, the monthly temperature and precipitation time series are extracted from the nearest CRU CL v2.0 grid point and then converted to the local temperature according to a temperature gradient (default: 6.5K km^{-1}). No vertical gradient is applied to precipitation, but we apply a correction factor p_f=2.5 to the original CRU time series (similar to Marzeion et al., 2012b). This correction factor can be seen as a global correction for orographic precipitation, avalanches, and wind-blown snow. It must be noted that this factor has few (if any) impact on the mass balance model performance in terms of bias. This is due to the automated calibration algorithm, which will adapt to a new factor by acting on the temperature sensitivity μ^*. To verify that the chosen precipitation factor is realistic, we use another metric: the standard deviation of the mass balance time-series. Comparisons between model and observations show that the model underestimates variability by about 10%: we could tune the precipitation factor towards higher values to reduce this discrepancy but refrain to do so, as we do not want to add an additional free parameter in the model.

A.2 WGMS glaciers

To calibrate and validate the mass balance model, OGGM relies on mass-balance observations provided by the World Glacier Monitoring Service (WGMS, 2017). The Fluctuations of Glaciers (FoG) database contains annual mass-balance values for several hundreds of glaciers worldwide. We exclude water-terminating glaciers and the time series with less than five years of data. Not all

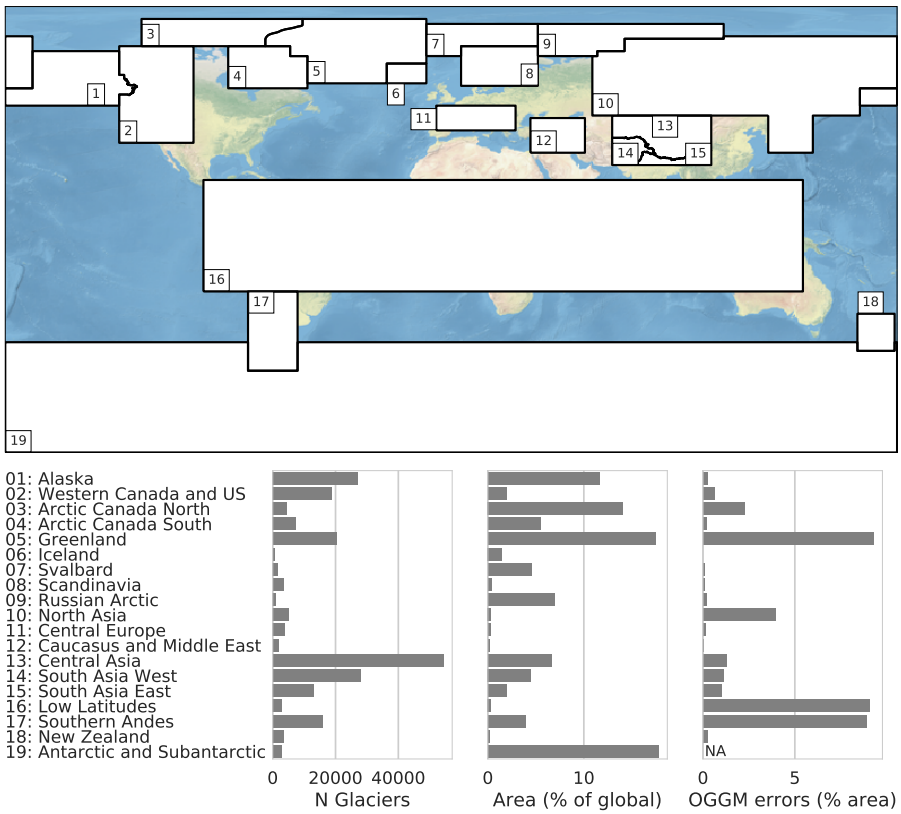

Figure A.1: **Upper panel**: map of the RGI regions; the red dots indicate the glacier locations and the blue circles the location of the 254 reference WGMS glaciers used by the OGGM calibration. **Lower panel**: region names and basic statistics of the database (number of glaciers per region, regional contribution to the global area in percent, and percentage of the regional area which cannot be modelled by OGGM).

of the remaining glaciers can be used by OGGM: we also need a corresponding RGI outline. Indeed, the WGMS and RGI databases have distinct glacier identifiers and it is not guaranteed that the glacier outline provided by the RGI fits the outline used by the local data providers to compute the specific mass balance. Since 2017, the WGMS provides a lookup table linking the two databases. We updated this list for the version 6 of the RGI, leaving us with 254 mass balance time series.

These data are not equally distributed over the glaciated regions (e.g. see Fig. A.1 and (Zemp et al., 2015)), and their quality is highly variable. In the absence of a better data basis (at least for the 20th century), we have to rely

on them for the calibration and validation of our model. Fortunately, these data play a relatively minor role in the model calibration as explained in Sect. 2.3.3. For future studies it might be advisable to use independent, regional geodetic mass balance estimates for validation as well.

A.3 RGI Regions

A map of the RGI regions and some basic statistics are presented in Fig. A.1.

Bibliography

Adhikari, S. and Marshall, S. J.: Glacier volume-area relation for high-order mechanics and transient glacier states, Geophysical Research Letters, 39, 1–6, 2012a.

Adhikari, S. and Marshall, S. J.: Parameterization of lateral drag in flowline models of glacier dynamics, Journal of Glaciology, 58, 1119–1132, 2012b.

Anderson, B., Lawson, W., and Owens, I.: Response of Franz Josef Glacier Ka Roimata o Hine Hukatere to climate change, Global and Planetary Change, 63, 23–30, 2008.

Åström, J. A., Vallot, D., Schäfer, M., Welty, E. Z., O'Neel, S., Bartholomaus, T. C., Liu, Y., Riikilä, T. I., Zwinger, T., Timonen, J., and Moore, J. C.: Termini of calving glaciers as self-organized critical systems, Nature Geoscience, 7, 874–878, 2014.

Bahr, D. B., Meier, M. F., and Peckham, S. D.: The physical basis of glacier volume-area scaling, Journal of Geophysical Research: Solid Earth, 102, 20 355–20 362, 1997.

Bahr, D. B., Dyurgerov, M., and Meier, M. F.: Sea-level rise from glaciers and ice caps: A lower bound, Geophysical Research Letters, 36, 2–5, 2009.

Bahr, D. B., Pfeffer, W. T., and Kaser, G.: Glacier volume estimation as an ill-posed inversion, Journal of Glaciology, 60, 922–934, 2014.

Bahr, D. B., Pfeffer, W. T., and Kaser, G.: A review of volume-area scaling of glaciers, Reviews of Geophysics, pp. 95–140, 2015.

Bendle, J.: Calving of freshwater glaciers., 2018.

Benn, D. I., Hulton, N. R., and Mottram, R. H.: 'Calving laws', 'sliding laws' and the stability of tidewater glaciers, Annals of Glaciology, 46, 123–130, 2007a.

Benn, D. I., Warren, C. R., and Mottram, R. H.: Calving processes and the dynamics of calving glaciers, Earth-Science Reviews, 82, 143–179, 2007b.

BIBLIOGRAPHY

Berthier, E., Schiefer, E., Clarke, G. K. C., Menounos, B., and Rémy, F.: Contribution of Alaskan glaciers to sea-level rise derived from satellite imagery, Nature Geoscience, 3, 92–95, 2010.

Bjørk, A. A., Aagaard, S., Lütt, A., Khan, S. A., Box, J. E., Kjeldsen, K. K., Larsen, N. K., Korsgaard, N. J., Cappelen, J., Colgan, W. T., Machguth, H., Andresen, C. S., Peings, Y., and Kjær, K. H.: Changes in Greenland's peripheral glaciers linked to the North Atlantic Oscillation, Nature Climate Change, 8, 48–52, 2018.

Blaszczyk, M., Jania, J. a., and Hagen, J. O.: Tidewater glaciers of Svalbard: Recent changes and estimates of calving fluxes, vol. 30, 2009.

Bolch, T., Sandberg Sørensen, L., Simonsen, S. B., Mölg, N., Machguth, H., Rastner, P., and Paul, F.: Mass loss of Greenland's glaciers and ice caps 2003–2008 revealed from ICESat laser altimetry data, Geophysical Research Letters, 40, 875–881, 2013.

Brondex, J., Gagliardini, O., Gillet-Chaulet, F., and Durand, G.: Sensitivity of grounding line dynamics to the choice of the friction law, Journal of Glaciology, 63, 854–866, 2017.

Brown, C. S., Meier, M. F., and Post, A.: 'Calving speed of Alaska tidewater Glaciers, with application to Columbia Glacier', U.S. Geological Survey Professional Paper, pp. 1258–C, 1982.

Budd, W. and Allison, I.: An empirical scheme for estimating the dynamics of unmeasured glaciers, International Association of Hydrological Sciences, in: Proceedings of the Moscow Symposium "Snow and Ice", 104, p. 246–256, 1975.

Budd, W. F., Keage, P. L., and Blundy, N. A.: Empirical studies of ice sliding., Journal of Glaciology, 23, 157–170, 1979a.

Budd, W. F., Keage, P. L., and Blundy, N. A.: Empirical Studies of Ice Sliding, Journal of Glaciology, 23, 157–170, 1979b.

Burgess, E. W., Forster, R. R., and Larsen, C. F.: Flow velocities of Alaskan glaciers, Nature Communications, 4, 1–8, 2013.

Carr, J., Vieli, A., Stokes, C., Jamieson, S., Palmer, S., Christoffersen, P., Dowdeswell, J., Nick, F., Blankenship, D., Young, D., and et al.: Basal topographic controls on rapid retreat of Humboldt Glacier, northern Greenland, Journal of Glaciology, 61, 137–150, 2015.

Carr, J. R., Stokes, C., and Vieli, A.: Recent retreat of major outlet glaciers on Novaya Zemlya, Russian Arctic, influenced by fjord geometry and sea-ice conditions, Journal of Glaciology, 60, 155–170, 2014.

Castellani, M.: An overview of the Glacier Thickness Database, 2019.

Choi, Y., Morlighem, M., Wood, M., and Bondzio, J. H.: Comparison of four calving laws to model Greenland outlet glaciers, The Cryosphere, 12, 3735–3746, 2018.

Church, J., Clark, P., Cazenave, A., Gregory, J., Jevrejeva, S., Levermann, A., Merrifield, M., Milne, G., Nerem, R., Nunn, P., Payne, A., Pfeffer, W., Stammer, D., and Unnikrishnan, A.: Sea Level Change, in: Climate Change 2013 - The Physical Science Basis, edited by Intergovernmental Panel on Climate Change, chap. 13, pp. 1137–1216, Cambridge University Press, Cambridge, 2013a.

Church, J., Clark, P., Cazenave, A., Gregory, J., Jevrejeva, S., Levermann, A., Merrifield, M., Milne, G., Nerem, R., Nunn, P., Payne, A., Pfeffer, W., Stammer, D., and Unnikrishnan, A.: Sea Level Change. In *Climate Change 2013: The Physical Science Basis. Contribution of Working Group I to the Fifth Assessment Report of the Intergovernmental Panel on Climate Change*, Cambridge University Press, Cambridge, United Kingdom and New York, NY, USA, 2013b.

Clarke, G. K. C., Anslow, F. S., Jarosch, A. H., Radić, V., Menounos, B., Bolch, T., and Berthier, E.: Ice Volume and Subglacial Topography for Western Canadian Glaciers from Mass Balance Fields, Thinning Rates, and a Bed Stress Model, Journal of Climate, 26, 4282–4303, 2013.

Clarke, G. K. C., Jarosch, A. H., Anslow, F. S., Radić, V., and Menounos, B.: Projected deglaciation of western Canada in the twenty-first century, Nature Geoscience, 8, 372–377, 2015.

Cogley, J. G.: Geodetic and direct mass-balance measurements: comparison and joint analysis, Annals of Glaciology, 50, 96–100, 2009a.

Cogley, J. G.: A more complete version of the World Glacier Inventory, Annals of Glaciology, 50, 32–38, 2009b.

Colgan, W., Box, J. E., Andersen, M. L., Fettweis, X., Csathó, B., Fausto, R. S., Van As, D., and Wahr, J.: Greenland high-elevation mass balance: inference and implication of reference period (1961–90) imbalance, Annals of Glaciology, 56, 105–117, 2015.

Cowton, T. R., Sole, A. J., Nienow, P. W., Slater, D. A., and Christoffersen, P.: Linear response of east Greenland's tidewater glaciers to ocean/atmosphere warming, Proceedings of the National Academy of Sciences, 115, 7907–7912, 2018.

Cuffey, K. and Paterson, W.: The Physics of Glaciers, 4th Edition, Academic Press, 2010.

Davies, B. and Lea, J.: Numerical Glacier Modelling Glossary, 2015.

De Smedt, B. and Pattyn, F.: Numerical modelling of historical front variations and dynamic response of Sofiyskiy glacier, Altai mountains, Russia, Annals of Glaciology, 37, 143–149, 2003.

Diolaiuti, G., Smiraglia, C., Vassena, G., and Motta, M.: Dry calving processes at the ice cliff of Strandline Glacier northern Victoria Land, Antarctica, Annals of Glaciology, 39, 201–208, 2004.

Enderlin, E. M., Howat, I. M., and Vieli, A.: The sensitivity of flowline models of tidewater glaciers to parameter uncertainty, The Cryosphere, 7, 1579–1590, 2013a.

Enderlin, E. M., Howat, I. M., and Vieli, A.: High sensitivity of tidewater outlet glacier dynamics to shape, The Cryosphere, 7, 1007–1015, 2013b.

Farinotti, D., Huss, M., Bauder, A., Funk, M., and Truffer, M.: A method to estimate the ice volume and ice-thickness distribution of alpine glaciers, Journal of Glaciology, 55, 422–430, 2009.

Farinotti, D., Brinkerhoff, D. J., Clarke, G. K. C., Fürst, J. J., Frey, H., Gantayat, P., Gillet-Chaulet, F., Girard, C., Huss, M., Leclercq, P. W., Linsbauer, A., Machguth, H., Martin, C., Maussion, F., Morlighem, M., Mosbeux, C., Pandit, A., Portmann, A., Rabatel, A., Ramsankaran, R., Reerink, T. J.,

Sanchez, O., Stentoft, P. A., Singh Kumari, S., van Pelt, W. J. J., Anderson, B., Benham, T., Binder, D., Dowdeswell, J. A., Fischer, A., Helfricht, K., Kutuzov, S., Lavrentiev, I., McNabb, R., Gudmundsson, G. H., Li, H., and Andreassen, L. M.: How accurate are estimates of glacier ice thickness? Results from ITMIX, the Ice Thickness Models Intercomparison eXperiment, The Cryosphere, 11, 949–970, 2017.

Farinotti, D., Huss, M., Fürst, J. J., Landmann, J., Machguth, H., Maussion, F., and Pandit, A.: A consensus estimate for the ice thickness distribution of all glaciers on Earth, Nature Geoscience, 12, 168–1973, 2019.

Farr, T. G., Rosen, P. A., Caro, E., Crippen, R., Duren, R., Hensley, S., Kobrick, M., Paller, M., Rodriguez, E., Roth, L., Seal, D., Shaffer, S., Shimada, J., Umland, J., Werner, M., Oskin, M., Burbank, D., and Alsdorf, D.: The Shuttle Radar Topography Mission, Reviews of Geophysics, 45, RG2004, 2007.

Fastook, J. L., Brecher, H. H., and Hughes, T. J.: Derived bedrock elevations, strain rates and stresses from measured surface elevations and velocities: Jakobshavns Isbræ, Greenland, Journal of Glaciology, 41, 161–173, 1995.

Fettweis, X., Box, J. E., Agosta, C., Amory, C., Kittel, C., Lang, C., van As, D., Machguth, H., and Gallée, H.: Reconstructions of the 1900–2015 Greenland ice sheet surface mass balance using the regional climate MAR model, The Cryosphere, 11, 1015–1033, 2017.

Fischer, A. and Kuhn, M.: Ground-penetrating radar measurements of 64 Austrian glaciers between 1995 and 2010, Annals of Glaciology, 54, 179–188, 2013.

Frey, H., Machguth, H., Huss, M., Huggel, C., Bajracharya, S., Bolch, T., Kulkarni, A., Linsbauer, A., Salzmann, N., and Stoffel, M.: Estimating the volume of glaciers in the Himalayan-Karakoram region using different methods, The Cryosphere, 8, 2313–2333, 2014.

Gantayat, P., Kulkarni, A. V., and Srinivasan: Estimation of ice thickness using surface velocities and slope: Case study at Gangotri Glacier, India., Journal of Glaciology, 60, 2014.

Gardner, A. S., Moholdt, G., Cogley, J. G., Wouters, B., Arendt, A. a., Wahr, J., Berthier, E., Hock, R., Pfeffer, W. T., Kaser, G., Ligtenberg, S. R. M., Bolch, T., Sharp, M. J., Hagen, J. O., van den Broeke, M. R., and Paul, F.: A

Reconciled Estimate of Glacier Contributions to Sea Level Rise: 2003 to 2009, Science., 340, 852–857, 2013.

Gärtner-Roer, I., Naegeli, K., Huss, M., Knecht, T., Machguth, H., and Zemp, M.: A database of worldwide glacier thickness observations, Global and Planetary Change, 122, 330–344, 2014.

Giesen, R. H. and Oerlemans, J.: Calibration of a surface mass balance model for global-scale applications, The Cryosphere, 6, 1463–1481, 2012.

Giesen, R. H. and Oerlemans, J.: Climate-model induced differences in the 21st century global and regional glacier contributions to sea-level rise, Climate Dynamics, 41, 3283–3300, 2013.

Gillies, S.: Shapely: manipulation and analysis of geometric objects, 2007.

Gillies, S.: Rasterio: geospatial raster I/O for Python programmers, 2013.

Glen, J. W.: The Creep of Polycrystalline Ice., Proceedings of the Royal Society A, 228, 519–538, 1995.

Goosse, H., Barriat, P.-Y., Dalaiden, Q., Klein, F., Marzeion, B., Maussion, F., Pelucchi, P., and Vlug, A.: Testing the consistency between changes in simulated climate and Alpine glacier length over the past millennium, Climate of the Past, 14, 1119–1133, 2018.

Gregory, J. M., White, N. J., Church, J. A., Bierkens, M. F. P., Box, J. E., van den Broeke, M. R., Cogley, J. G., Fettweis, X., Hanna, E., Huybrechts, P., Konikow, L. F., Leclercq, P. W., Marzeion, B., Oerlemans, J., Tamisiea, M. E., Wada, Y., Wake, L. M., and van de Wal, R. S. W.: Twentieth-Century Global-Mean Sea Level Rise: Is the Whole Greater than the Sum of the Parts?, Journal of Climate, 26, 4476–4499, 2013a.

Gregory, J. M., White, N. J., Church, J. A., Bierkens, M. F. P., Box, J. E., Van Den Broeke, M. R., Cogley, J. G., Fettweis, X., Hanna, E., Huybrechts, P., Konikow, L. F., Leclercq, P. W., Marzeion, B., Oerlemans, J., Tamisiea, M. E., Wada, Y., Wake, L. M., and Van De Wal, R. S. W.: Twentieth-century global-mean sea level rise: Is the whole greater than the sum of the parts?, Journal of Climate, 26, 4476–4499, 2013b.

Grinsted, A.: An estimate of global glacier volume, Cryosphere, 7, 141–151, 2013.

Haeberli, W. and Hoelzle, M.: Application of inventory data for estimating characteristics of and regional climate-change effects on mountain glaciers: a pilot study with the European Alps, Annals of Glaciology, 21, 206–212, 1995.

Harris, I., Jones, P., Osborn, T., and Lister, D.: Updated high-resolution grids of monthly climatic observations - the CRU TS3.10 Dataset, International Journal of Climatology, 34, 623–642, 2014.

Harrison, W. D.: How do glaciers respond to climate? Perspectives from the simplest models, Journal of Glaciology, 59, 949–960, 2013.

Howat, I. M., Negrete, A., and Smith, B. E.: The Greenland Ice Mapping Project (GIMP) land classification and surface elevation data sets, Cryosphere, 8, 1509–1518, 2014.

Hoyer, S. and Hamman, J. J.: xarray: N-D labeled Arrays and Datasets in Python, Journal of Open Research Software, 5, 1–6, 2017.

Hunter, J. D.: Matplotlib: A 2D Graphics Environment, Computing in Science Engineering, 9, 90–95, 2007.

Huss, M.: Present and future contribution of glacier storage change to runoff from macroscale drainage basins in Europe, Water Resources Research, 47, n/a–n/a, 2011.

Huss, M. and Farinotti, D.: Distributed ice thickness and volume of all glaciers around the globe, Journal of Geophysical Research: Earth Surface, 117, F04 010, 2012.

Huss, M. and Hock, R.: A new model for global glacier change and sea-level rise, Frontiers in Earth Science, 3, 1–22, 2015.

Hutter, K.: The effect of longitudinal strain on the shear stress of an ice sheet: in defence of using streched coordinates, J. Glaciol., 27, 39–56, 1981.

Hutter, K.: Theoretical glaciology: material science of ice and the mechanics of glaciers and ice sheets, 1983.

Immerzeel, W. W., van Beek, L. P. H., Konz, M., Shrestha, a. B., and Bierkens, M. F. P.: Hydrological response to climate change in a glacierized catchment in the Himalayas, Climatic Change, 110, 721–736, 2012.

Jamieson, S. S. R., Vieli, A., Livingstone, S. J., Cofaigh, C. Ó., Stokes, C., Hillenbrand, C.-D., and Dowdeswell, J. a.: Ice-stream stability on a reverse bed slope, Nature Geoscience, 5, 799–802, 2012.

Jarosch, a. H., Schoof, C. G., and Anslow, F. S.: Restoring mass conservation to shallow ice flow models over complex terrain, Cryosphere, 7, 229–240, 2013.

Jarvis, A., Reuter, H., Nelson, A., and Guevara, E.: Hole-filled SRTM for the globe Version 4, 2008.

Jones, E., Oliphant, T., Peterson, P., et al.: SciPy: Open source scientific tools for Python, 2001.

Joughin, I., B. S. I. H. and Scambos., T.: MEaSUREs Multi-year Greenland Ice Sheet Velocity Mosaic, Version 1., 2016.

Kaser, G., Grosshauser, M., and Marzeion, B.: Contribution potential of glaciers to water availability in different climate regimes, P. Natl. Acad. Sci. Usa., 107, 20 223–20 227, 2010.

Kienholz, C., Hock, R., and Arendt, A. a.: A new semi-automatic approach for dividing glacier complexes into individual glaciers, Journal of Glaciology, 59, 925–937, 2013.

Kienholz, C., Rich, J. L., Arendt, a. a., and Hock, R.: A new method for deriving glacier centerlines applied to glaciers in Alaska and northwest Canada, The Cryosphere, 8, 503–519, 2014.

Kienholz, C., Herreid, S., Rich, J. L., Arendt, A. A., Hock, R., and Burgess, E. W.: Derivation and analysis of a complete modern-date glacier inventory for Alaska and northwest Canada, Journal of Glaciology, 61, 403–420, 2015.

King, M. D., Howat, I. M., Jeong, S., Noh, M. J., Wouters, B., Noël, B., and van den Broeke, M. R.: Seasonal to decadal variability in ice discharge from the Greenland Ice Sheet, The Cryosphere, 12, 3813–3825, 2018.

King, M. D., Howat, I. M., Candela, S. G., Noh, M. J., Jeong, S., Noël, B. P. Y., van den Broeke, M. R., Wouters, B., and Negrete, A.: Dynamic ice loss from the Greenland Ice Sheet driven by sustained glacier retreat, Communications Earth & Environment, 1, 1, 2020.

Larsen, C. F., Motyka, R. J., Arendt, A. A., Echelmeyer, K. A., and Geissler, P. E.: Glacier changes in southeast Alaska and northwest British Columbia and contribution to sea level rise, Journal of Geophysical Research, 112, F01 007, 2007.

Larsen, C. F., Burgess, E., Arendt, A. A., O'Neel, S., Johnson, A. J., and Kienholz, C.: Surface melt dominates Alaska glacier mass balance, Geophysical Research Letters, 42, 5902–5908, 2015.

Leclercq, P. W., Oerlemans, J., and Cogley, J. G.: Estimating the Glacier Contribution to Sea-Level Rise for the Period 1800-2005, Surveys in Geophysics, 32, 519–535, 2011.

Leclercq, P. W., Oerlemans, J., Basagic, H. J., Bushueva, I., Cook, A. J., and Le Bris, R.: A data set of worldwide glacier length fluctuations, The Cryosphere, 8, 659–672, 2014.

Li, H., Ng, F., Li, Z., Qin, D., and Cheng, G.: An extended "perfect-plasticity" method for estimating ice thickness along the flow line of mountain glaciers, Journal of Geophysical Research (Earth Surface), 117, 1020–, 2012.

Linsbauer, A., Paul, F., and Haeberli, W.: Modeling glacier thickness distribution and bed topography over entire mountain ranges with GlabTop: Application of a fast and robust approach, Journal of Geophysical Research: Earth Surface, 117, 2012.

Liu, H., Jezek, K. C., Li, B., and Zhao, Z.: Radarsat Antarctic Mapping Project Digital Elevation Model, Version 2, Boulder, Colorado USA. NASA National Snow and Ice Data Center Distributed Active Archive Center, 2015.

Lüthi, M. P.: Transient response of idealized glaciers to climate variations., The journal of glaciology, 55(193), 918–930, 2009.

Machguth, H., Rastner, P., Bolch, T., Mölg, N., Sørensen, L. S., Adalgeirsdottir, G., van Angelen, J. H., van den Broeke, M. R., and Fettweis, X.: The future sea-level rise contribution of Greenland's glaciers and ice caps, Environmental Research Letters, 8, 025 005, 2013.

Mackintosh, A. N., Anderson, B. M., and Pierrehumbert, R. T.: Reconstructing Climate from Glaciers, Annual Review of Earth and Planetary Sciences, 45, 649–680, 2017.

Mankoff, K. D., Colgan, W., Solgaard, A., Karlsson, N. B., Ahlstrøm, A. P., van As, D., Box, J. E., Khan, S. A., Kjeldsen, K. K., Mouginot, J., and Fausto, R. S.: Greenland Ice Sheet solid ice discharge from 1986 through 2017, Earth System Science Data, 11, 769–786, 2019.

Marzeion, B., Hofer, M., Jarosch, A. H., Kaser, G., and Mölg, T.: A minimal model for reconstructing interannual mass balance variability of glaciers in the European Alps, The Cryosphere, 6, 71–84, 2012a.

Marzeion, B., Jarosch, a. H., and Hofer, M.: Past and future sea-level change from the surface mass balance of glaciers, The Cryosphere, 6, 1295–1322, 2012b.

Marzeion, B., Cogley, J. G., Richter, K., and Parkes, D.: Attribution of global glacier mass loss to anthropogenic and natural causes, Science, 2014a.

Marzeion, B., Jarosch, A. H., and Gregory, J. M.: Feedbacks and mechanisms affecting the global sensitivity of glaciers to climate change, The Cryosphere, 8, 59–71, 2014b.

Marzeion, B., Leclercq, P. W., Cogley, J. G., and Jarosch, a. H.: Brief Communication: Global glacier mass loss reconstructions during the 20th century are consistent, The Cryosphere Discussions, 9, 3807–3820, 2015.

Marzeion, B., Kaser, G., Maussion, F., and Champollion, N.: Limited influence of climate change mitigation on short-term glacier mass loss, Nature Climate Change, 8, 2018.

Maussion, F.: A new WGMS to RGI lookup table, 2017.

Maussion, F., Siller, M., and Rothenberg, D.: fmaussion/salem: v0.2.1, 2017.

Maussion, F., Butenko, A., Champollion, N., Dusch, M., Eis, J., Fourteau, K., Gregor, P., Jarosch, A. H., Landmann, J., Oesterle, F., Recinos, B., Rothenpieler, T., Vlug, A., Wild, C. T., and Marzeion, B.: The Open Global Glacier Model (OGGM) v1.1, Geoscientific Model Development, 12, 909–931, 2019.

McKinney, W.: Data Structures for Statistical Computing in Python, Proceedings of the 9th Python in Science Conference, 1697900, 51–56, 2010.

Mcnabb, R., Hock, R., O'Neel, S., Rasmussen, L., Ahn, Y., Braun, M., Conway, H., Herreid, S., Joughin, I., Pfeffer, W., Smith, B., and Truffer, M.: Using surface velocities to calculate ice thickness and bed topography: a case study at Columbia Glacier, Alaska, USA, Journal of Glaciology, 58, 1151–1164, 2012.

McNabb, R. W. and Hock, R.: Alaska tidewater glacier terminus positions, 1948-2012, Journal of Geophysical Research: Earth Surface, 119, 153–167, 2014.

McNabb, R. W., Hock, R., and Huss, M.: Variations in Alaska tidewater glacier frontal ablation, 1985-2013, Journal of Geophysical Research: Earth Surface, 120, 120–136, 2015.

Mercenier, R., Lüthi, M. P., and Vieli, A.: Calving relation for tidewater glaciers based on detailed stress field analysis, The Cryosphere, 12, 721–739, 2018.

Mernild, S. H., Lipscomb, W. H., Bahr, D. B., Radić, V., and Zemp, M.: Global glacier changes: A revised assessment of committed mass losses and sampling uncertainties, Cryosphere, 7, 1565–1577, 2013.

Morlighem, M., Rignot, E., Seroussi, H., Larour, E., Ben Dhia, H., and Aubry, D.: A mass conservation approach for mapping glacier ice thickness, Geophysical Research Letters, 38, n/a–n/a, 2011.

Mouginot, J., Rignot, E., Bjørk, A. A., van den Broeke, M., Millan, R., Morlighem, M., Noël, B., Scheuchl, B., and Wood, M.: Forty-six years of Greenland Ice Sheet mass balance from 1972 to 2018, Proceedings of the National Academy of Sciences, 116, 9239–9244, 2019.

New, M., Lister, D., Hulme, M., and Makin, I.: A high-resolution data set of surface climate over global land areas, Climate Research, 21, 1–25, 2002.

Nick, F., van der Veen, C., Vieli, A., and Benn, D.: A physically based calving model applied to marine outlet glaciers and implications for the glacier dynamics, Journal of Glaciology, 56, 781–794, 2010.

Nick, F. M.: Modelling the behaviour of tidewater glaciers, Ph.D. thesis, Universiteit Utrecht, 2006.

Nick, F. M., Vieli, A., Andersen, M. L., Joughin, I., Payne, A., Edwards, T. L., Pattyn, F., and van de Wal, R. S. W.: Future sea-level rise from Greenland's main outlet glaciers in a warming climate, Nature, 497, 235 EP –, 2013.

NOAA National Centers for Environmental Information: NOAA National Centers for Environmental Information (2004): Multibeam Bathymetry Database (MBBDB), [cruise]., 2004.

Noël, B., van de Berg, W. J., Machguth, H., Lhermitte, S., Howat, I., Fettweis, X., and van den Broeke, M. R.: A daily, 1 km resolution data set of downscaled Greenland ice sheet surface mass balance (1958–2015), The Cryosphere, 10, 2361–2377, 2016.

Noël, B., van de Berg, W. J., Lhermitte, S., Wouters, B., Machguth, H., Howat, I., Citterio, M., Moholdt, G., Lenaerts, J. T. M., and van den Broeke, M. R.: A tipping point in refreezing accelerates mass loss of Greenland's glaciers and ice caps, Nature Communications, 8, 14 730, 2017.

Noël, B., van de Berg, W. J., van Wessem, J. M., van Meijgaard, E., van As, D., Lenaerts, J. T. M., Lhermitte, S., Kuipers Munneke, P., Smeets, C. J. P. P., van Ulft, L. H., van de Wal, R. S. W., and van den Broeke, M. R.: Modelling the climate and surface mass balance of polar ice sheets using RACMO2 – Part 1: Greenland (1958–2016), The Cryosphere, 12, 811–831, 2018.

Noël, B., van de Berg, W. J., Lhermitte, S., and van den Broeke, M. R.: Rapid ablation zone expansion amplifies north Greenland mass loss, Science Advances, 5, 2019.

Nye, J. F.: The Mechanics of Glacier Flow, Journal of Glaciology, 2, 82–93, 1952.

Nye, J. F.: The Flow of a Glacier in a Channel of Rectangular, Elliptic or Parabolic Cross-Section, Journal of Glaciology, 5, 661–690, 1965.

Oerlemans, J.: Quantifying Global Warming from the Retreat of Glaciers, Science, 264, 243–245, 1994.

Oerlemans, J.: A flowline model for Nigardsbreen, Norway: projection of future glacier length based on dynamic calibration with the historic record, Journal of glaciology, 24, 382–389, 1997.

Oerlemans, J.: Extracting a Climate Signal from 169 Glacier Records, Science, 308, 675–677, 2005.

Oerlemans, J. and Nick, F.: A minimal model of a tidewater glacier, Annals of Glaciology, 42, 1–6, 2005.

Oerlemans, J., Jania, J., and Kolondra, L.: Application of a minimal glacier model to Hansbreen, Svalbard, The Cryosphere, 5, 1–11, 2011.

Pattyn, F., Schoof, C., Perichon, L., Hindmarsh, R. C. A., Bueler, E., de Fleurian, B., Durand, G., Gagliardini, O., Gladstone, R., Goldberg, D., Gudmundsson, G. H., Huybrechts, P., Lee, V., Nick, F. M., Payne, A. J., Pollard, D., Rybak, O., Saito, F., and Vieli, A.: Results of the Marine Ice Sheet Model Intercomparison Project, MISMIP, The Cryosphere, 6, 573–588, 2012.

Paul, F. and Linsbauer, A.: Modeling of glacier bed topography from glacier outlines, central branch lines, and a DEM, International Journal of Geographical Information Science, 26, 1173–1190, 2012.

Pfeffer, W. T., Dyurgerov, M., Kaplan, M., Dwyer, J., Sassolas, C., Jennings, A., Raup, B., and Manley, W.: Numerical modeling of Late Glacial Laurentide advance of ice across Hudson Strait: Insights into terrestrial and marine geology, mass balance, and calving flux, Paleoceanography, 12, 97–110, 1997.

Pfeffer, W. T., Arendt, A. a., Bliss, A., Bolch, T., Cogley, J. G., Gardner, A. S., Hagen, J.-O., Hock, R., Kaser, G., Kienholz, C., Miles, E. S., Moholdt, G., Mölg, N., Paul, F., Radić, V., Rastner, P., Raup, B. H., Rich, J., and Sharp, M. J.: The Randolph Glacier Inventory: a globally complete inventory of glaciers, Journal of Glaciology, 60, 537–552, 2014.

Pope, A.: GLOSSARY OF GLACIER MASS BALANCE AND RELATED TERMS. J.G. Cogley, R. Hock, L.A. Rasmussen, A.A. Arendt, A. Bauder, R.J. Braithwaite, P. Jansson, G. Kaser, M. Möller, L. Nicholson, and M. Zemp. 2011. Paris: UNESCO-IHP (IHP-VII Technical documents in hydrology 86, IACS contribution 2), vi 114p, illustrated, soft cover. (Free download from URL: http://unesdoc.unesco.org/images/0019/001925/192525E.pdf or ordered as hard copy, at no charge, from ihp@unesco.org)., Polar Record, 48, e15, 2012.

Porter, C., Morin, P., Howat, I., Noh, M.-J., Bates, B., Peterman, K., Keesey, S., Schlenk, M., Gardiner, J., Tomko, K., Willis, M., Kelleher, C., Cloutier, M., Husby, E., Foga, S., Nakamura, H., Platson, M., Wethington, Michael, J., Williamson, C., Bauer, G., Enos, J., Arnold, G., Kramer, W., Becker, P., Doshi, A., D'Souza, C., Cummens, P., Laurier, F., and Bojesen, M.: ArcticDEM, 2018.

Price, S., Lipscomb, W., Hoffman, M., Hagdorn, M., Rutt, I., Payne, T., Hebeler, F., and Kennedy, J. H.: CISM 2.0.5 Documentation, 2015.

Radić, V. and Hock, R.: Regionally differentiated contribution of mountain glaciers and ice caps to future sea-level rise, Nature Geoscience, 4, 91–94, 2011.

Radić, V. and Hock, R.: Glaciers in the Earth's Hydrological Cycle: Assessments of Glacier Mass and Runoff Changes on Global and Regional Scales, Surveys in Geophysics, 35, 813–837, 2014.

Radić, V., Bliss, A., Beedlow, a. C., Hock, R., Miles, E., and Cogley, J. G.: Regional and global projections of twenty-first century glacier mass changes in response to climate scenarios from global climate models, Climate Dynamics, 42, 37–58, 2014.

Rasmussen, L. A.: Bed Topography and Mass-Balance Distribution of Columbia Glacier, Alaska, U.S.A., Determined from Sequential Aerial Photography, Journal of Glaciology, 34, 208–216, 1988.

Rasmussen, L. A., Conway, H., Krimmel, R. M., and Hock, R.: Surface mass balance, thinning and iceberg production, Columbia Glacier, Alaska, 1948-2007, Journal of Glaciology, 57, 431–440, 2011.

Rastner, P., Bolch, T., Mölg, N., Machguth, H., Le Bris, R., and Paul, F.: The first complete inventory of the local glaciers and ice caps on Greenland, The Cryosphere, 6, 1483–1495, 2012.

Recinos, B., Maussion, F., Rothenpieler, T., and Marzeion, B.: Impact of frontal ablation on the ice thickness estimation of marine-terminating glaciers in Alaska, The Cryosphere, 13, 2657–2672, 2019.

RGI Consortium: Randolph Glacier Inventory – A Dataset of Global Glacier Outlines: Version 6.0, Tech. rep., Global Land Ice Measurements from Space, Colorado, USA, 2017.

Richardson, S. D. and Reynolds, J. M.: An overview of glacial hazards in the Himalayas, Quaternary International, 65-66, 31–47, 2000.

Rignot, E. and Kanagaratnam, P.: Changes in the Velocity Structure of the Greenland Ice Sheet, Science, 311, 986–990, 2006.

Roe, G. H.: What do glaciers tell us about climate variability and climate change?, Journal of Glaciology, 57, 567–578, 2011.

Roe, G. H. and O'Neal, M. A.: The response of glaciers to intrinsic climate variability: Observations and models of late-holocene variations in the Pacific northwest, Journal of Glaciology, 55, 839–854, 2009.

Shepherd, A., Ivins, E., Rignot, E., Smith, B., van den Broeke, M., Velicogna, I., Whitehouse, P., Briggs, K., Joughin, I., Krinner, G., Nowicki, S., Payne, T., Scambos, T., Schlegel, N., A, G., Agosta, C., Ahlstrøm, A., Babonis, G., Barletta, V. R., Bjørk, A. A., Blazquez, A., Bonin, J., Colgan, W., Csatho, B., Cullather, R., Engdahl, M. E., Felikson, D., Fettweis, X., Forsberg, R., Hogg, A. E., Gallee, H., Gardner, A., Gilbert, L., Gourmelen, N., Groh, A., Gunter, B., Hanna, E., Harig, C., Helm, V., Horvath, A., Horwath, M., Khan, S., Kjeldsen, K. K., Konrad, H., Langen, P. L., Lecavalier, B., Loomis, B., Luthcke, S., McMillan, M., Melini, D., Mernild, S., Mohajerani, Y., Moore, P., Mottram, R., Mouginot, J., Moyano, G., Muir, A., Nagler, T., Nield, G., Nilsson, J., Noël, B., Otosaka, I., Pattle, M. E., Peltier, W. R., Pie, N., Rietbroek, R., Rott, H., Sandberg Sørensen, L., Sasgen, I., Save, H., Scheuchl, B., Schrama, E., Schröder, L., Seo, K.-W., Simonsen, S. B., Slater, T., Spada, G., Sutterley, T., Talpe, M., Tarasov, L., van de Berg, W. J., van der Wal, W., van Wessem, M., Vishwakarma, B. D., Wiese, D., Wilton, D., Wagner, T., Wouters, B., Wuite, J., and Team, T. I.: Mass balance of the Greenland Ice Sheet from 1992 to 2018, Nature, 579, 233–239, 2020.

Strahler, A. N.: Hypsometric (Area - Altitude) Analysis of Erosional Topography, Geological Society of America Bulletin, 63, 1117–1142, 1952.

Straneo, F., Heimbach, P., Sergienko, O., Hamilton, G., Catania, G., Griffies, S., Hallberg, R., Jenkins, A., Joughin, I., Motyka, R., Pfeffer, W. T., Price, S. F., Rignot, E., Scambos, T., Truffer, M., and Vieli, A.: Challenges to Understanding the Dynamic Response of Greenland's Marine Terminating Glaciers to Oceanic and Atmospheric Forcing, Bulletin of the American Meteorological Society, 94, 1131–1144, 2013.

Todd, J. and Christoffersen, P.: Are seasonal calving dynamics forced by buttressing from ice mélange or undercutting by melting? Outcomes from full-Stokes simulations of Store Glacier, West Greenland, The Cryosphere, 8, 2353–2365, 2014.

Todd, J., Christoffersen, P., Zwinger, T., Rabåck, P., Chauché, N., Benn, D., Luckman, A., Ryan, J., Toberg, N., Slater, D., and Hubbard, A.: A Full-Stokes 3-D Calving Model Applied to a Large Greenlandic Glacier, Journal of Geophysical Research: Earth Surface, 123, 410–432, 2018.

Turton, J.: Image of the Week - The Greenland Ocean-ice interaction project (GROCE): teamwork to predict a glacier's future, 2019.

Ultee, L. and Bassis, J. N.: The future is Nye: an extension of the perfect plastic approximation to tidewater glaciers, Journal of Glaciology, 62, 1143–1152, 2016.

Van der Veen, C. J.: Tidewater calving, Journal of Glaciology, 42, 375–385, 1996.

van der Veen, C. J.: Calving glaciers, Progress in Physical Geography: Earth and Environment, 26, 96–122, 2002.

van der Walt, S., Colbert, S. C., and Varoquaux, G.: The NumPy array: A structure for efficient numerical computation, Computing in Science and Engineering, 13, 22–30, 2011.

van der Walt, S., Schönberger, J. L., Nunez-Iglesias, J., Boulogne, F., Warner, J. D., Yager, N., Gouillart, E., and Yu, T.: scikit-image: image processing in Python, PeerJ, 2, e453, 2014.

Vaughan, D., Comiso, J., Allison, I., Carrasco, J., Kaser, G., Kwok, R., Mote, P., Murray, T., Paul, F., Ren, J., Rignot, E., Solomina, O., Steffen, K., and Zhang, T.: Observations: Cryosphere. In *Climate Change 2013: The Physical Science Basis. Contribution of Working Group I to the Fifth Assessment Report of the Intergovernmental Panel on Climate Change*, Cambridge University Press, Cambridge, United Kingdom and New York, NY, USA, 2013.

Vieli, A., Funk, M., and Blatter, H.: Tidewater glaciers: frontal flow acceleration and basal sliding, Annals of Glaciology, 31, 217–221, 2000.

Vieli, A., Funk, M., and Blatter, H.: Flow dynamics of tidewater glaciers: a numerical modelling approach, Journal of Glaciology, 47, 595–606, 2001.

Vieli, A., Jania, J., and Kolondra, L.: The retreat of a tidewater glacier: observations and model calculations on Hansbreen, Spitsbergen, Journal of Glaciology, 48, 592–600, 2002.

Wessel, B., Huber, M., Wohlfart, C., Marschalk, U., Kosmann, D., and Roth, A.: Accuracy assessment of the global TanDEM-X Digital Elevation Model with GPS data, ISPRS Journal of Photogrammetry and Remote Sensing, 139, 171 – 182, 2018.

WGMS: Fluctuations of Glaciers Database. World Glacier Monitoring Service, Zurich, Switzerland, 2017.

Winkelmann, R., Martin, M. A., Haseloff, M., Albrecht, T., Bueler, E., Khroulev, C., and Levermann, A.: The Potsdam Parallel Ice Sheet Model (PISM-PIK) - Part 1: Model description, Cryosphere, 5, 715–726, 2011.

Zemp, M., Hoelzle, M., and Haeberli, W.: Six decades of glacier mass-balance observations: a review of the worldwide monitoring network, Ann. Glaciol., 50, 101–111, 2009.

Zemp, M., Frey, H., Gärtner-Roer, I., Nussbaumer, S. U., Hoelzle, M., Paul, F., Haeberli, W., Denzinger, F., Ahlstrøm, A. P., Anderson, B., Bajracharya, S., Baroni, C., Braun, L. N., Càceres, B. E., Casassa, G., Cobos, G., Dàvila, L. R., Delgado Granados, H., Demuth, M. N., Espizua, L., Fischer, A., Fujita, K., Gadek, B., Ghazanfar, A., Hagen, J. O., Holmlund, P., Karimi, N., Li, Z., Pelto, M., Pitte, P., Popovnin, V. V., Portocarrero, C. A., Prinz, R., Sangewar, C. V., Severskiy, I., Sigurdsson, O., Soruco, A., Usubaliev, R., and Vincent, C.: Historically unprecedented global glacier decline in the early 21st century, Journal of Glaciology, 61, 745–762, 2015.

Zemp, M., Huss, M., Thibert, E., Eckert, N., McNabb, R., Huber, J., Barandun, M., Machguth, H., Nussbaumer, S. U., Gärtner-Roer, I., Thomson, L., Paul, F., Maussion, F., Kutuzov, S., and Cogley, J. G.: Global glacier mass changes and their contributions to sea-level rise from 1961 to 2016, Nature, 568, 382–386, 2019.

Versicherung an Eides Statt / Affirmation in lieu of an oath

gem. § 6 Abs. 5 der Promotionsordnung Dr. rer. nat. im Fachbereich 8 vom 22.06.2011 /
according to § 6 (5) of the Doctoral Degree Rules and Regulations of 22 June, 2011

Ich / I, Beatriz Margarita Recinos Rivas, .
(Vorname / First Name, Name / Name, Anschrift / Address, ggf. Matr.-Nr. / student ID no., if applicable)

versichere an Eides Statt durch meine Unterschrift, dass ich die vorliegende Dissertation selbständig und ohne fremde Hilfe angefertigt und alle Stellen, die ich wörtlich dem Sinne nach aus Veröffentlichungen entnommen habe, als solche kenntlich gemacht habe, mich auch keiner anderen als der angegebenen Literatur oder sonstiger Hilfsmittel bedient habe und die zu Prüfungszwecken beigelegte elektronische Version (PDF) der Dissertation mit der abgegebenen gedruckten Version identisch ist. / *With my signature I affirm in lieu of an oath that I prepared the submitted dissertation independently and without illicit assistance from third parties, that I appropriately referenced any text or content from other sources, that I used only literature and resources listed in the dissertation, and that the electronic (PDF) and printed versions of the dissertation are identical.*

Ich versichere an Eides Statt, dass ich die vorgenannten Angaben nach bestem Wissen und Gewissen gemacht habe und dass die Angaben der Wahrheit entsprechen und ich nichts verschwiegen habe. */ I affirm in lieu of an oath that the information provided herein to the best of my knowledge is true and complete.*

Die Strafbarkeit einer falschen eidesstattlichen Versicherung ist mir bekannt, namentlich die Strafandrohung gemäß § 156 StGB bis zu drei Jahren Freiheitsstrafe oder Geldstrafe bei vorsätzlicher Begehung der Tat bzw. gemäß § 161 Abs. 1 StGB bis zu einem Jahr Freiheitsstrafe oder Geldstrafe bei fahrlässiger Begehung. / *I am aware that a false affidavit is a criminal offence which is punishable by law in accordance with § 156 of the German Criminal Code (StGB) with up to three years imprisonment or a fine in case of intention, or in accordance with § 161 (1) of the German Criminal Code with up to one year imprisonment or a fine in case of negligence.*

_____ _____

Ort / Place, Datum / Date Unterschrift / Signature